DESIGN OF A SELF-ADJUSTING AND SELF-POWERED DYNAMIC VIBRATION ABSORBER

by

Bedri Seyhan

B.S., Mechanical Engineering, Istanbul Technical University, 2019

Submitted to the Institute for Graduate Studies in
Science and Engineering in partial fulfillment of
the requirements for the degree of
Master of Science

Graduate Program in Mechanical Engineering
Boğaziçi University

2022

DESIGN OF A SELF-ADJUSTING AND SELF-POWERED DYNAMIC VIBRATION ABSORBER

APPROVED BY:

Prof. Çetin Yılmaz . . . . . .
(Thesis Supervisor)

Assoc. Prof. Evren Samur . . . . . .

Assist. Prof. Polat Şendur . . . . . .

DATE OF APPROVAL: 04.07.2022

ACKNOWLEDGEMENTS

First of all, I would like to thank my thesis advisor Prof. Çetin Yılmaz for his great support during my study, in terms of both teaching and leading the way. His understanding, kindness and patience were invaluable to me at all stages of this thesis.

I would like to thank the members of my thesis committee Assoc. Prof. Evren Samur and Assist. Prof. Polat Şendur for their contributions.

I am thankful to all my supervisors, teachers, research assistants and the staff at the mechanical engineering department who have contributed to the development of my engineering and academic skills.

I am grateful for the company, encouragement and support of my friends Emirhan Tıknaz and Onat Baykara during my studies and master program.

Special thanks to my colleagues and managers at Arçelik, especially Can Arer, for always providing me the time and support I need to finish my thesis.

Finally, I thank my family for their love, support and encouragement. I feel lucky to have their continuous supports from the beginning to the end.

ABSTRACT

DESIGN OF A SELF-ADJUSTING AND SELF-POWERED DYNAMIC VIBRATION ABSORBER

In this study, an adaptive self-tuning base-excited resonator, which can be used as a vibration absorber system, is described. A self-powered tuning subsystem that only uses external vibration energy is designed. Hence, no electronic sensor or actuator is used and the fully mechanical system functions without an external electrical source. The system contains a lever, whose effective length can change, which in turn changes the resonance frequency of the system. When the resonance frequency matches the excitation frequency, the instant center of zero velocity of the lever coincides with the hinge attached to the base. As the excitation frequency changes, the system changes the lever ratio in such way to bring out resonance frequency to coincide with the excitation frequency to absorb excitation at the base and transfer the vibration to the main mass of the absorber. The system self-tunes to the optimum lever ratio for maximum vibration output. The equation of motion of the system is derived and the location of the instant center is calculated analytically. In addition, simulations are carried out to compare and confirm the response of the system. The numerical simulations verify that the resonance condition is achieved in the working frequency range.

ÖZET

KENDİNİ AYARLAYABİLEN VE KENDİ GÜCÜNÜ SAĞLAYAN BİR DİNAMİK TİTREŞİM YUTUCUSU TASARIMI

Bu çalışmada dinamik titreşim yutucusu olarak kullanılabilecek, uyarlanabilir, kendini ayarlayan, taban uyarımlı bir rezonatör anlatılmıştır. Yalnızca harici titreşim enerjisini kullanarak kendi gücünü sağlayan bir ayarlama alt sistemi tasarlanmıştır. Bu sayede sistem, elektronik sensör veya eyleyici kullanmadan ve tamamen mekanik olarak harici bir elektrik kaynağı olmadan çalışır. Sistem, etkin uzunluğu değişebilen ve değiştikçe sistemin rezonans frekansını değiştiren bir kaldıraç içerir. Rezonans frekansı uyarma frekansı ile eşleştiğinde, kaldıracın anlık dönme merkezi tabana bağlı menteşe ile çakışır. Uyarma frekansı değiştikçe sistem, tabandaki uyarıyı absorbe etmek ve titreşimi dinamik titreşim yutucusunun ana kütlesine aktarmak için rezonans frekansını uyarma frekansıyla çakışacak şekilde kaldıraç oranını ayarlar. Sistem, maksimum titreşim çıkışı için optimum kaldıraç oranını ayarlar. Sistemin hareket denklemi türetilmiş ve anlık dönme merkezin konumu analitik olarak hesaplanmıştır. Ek olarak, sistemin tepkisini karşılaştırmak ve doğrulamak amacıyla simülasyonlar yapılmıştır. Nümerik simülasyonlar ile rezonans koşulunun çalışma frekansı aralığında sağlandığı doğrulanmıştır.

TABLE OF CONTENTS

ACKNOWLEDGEMENTS iii
ABSTRACT iv
ÖZET v
TABLE OF CONTENTS vi
LIST OF FIGURES viii
LIST OF TABLES xiv
LIST OF SYMBOLS xv
LIST OF ABBREVIATIONS xvii
1. INTRODUCTION 1
1.1 Objective and Motivation of Study 1
1.2 Literature Review 2
1.3 Overview of Thesis 6
2. DEVELOPMENT OF THE SELF-TUNING ALGORITHM 7
2.1 Dynamic Vibration Absorbers 7
2.2 Dynamic Anti-Resonant Vibration Isolator 10
2.3 Development of the Self-Tuning Algorithm 12
3. NUMERICAL VERIFICATION 17
3.1 Lever-Type Self-Tuning Adaptive Vibration Absorber Model 17
3.2 Parametric Design Studies 24
3.3 Tracking Performance of the Modified System Under Changing Frequency Condition 33
3.4 Implementation of the Self-Tuning Vibration Absorber 36
3.4.1 Tracking Performance of the Self-Tuning Absorber System Under Changing Frequency Condition 61
3.5 Modification of the System to Increase Working Frequency Range 63
4. CONCLUSION 66
4.1 Summary 66
4.2 Future Work 66
REFERENCES 68
APPENDIX A: ELSEVIER LICENSE NUMBER 5375511216243 72

APPENDIX B: ELSEVIER LICENSE
NUMBER 5375510063227 73
APPENDIX C: ELSEVIER LICENSE
NUMBER 5375500220278 74

LIST OF FIGURES

Figure 1.1. SMA based ATVA [1] 3

Figure 1.2. Negative stiffness mechanism [6] 4

Figure 2.1. Dynamic vibration absorber subject to base excitation 7

Figure 2.2. Transmissibility plot for a dynamic vibration absorber with $k_1 = 1$ N/m, $k_2 = 0.1$ N/m, $m_1 = 1$ kg, $m_2 = 0.1$ kg 9

Figure 2.3. Lumped parameter model of level-type isolator [31] 10

Figure 2.4. Transmissibility & phase angle plot of a lever-type vibration absorber [31] 12

Figure 2.5. Location of instantaneous center of zero velocity for case 1 [31] 13

Figure 2.6. Location of instantaneous center of zero velocity for case 2 [31] 13

Figure 2.7. Location of instantaneous center of zero velocity for case 3 [31] 14

Figure 2.8. Location of instantaneous center of zero velocity for case 4 [31] 14

Figure 2.9. Location of instantaneous center of zero velocity for case 5 [31] 14

Figure 2.10. Self-tuning operation 15

Figure 2.11. Flowchart of the self-tuning control algorithm 16

Figure 3.1 Lever-type self-tuning adaptive vibration absorber 17

Figure 3.2. V-shaped tuning mechanism 18

Figure 3.3. 1st mode shape at 7.4 Hz 19

Figure 3.4. 2nd mode shape at 22.5 Hz 20

Figure 3.5. Displacement of levered absorber mass 21

Figure 3.6. Amplitude of the main absorber mass 22

Figure 3.7. Equilibrium position for the initial resonance frequency (22.5 Hz)..... 22

Figure 3.8. Equilibrium position after tuning to 32 Hz 23

Figure 3.9. Equilibrium position after tuning to 20 Hz 23

Figure 3.10. Effect of friction coefficient on the displacement of the levered absorber mass during self-tuning to high and low excitation frequencies compared to the natural frequency 24

Figure 3.11. Effect of vertical spring stiffness on the displacement of the levered absorber mass during self-tuning to high and low excitation frequencies compared to the natural frequency 25

Figure 3.12. Effect of vertical damping constant on the displacement of the levered absorber mass during self-tuning to high and low excitation frequencies compared to the natural frequency 26

Figure 3.13. Effect of torsional spring stiffness on the displacement of the levered absorber mass during self-tuning to high and low excitation frequencies compared to the natural frequency 27

Figure 3.14. Effect of torsional damping constant on the displacement of the levered absorber mass during self-tuning to high and low excitation frequencies compared to the natural frequency 28

Figure 3.15. Effect of input excitation amplitude on the displacement of the levered absorber mass during self-tuning to high and low excitation frequencies compared to the natural frequency 29

Figure 3.16. Displacement of the levered absorber mass during self-tuning to high and low excitation frequencies compared to the natural frequency for the original system (blue dashed line) and modified system (red solid line). 30

Figure 3.17. Amplitude of the main absorber mass in the modified system 31

Figure 3.18. Amplitude of the main absorber mass during self-tuning to high and low excitation frequencies compared to the natural frequency for the original system (red solid line) and modified system (blue dashed line) 31

Figure 3.19. Displacement of the levered absorber mass during self-tuning to high and low excitation frequencies compared to the natural frequency for the optimized system (red dotted line), lower main damping constant value (blue dashed line), and larger main damping constant value (green solid line)..... 32

Figure 3.20. Amplitude of the main absorber mass during self-tuning to high and low excitation frequencies compared to the natural frequency for the optimized system (red dotted line), lower main damping constant value (blue dashed line), and larger main damping constant value (green solid line)..... 33

Figure 3.21. Amplitude of the main absorber mass under increasing excitation frequency..... 34

Figure 3.22. Displacement of the levered absorber mass during self-tuning to increasing excitation frequency..... 34

Figure 3.23. Amplitude of the main absorber mass under decreasing excitation frequency 35

Figure 3.24. Displacement of the levered absorber mass during self-tuning to decreasing excitation frequency 35

Figure 3.25. The self-tuning absorber system implemented on a main mass suspended by a main spring 36

Figure 3.26. Transmissibility plot for a passive dynamic vibration absorber with $k_1 = 246\ N/m$, $k_2 = 24.6\ N/m$, $m_1 = 12.3$ kg, $m_2 = 1.23$ kg, $c_1 = 0\ Ns/m$, $c_2 = 15.6\ Ns/m$ 38

Figure 3.27. Response of the self-tuning absorber system implemented on a main mass suspended by a main spring when subject to 20 Hz base-excitation. (a) Main mass amplitude, (b) Main absorber mass amplitude, (c) Lever absorber mass displacement, (d) Position of the levered mass after self-tuning to 20 Hz 42

Figure 3.28. Response of the self-tuning absorber system implemented on a main mass suspended by a main spring when subject to 22.5 Hz base-excitation. (a) Main mass amplitude, (b) Main absorber mass amplitude, (c) Lever absorber mass displacement, (d) Position of the levered mass after self-tuning to 22.5 Hz 44

Figure 3.29. Response of the self-tuning absorber system implemented on a main mass suspended by a main spring when subject to 25 Hz base-excitation. (a) Main mass amplitude, (b) Main absorber mass amplitude, (c) Lever absorber mass displacement, (d) Position of the levered mass after self-tuning to 25 Hz 46

Figure 3.30. Response of the self-tuning absorber system implemented on a main mass suspended by a main spring when subject to 27.5 Hz base-excitation. (a) Main mass amplitude, (b) Main absorber mass amplitude, (c) Lever absorber mass displacement, (d) Position of the levered mass after self-tuning to 27.5 Hz 48

Figure 3.31. Response of the self-tuning absorber system implemented on a main mass suspended by a main spring when subject to 30 Hz base-excitation. (a) Main mass amplitude, (b) Main absorber mass amplitude, (c) Lever absorber mass displacement, (d) Position of the levered mass after self-tuning to 30 Hz 50

Figure 3.32. Response of the self-tuning absorber system implemented on a main mass suspended by a main spring when subject to 20 Hz base-excitation. (a) Main mass amplitude, (b) Main absorber mass amplitude, (c) Lever absorber mass displacement 52

Figure 3.33. Response of the self-tuning absorber system implemented on a main mass suspended by a main spring when subject to 22.5 Hz base-excitation. (a) Main mass amplitude, (b) Main absorber mass amplitude, (c) Lever absorber mass displacement 53

Figure 3.34. Response of the self-tuning absorber system implemented on a main mass suspended by a main spring when subject to 25 Hz base-excitation. (a) Main mass amplitude, (b) Main absorber mass amplitude, (c) Lever absorber mass displacement 54

Figure 3.35. Response of the self-tuning absorber system implemented on a main mass suspended by a main spring when subject to 27.5 Hz base-excitation. (a) Main mass amplitude, (b) Main absorber mass amplitude, (c) Lever absorber mass displacement 55

Figure 3.36. Response of the self-tuning absorber system implemented on a main mass suspended by a main spring when subject to 30 Hz base-excitation. (a) Main mass amplitude, (b) Main absorber mass amplitude, (c) Lever absorber mass displacement 56

Figure 3.37. The passive dynamic vibration absorber system 57

Figure 3.38. Transmissibility plot for a passive dynamic vibration absorber with $k_1 = 246\ N/m$, $k_2 = 24.6\ N/m$, $m_1 = 12.3$ kg, $m_2 = 1.23$ kg, $c_1 = 0\ Ns/m$, $c_2 = 3.9\ Ns/m$ 58

Figure 3.39. Main mass amplitude of the dynamic vibration absorber system when subject to 0.1 mm base-excitation at different frequencies (a) 20 Hz, (b) 22.5 Hz, (c) 25 Hz, (d) 27.5 Hz, (e) 30 Hz 60

Figure 3.40. Amplitude of the main mass under changing excitation frequency 62

Figure 3.41. Amplitude of the main absorber mass under changing excitation frequency 62

Figure 3.42. Displacement of the levered absorber mass during self-tuning to changing excitation frequency 62

Figure 3.43. Original system with 160 mm hinge spacing 63

Figure 3.44. New system with 60 mm hinge spacing 63

Figure 3.45. Displacement of levered absorber mass for the system with modified hinge spacing 64

Figure 3.46. Amplitude of the main absorber mass for the system with modified hinge spacing 64

LIST OF TABLES

Table 3.1. Parameter values of the model 17

Table 3.2. Stiffness and damping values in the V-shaped self-tuning mechanism ... 19

Table 3.3. Contact parameters between the wings and the lever 19

Table 3.4. Parameter modifications to minimize self-tuning time 30

Table 3.5. Steady state amplitude of the main mass for various excitation frequencies for 0.1 mm input amplitude 63

LIST OF SYMBOLS

A	Amplitude
c	Main damping constant
c_1	Damping constant between m_1 and base
c_2	Damping constant between m_1 and m_2
c_t	Torsional damping constant
c_v	Vertical damping constant
F_1	Force towards left
F_2	Force towards right
F_{net}	Net force
k_1	Spring stiffness between m_1 and base
k_2	Spring stiffness between m_1 and m_2
k	Main spring stiffness
k_t	Torsional spring stiffness
k_v	Vertical spring stiffness
l_1	Length of lever
l_2	Hinge spacing
m_1	Mass connected to the base via k_1 and c_1
m_2	Mass connected to m_1 via k_2 and c_2
m	Main absorber mass
m_{is}	Levered absorber mass
t	Time
T	Kinetic energy
$Tr(\omega)$	Transmissibility
V_1	Left velocity
V_2	Right velocity
V	Potential energy
x_1	Displacement of m_1
x_2	Displacement of m_2

X_1	Amplitude of m_1 motion
X_2	Amplitude of m_2 motion
y	Displacement of the base
Y	Amplitude of base excitation
α	Lever ratio
θ	Lever angle
μ	Mass ratio
π	Pi constant
$\emptyset$	Phase angle
ω	Excitation frequency
ω_0	Natural frequency
ω_p	Resonance frequency
ω_z	Anti-Resonance frequency

LIST OF ABBREVIATIONS

2DOF	Two degree of freedom
ATVA	Adaptive tuned vibration absorbers
DAVI	Dynamic anti-resonant vibration isolator
DOF	Degree of freedom
DVA	Dynamic vibration absorber
MRE	Magnetorheological
SDOF	Single degree of freedom
SMA	Shape memory alloys
TVA	Tuned vibration absorber

1. INTRODUCTION

1.1. Objective & Motivation of Study

Vibration is an important topic for many industries such as automotive, aerospace, defense and consumer goods. Crucial problems in machines are often caused by vibrations. Vibrations are directly related to the life span of machinery and unwanted vibrations may cause negative impacts and failures. These failures may happen in all types of systems where machines are involved and can cause traumatic incidents. Therefore, machines should be designed accordingly and vibration control of machines is vital.

Every machine generates vibrations and have a set of natural frequencies. Unwanted responses with high amplitudes may occur when the excitation frequencies match these natural frequencies. Consequently, the systems may fail. Studies have been conducted to solve these problems, however some solutions involve expensive design changes. Vibration absorber systems offer a cost effective solution. However, if the excitation frequency varies, passive vibration absorbers become ineffective. In order to adapt to varying excitation conditions, active or adaptive (semi-active) systems are used. These kind of systems generally require electronic sensors, actuators, control circuitry and external electrical energy for the tuning process. There are some studies on self-tuning passive torsional vibration absorbers. However, to the author's knowledge, there is no study on passive, mechanical self-powered and self-tuning translational vibration absorbers.

In this thesis, the aim is to design a self-tuning and self-powered vibration absorber system. The input vibration energy is aimed to power the tuning subsystem. Hence, there will not be any electronic sensor or actuator and the system is expected to function without an outside electrical source.

First, the design will be described and the mathematical formulations will be given. Then, multi-body dynamic simulations will be done using MSC ADAMS software. Consequently, comparative results will be shown.

1.2. Literature Review

Vibration can be controlled or suppressed by the usage of vibration absorbers. The frequency of a system can change by time especially when the system is in a dynamic environment, and these systems may or may not adapt to these conditions depending on their design. Vibration absorbers can be classified into three types; passive, active and semi-active (adaptive) vibration absorbers.

Vibration suppression can simply be made by passive absorber usage. In this method no external control, sensor or actuator is used, hence it is a cheap and basic method. However, the frequency range, which the system works, can be quite narrow. Moreover, in the cases where excitation frequency differs from the tuned values, resonance may occur for the overall system.

Vibration suppression with the usage of active absorbers is achieved by detecting the frequencies of the system using sensors, and actuators are utilized to counteract the movements. Unlike passive systems, active systems can work in a wider range of frequency. However, actuator, sensor and control circuitry usage make the systems complex, hence it is not very practical. Besides, external energy is required for active control.

Adaptive vibration absorption has common parts with active and passive systems. Similar to passive systems, vibrating subsystem does not require external electrical energy input for its operation. On the other hand, similar to active systems certain measurement devices are used in order to tune the system for the changing frequencies.

This thesis focuses on adaptive vibration absorbers. There are various adaptive vibration absorber designs in the literature. However, these systems generally require electronic sensors, actuators, control circuitry or external electrical energy for the tuning process.

Shape memory alloys (SMA), with their variable material properties, suggest a good adaptive mechanism. Heating an SMA causes a change in the elastic modulus of the material. Several studies have been conducted using this method [1-5].

Williams et al. show an adaptive tuned vibration absorber (ATVA) using spring elements composed of three pairs of SMA wires and one pair of steel wires was constructed and tested. On-off actuation of the SMA elements created an ATVA with four discrete tuned frequencies. Characterization testing of the absorber showed variation of the natural frequency of the ATVA of approximately 15%. The ATVA was applied to a primary system and the frequency response of the system at various states of ATVA actuation was determined. Manual tuning of the ATVA actuation during a stepped-sine base excitation of the primary system showed a wider notch of attenuation than was possible with a non-adaptive absorber. Results of the tests indicate that an adaptive absorber incorporating SMA as a tuning element has potential as a simple, high-performance adaptive-passive technique for vibration control [1].

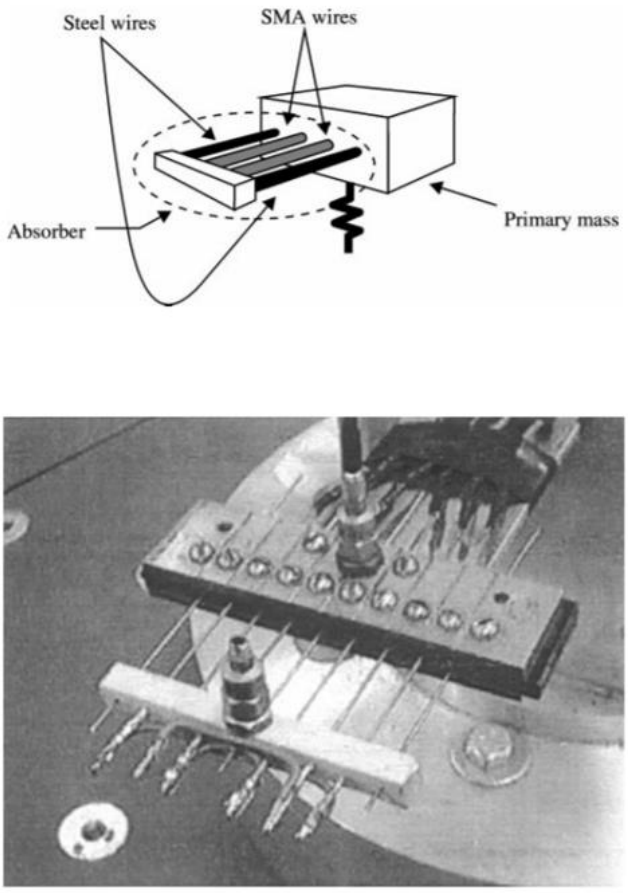


Figure 1.1. SMA based ATVA [1].

In terms of absorbing low frequency disturbances and other challenging environments negative stiffness subsystems are very effective. Vibration suppression in this method is accomplished by using an arrangement of springs and negative-stiffness mechanism. This method has been used in various studies [6-10].

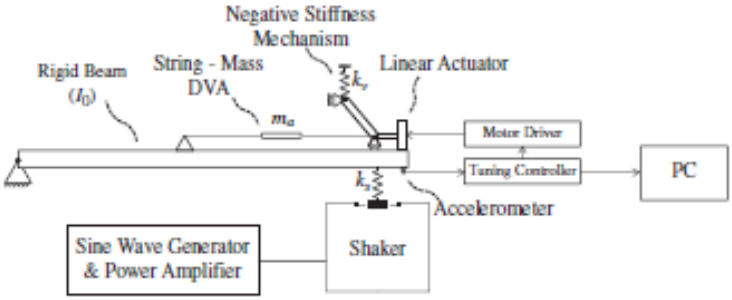


Figure 1.2. Negative stiffness mechanism [6].

Magnetorheological materials have a variable resistance for shear due to the magnetic field applied on them. The changes in the material properties of these smart materials can be used to create a variable stiffness element for an absorption system [11-15]. In the research of Hoang et al., a magnetorheological elastomer has been used in an ATVA system for a vehicular powertrain transient vibration reduction [11]. In the study of Hirunyapruk et al., magnetorheological fluid has been used to change the stiffness and tune vibration. The shear stiffness of the fluid is adjusted by varying the magnetic field by changing the current supplied by electromagnets [13]. Electromagnets were acting as the active mass of the absorber and were designed to provide the required magnetic field to alter the stiffness of the MRE layers in Rasooli et al. [16].

Other than negative stiffness elements, variable stiffness springs can be used to achieve vibration absorption or isolation. These variable stiffness springs allow the system to adapt to the changing operating conditions [17-21]. In the work of Cronje et al., a variable stiffness system was designed using leaf springs and a wax actuator. By heating the wax, the effective stiffness of the system can be changed [19]. Moreover, other than springs, non-uniform structures with variable stiffness properties such as composite or cantilever beams

can be used for the same purpose [22]. In the studies of Bonello et al., system where the stiffness is varied by adjusting the curvature of the beam was proposed [23].

Helical spring were used as the tunable stiffness element in the study conducted by Franchek et al. [24]. Patents were granted for similar system designs using springs [25, 26].

Mass is used as another control parameter for vibration suppression. In the studies of Almashhor and Asiri, absorber mass takes the shape of a tank filled with fluid and by varying the amount of fluid inside the tank, the mass is adjusted in order to create a tunable system [27].

Other applications can be seen in the automotive industry. Torsional vibration absorption can be achieved using pendulum type absorbers on crankshafts [28, 29]. Pendulum type vibration absorbers can be tuned to specific engine orders. Resonance frequency adapts to the motor speed; therefore, a fully mechanical self-tuning operation is obtained.

In the work of Shen et al., an amplifying mechanism and a grounded stiffness element are introduced into a grounded DVA; which improved the low-frequency control performance of the DVA, by changing the mass ratio and magnification ratio for three case: the optimum grounded stiffness ratio, i.e., negative, zero and positive [30].

When the literature is investigated, it is seen that there is no work on adaptive self-tuning and self-powered lever-type vibration absorbers that are fully mechanical (no use of electronic sensors, controllers or actuators). In this study, an adaptive lever-type vibration absorber, which employs mechanical means to tune itself with no external electrical energy is developed. To achieve self-sensing actuation with vibratory energy, a vibro-impact actuator is utilized.

1.3. Overview of The Thesis

The first chapter of this thesis consists of a brief introduction to the subject, objective & motivation summary. Literature search with critical topics/methods are highlighted.

The second chapter is where the analytical equations are shown and the self-tuning algorithm is developed. The control algorithm logic is explained in a flow-chart.

In the third chapter, numerical model is formed and calculations are verified. Optimization studies are carried out to minimize tuning time and to obtain a robust system. Tracking performance of the system is tested by changing the excitation frequency. Moreover, implementation of the self-tuning mechanism and tracking control of the new system in changing frequency conditions are also tested. Finally, working frequency range of the system is increased by modifying the system dimensions.

Lastly, on the fourth chapter the results are summarized and discussed. In addition, possible future work studies are suggested.

2. DEVELOPMENT OF THE SELF-TUNING ALGORITHM

Vibration, also known as oscillation can be defined as a periodic movement of an elastic body or medium in alternately opposite direction from the position of equilibrium when an excitation is applied. Vibration can be investigated in time or frequency domains and the simplest form of vibration is sinusoidal or harmonic.

In this thesis, harmonic input will be given to a base-excited system. The system is expected to tune to a fixed excitation frequency. It should also track a varying excitation frequency.

2.1. Dynamic Vibration Absorbers

Figure below shows an undamped passive dynamic vibration absorber subject to base excitation. Displacement functions of the relevant areas are given over the figure.

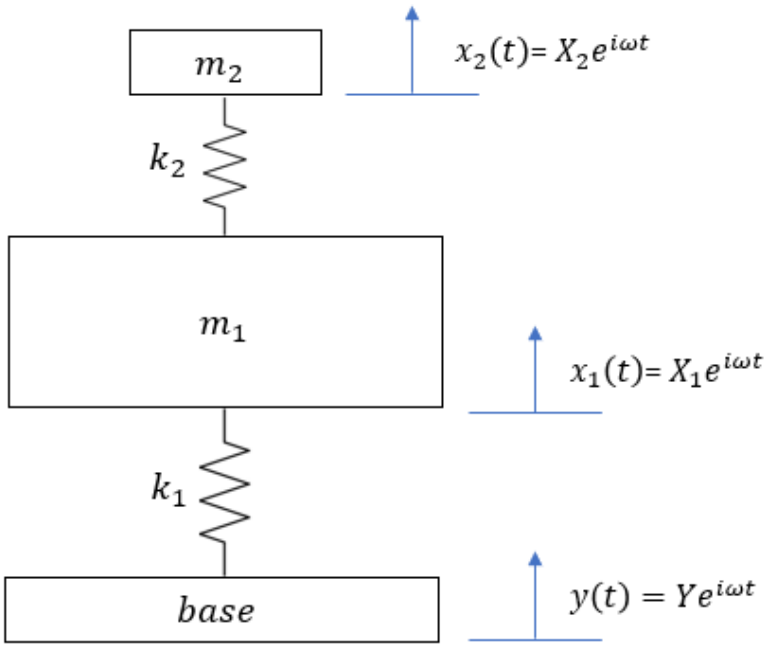


Figure 2.1. Dynamic vibration absorber subject to base excitation.

The equations of motion of the system can be seen as:

$$\begin{bmatrix} m_1 & 0 \\ 0 & m_2 \end{bmatrix} \begin{bmatrix} \ddot{x}_1 \\ \ddot{x}_2 \end{bmatrix} + \begin{bmatrix} k_1 + k_2 & -k_2 \\ -k_2 & k_2 \end{bmatrix} \begin{bmatrix} x_1 \\ x_2 \end{bmatrix} = \begin{bmatrix} k_1 y \\ 0 \end{bmatrix}. \tag{2.1}$$

Assuming harmonic base excitation as:

$$y(t) = Y e^{i\omega t}, \tag{2.2}$$

$x_1(t)$ and $x_2(t)$ can be obtained as follows:

$$x_1(t) = X_1 e^{i\omega t}, \tag{2.3}$$

$$x_2(t) = X_2 e^{i\omega t}. \tag{2.4}$$

Then, equation of motion (Equation 2.1) can be rewritten as

$$A \begin{bmatrix} X_1 \\ X_2 \end{bmatrix} e^{i\omega t} = \begin{bmatrix} k_1 Y \\ 0 \end{bmatrix} e^{i\omega t}, \tag{2.5}$$

where A is given as

$$A = \begin{bmatrix} (k_1 + k_2 - \omega^2 m_1) & -k_2 \\ -k_2 & (k_2 - \omega^2 m_2) \end{bmatrix}. \tag{2.6}$$

Then, the displacement amplitudes of $x_1(t)$ and $x_2(t)$ can be found as

$$\begin{bmatrix} X_1 \\ X_2 \end{bmatrix} = A^{-1} \begin{bmatrix} k_1 \\ 0 \end{bmatrix} Y. \tag{2.7}$$

Equation (2.7) can be rearranged to obtain the transmissibilities ($\frac{X_1}{Y}$ and $\frac{X_2}{Y}$) as

$$\begin{bmatrix} X_1/Y \\ X_2/Y \end{bmatrix} = A^{-1} \begin{bmatrix} k_1 \\ 0 \end{bmatrix}. \tag{2.8}$$

The main mass is m_1, so $\frac{X_1}{Y}$ is investigated. When Equation (2.6) is used in Equation (2.8), $\frac{X_1}{Y}$ can be obtained as:

$$\left|\frac{X_1}{Y}\right| = \left|\frac{(k_2 - \omega^2 m_2) k_1}{(k_1 + k_2 - \omega^2 m_1)(k_2 - \omega^2 m_2) - {k_2}^2}\right|. \tag{2.9}$$

Moreover, the numerator of Equation (2.9) becomes zero at the antiresonance frequency:

$$\omega_z = \sqrt{\frac{k_2}{m_2}}. \tag{2.10}$$

By tuning ω_z to the excitation frequency, transmissibility can be reduced to zero. At the antiresonance condition, the following equation holds:

$$k_1 Y = -k_2 X_2. \tag{2.11}$$

According to Equation (2.11), the net force on m_1 in Figure 2.1 is zero. Hence, it remains stationary. As an example, the following parameters are used in Equation (2.9):

$$k_1 = 1 \text{ N/m},$$

$$k_2 = 0.1 \text{ N/m},$$

$$m_1 = 1 \text{ kg},$$

$$m_2 = 0.1 \text{ kg}.$$

Figure 2.2 shows the transmissibility plot for the mass m_1. Notice that the antiresonance notch is very narrow. Hence, transmissibility is close to zero around the close vicinity of the antiresonance frequency. Moreover, the isolation frequency range in which transmissibility is less than 1 is between 0.957-1.049 rad/s. In order to achieve a wider bandwidth around the antiresonance frequency, antiresonance can be generated with a levered-mass.

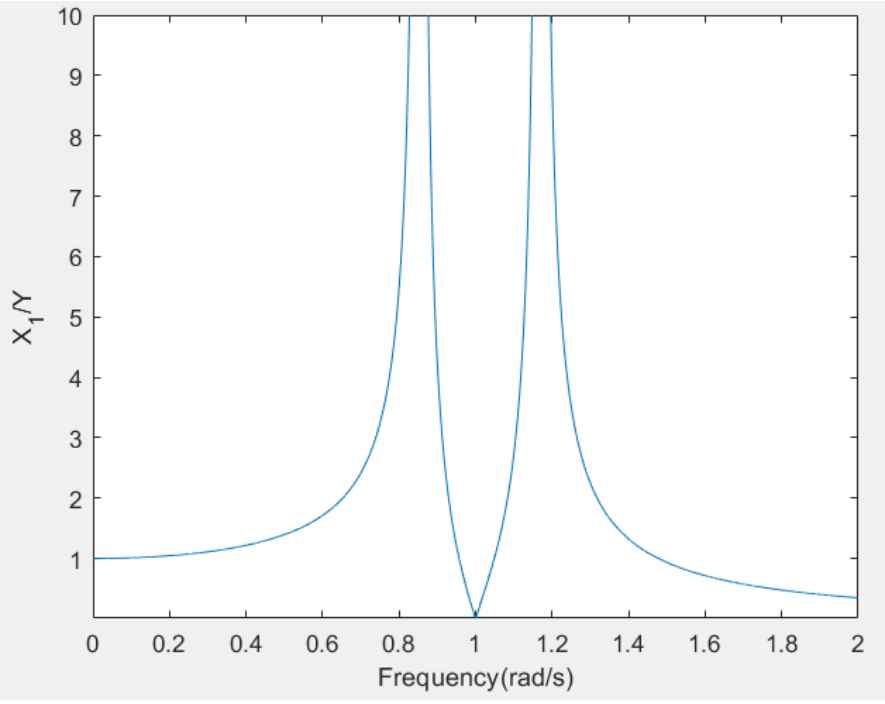


Figure 2.2. Transmissibility plot for a dynamic vibration absorber with $k_1 = 1$ N/m, $k_2 = 0.1$ N/m, $m_1 = 1$ kg, $m_2 = 0.1$ kg.

2.2. Dynamic Anti-Resonant Vibration Isolator

Dynamic anti-resonant vibration isolators (DAVI) can be classified by the position of the isolator's center of gravity with respect to the hinges attached to the base and the payload mass. It is shown that "Type II" lever-type DAVI offers the widest antiresonance notch compared to "Type I" DAVI or dynamic vibration absorber. The lever and isolator mass of these systems add a zero in the frequency spectrum; however, since the lever is connected to the base and the payload at the same time, the number of DOF does not change. In other words, while a dynamic vibration absorber is 2DOF, a dynamic anti-resonant vibration isolator is SDOF. The movement of the lever in the isolator is planar with translation and rotation. This type of planar motion of a rigid body is described as a rotation about an instantaneous center of zero velocity. At the frequency of maximum isolation, the instantaneous center of velocity coincides with hinge attached to the payload mass. Hence, the payload remains stationary. Moreover, at resonance, the instantaneous center of velocity coincides with the hinge attached to the base. Hence, this situation describes perfect tuning to the excitation frequency.

In this thesis, the lever-type isolator [31] will be used as a resonator so that when it is attached on an excitation source or vibrating mass, it can act like a dynamic vibration absorber. Thus, the payload mass will act like the main absorber mass. Moreover, the levered mass will also move coupled to the main absorber mass, so it also affects the resonance frequency of the system. In fact, as the lever ratio changes, the effective mass of the absorber system will vary which in turn will vary the resonance frequency.

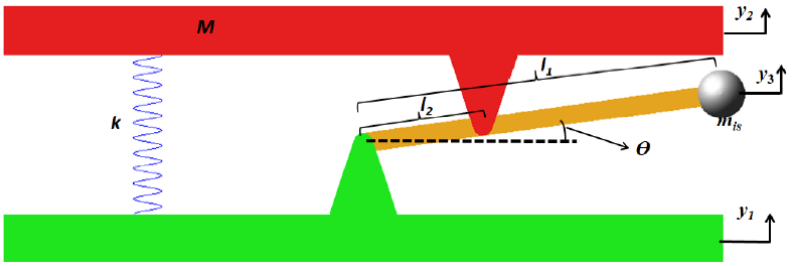


Figure 2.3. Lumped parameter model of the level-type isolator [31].

In Figure 2.3, the length of the lever is l_1, the hinge spacing is l_2, the angle between the horizontal line and lever is θ and the displacements of the base, main absorber mass, lever tip are denoted as y_1, y_2, y_3, respectively. When the base is excited by a sinusoidal displacement and θ is small, y_3 is obtained in terms of other displacements:

$$y_3 = \alpha y_2 - (\alpha - 1)y_1, \tag{2.12}$$

where

$$\alpha = \frac{l_1}{l_2} > 1. \tag{2.13}$$

From Equation (2.13), the kinetic (T) and potential energy (V) equations can be obtained as:

$$T = \frac{1}{2}M\dot{y}_2^2 + \frac{1}{2}m_{is}[\alpha y_2 - (\alpha - 1)y_1]^2, \tag{2.14}$$

$$V = \frac{1}{2}k(y_2 - y_1)^2. \tag{2.15}$$

The Lagrange equation is given below:

$$\frac{d}{dt}\left(\frac{\delta T}{\delta \dot{y}_2}\right) - \frac{\delta T}{\delta y_2} + \frac{\delta V}{\delta y_2} = 0. \tag{2.16}$$

Substituting equations (2.14) and (2.15) into the Lagrange equation, the equation of motion can be obtained as:

$$(1 + \mu\alpha^2)\ddot{y}_2 + \omega_0^2 y_2 = \mu(\alpha^2 - \alpha)\ddot{y}_1 + \omega_0^2 y_1, \tag{2.17}$$

where

$$\mu = \frac{m_{is}}{M}, \tag{2.18}$$

$$\omega_0 = \sqrt{\frac{k}{M}}. \tag{2.19}$$

For a periodic input to the system in the form of $y_1(t) = Y_1 e^{i\omega t}$, a periodic solution of the form $y_2(t) = Y_2 e^{i\omega t}$ can be assumed, hence:

$$[\omega_0^2 - \omega^2(1 + \mu\alpha^2)]Y_2 = [\omega_0^2 - \omega^2\mu(\alpha^2 - \alpha)]Y_1. \tag{2.20}$$

From the above equations, the resonance frequency can be obtained as below:

$$\omega_p = \omega_0\sqrt{\frac{1}{(1+\mu\alpha^2)}}. \tag{2.21}$$

The anti-resonance frequency is:

$$\omega_z = \omega_0 \sqrt{\frac{1}{\mu\alpha(\alpha-1)}}. \tag{2.22}$$

The transmissibility can be obtained by using equations (2.21) and (2.22):

$$Tr(\omega) = \frac{Y_2}{Y_1} = \frac{(1-\frac{\omega^2}{\omega_z^2})}{(1-\frac{\omega^2}{\omega_p^2})}. \tag{2.23}$$

The phase angle is:

$$\emptyset = \begin{cases} 0, & \omega < \omega_p \\ \pi, & \omega_p < \omega < \omega_z \\ 0, & \omega_z < \omega. \end{cases} \tag{2.24}$$

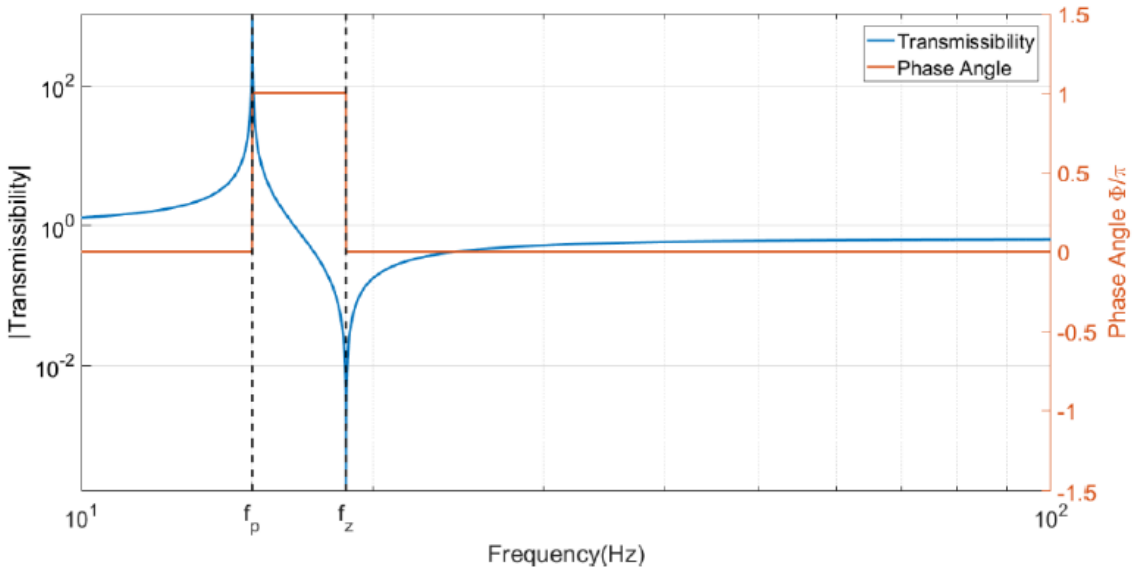


Figure 2.4. Transmissibility & phase angle plot of a lever-type vibration absorber [31].

2.3. Development of the Self-Tuning Algorithm

Figure 2.4 highlights 5 conditions given below:

1. $\omega < \omega_p < \omega_z$: $\emptyset = 0$, $|Y_2| > |Y_1|$, base and main mass move in-phase
2. $\omega = \omega_p < \omega_z$: At the resonance frequency, $Y_2 \to \infty$

3. $\omega_p < \omega < \omega_z$: $\emptyset = \pi$, base and main mass move out-of-phase
4. $\omega_p < \omega = \omega_z$: At the anti-resonance frequency, $Y_2 = 0$
5. $\omega_p < \omega_z < \omega$: $\emptyset = 0$, $|Y_1| > |Y_2|$, base and main mass move in-phase

When the excitation amplitude and frequency values are given, their amplitudes and phases are known by the equations given above. The ratio of the velocity of the main mass hinge and base hinge, as well as the ratio of their displacement and acceleration, is a function of excitation frequency and can also be obtained by the equations given previously (transmissibility and phase angle). Consequently, for the five cases above mentioned, the instantaneous center of zero velocity positions can be described schematically as:



Figure 2.5. Location of instantaneous center of zero velocity for case 1 [31].

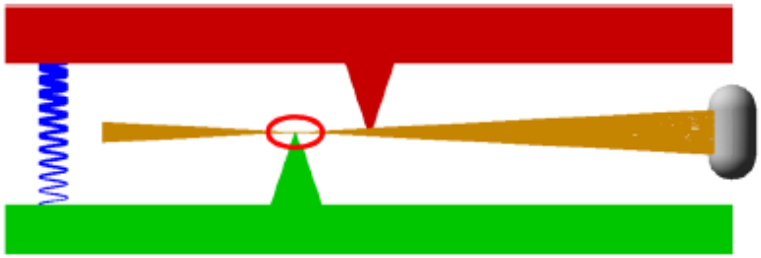


Figure 2.6. Location of instantaneous center of zero velocity for case 2 [31].

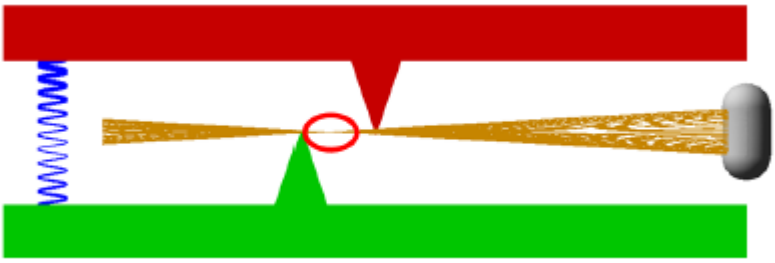


Figure 2.7. Location of instantaneous center of zero velocity for case 3 [31].



Figure 2.8. Location of instantaneous center of zero velocity for case 4 [31].

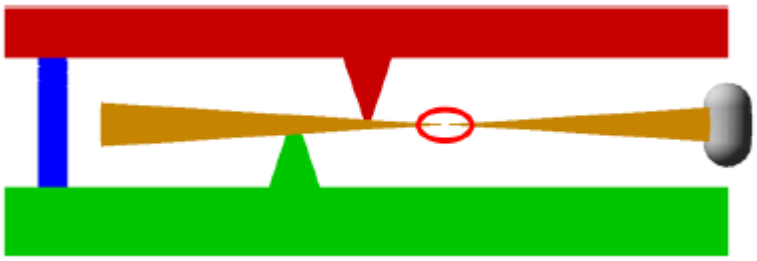


Figure 2.9. Location of instantaneous center of zero velocity for case 5 [31].

The derivations and the model structure is based on Figure (2.8) in which tuning to anti-resonance condition (case 4) was successfully accomplished. In our system resonance tuning will be aimed so that it can be used as a self-tuning resonator/absorber. Therefore, the tuning system will be modified.

In this thesis, the input excitation will cause impact forces around the base hinge, creating right and left forces on the lever (see Figure 2.10). These forces will be proportional to the impact velocities at two equidistant points around the base hinge. When these two forces are equal, the lever will not move in any direction, thus the system will converge into case 2 (Figure 2.6). If the two forces are not equal, then the lever will move along the net

force direction and eventually converge to case 2. So, if there is constant base excitation frequency, the system will tune to that excitation frequency. Moreover, if the excitation frequency changes, the system will track the changing excitation frequency. This will be achieved purely by mechanical means without using electronic circuits, sensors, actuators or electrical power.

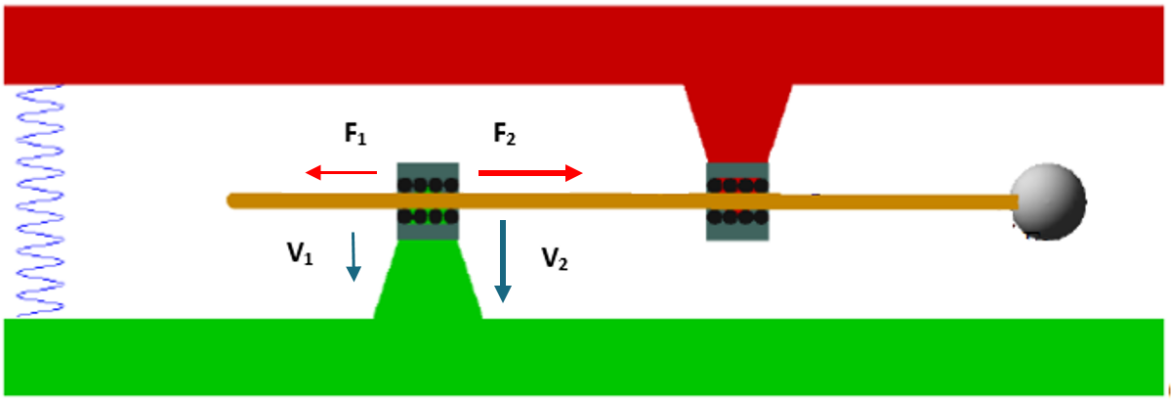


Figure 2.10. Self-tuning operation. Here, instantaneous center of velocity is assumed to be on the left of the base hinge, hence F_2 is larger than F_1 and the lever is pushed to the right.

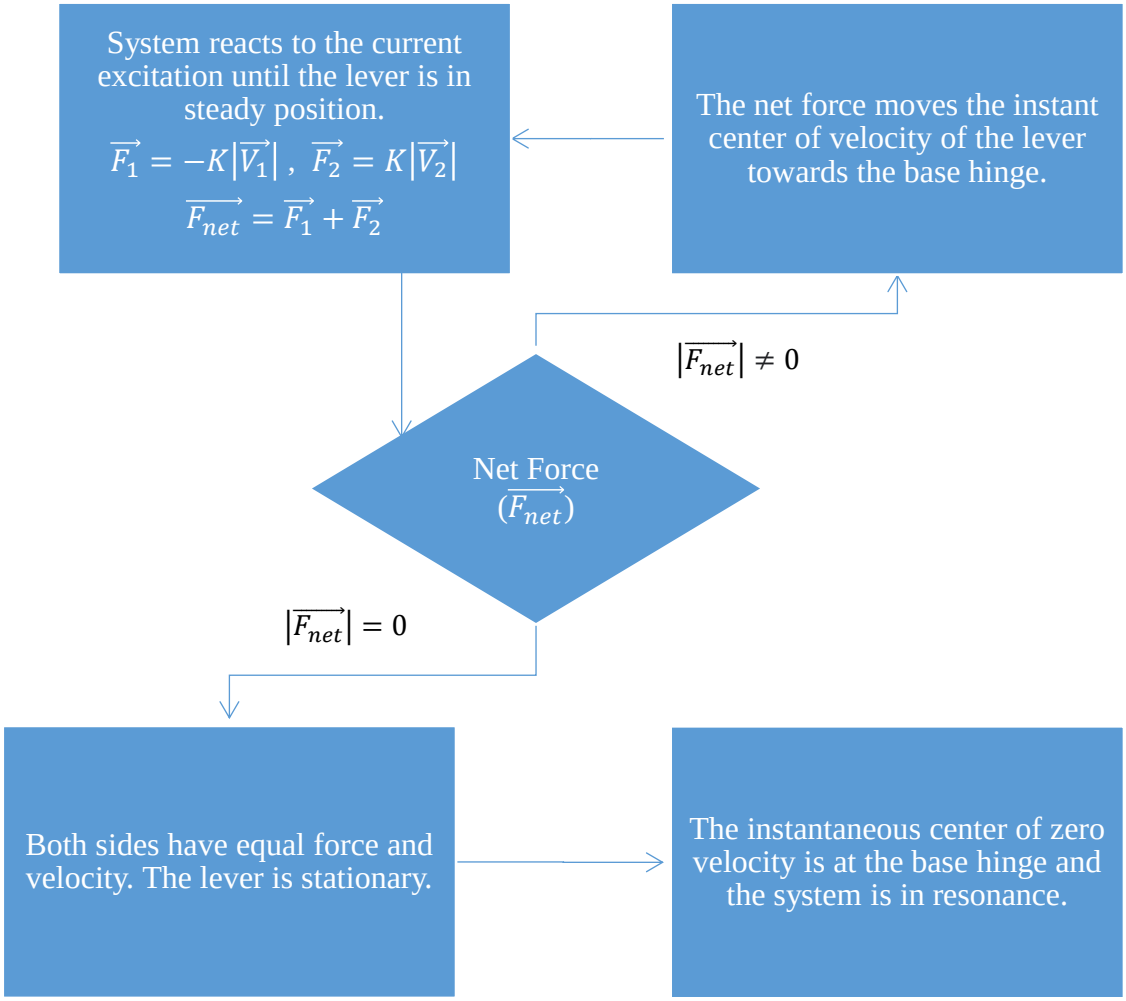


Figure 2.11. Flowchart of the self-tuning algorithm.

3. NUMERICAL VERIFICATION

3.1. Lever-Type Self-Tuning Adaptive Vibration Absorber Model

Model of the lever-type self-tuning adaptive vibration absorber is created using MSC ADAMS software and depicted in Figure 3.1. This base-excited system is aimed to tune to resonance condition so that it can absorb the vibrations coming from the base.

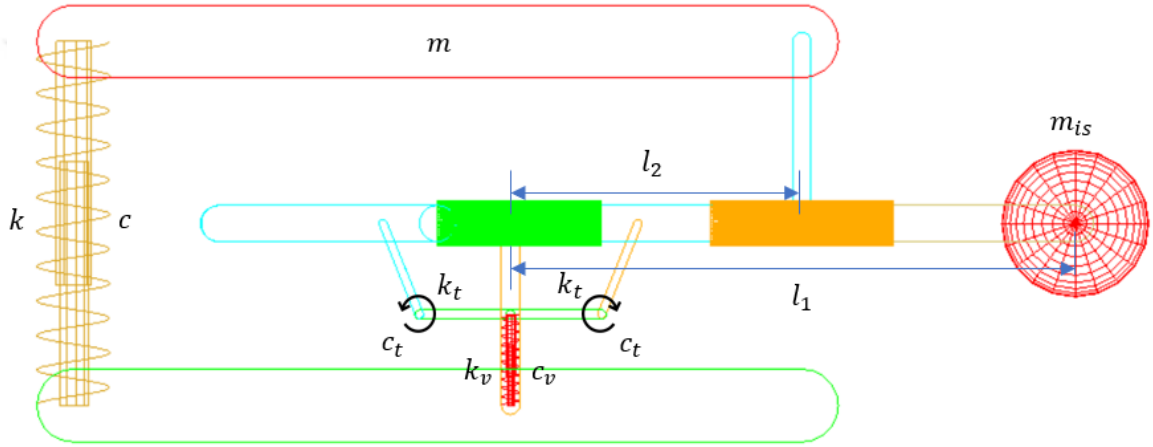


Figure 3.1. Lever-type self-tuning adaptive vibration absorber.

The base-excited system is SDOF, hence the levered absorber mass m_{is} and the main absorber mass m have coupled motion. As the lever ratio changes by changing l_1, the resonance frequency of the system can be changed. Parameters of the system are selected similar to the ones in the previous studies. (see Table 3.1).

Table 3.1. Parameter values of the model.

Main absorber mass (m)	0.93 kg
Levered absorber mass (m_{is})	0.3 kg
Main spring stiffness	44 N/mm
Main damping constant	0.028 N-sec/mm
Distance between base hinge & end mass (l_1)	310 mm
Distance between two hinges (l_2)	160 mm

The model includes a base part which can translate vertically with respect to the ground. The base part is connected to the main absorber mass on the top via a spring. The main absorber mass is constrained to move in the vertical direction.

Two vertical links are attached to each of these top and bottom parts with hollow cylinders connected to the other end with revolute joints. A lever is placed inside these hollow cylinders so that it can rotate about the revolute joints and translate along the axes of the hollow cylinders. A mass is attached to the tip of the lever so that its effective inertia can be changed by translating the lever with respect to the hollow cylinders.

The most critical component which creates the self-tuning effect is a V-shaped mechanism that consists of a base and two wings. This mechanism is supported by a vertical spring. The wings hit the lever at two different points and the lever moves with the effect of the tangential component of the reaction forces. The wings are connected to the base with revolute joints and torsional springs that provide stiffness and damping. The stiffness and damping values for the torsional (k_t, c_t) and vertical (k_v, c_v) springs are given in the following table. Similarly, contact properties which are defined between the wings and the lever are show in the following table.

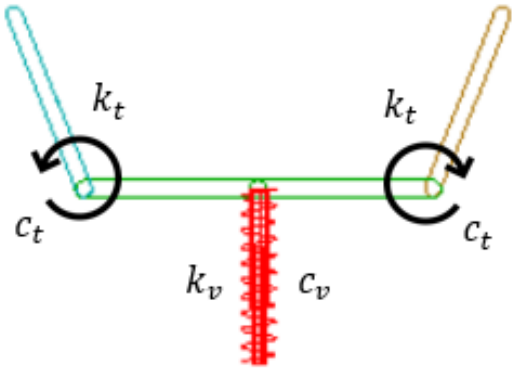


Figure 3.2. V-shaped tuning mechanism.

Table 3.2. Stiffness and damping values in the V-shaped self-tuning mechanism.

	Stiffness	**Damping**
Torsional Springs	100 [N-mm/deg]	1 [N-mm-sec/deg]
Vertical Spring	0.3 [N/mm]	5 x 10^{-6} [N-sec/mm]

Table 3.3. Contact parameters between the wings and the lever.

Contact Stiffness	1 N/mm
Force Exponent	2.2
Damping	0.1 N-sec/mm
Penetration Depth	1 mm
Static Friction Coefficient	0.8
Dynamic Friction Coefficient	0.8

The natural frequencies of this initial model for different modes are 7.4 Hz and 22.5 Hz. The mode shapes can be seen in Figure 3.3 and Figure 3.4.

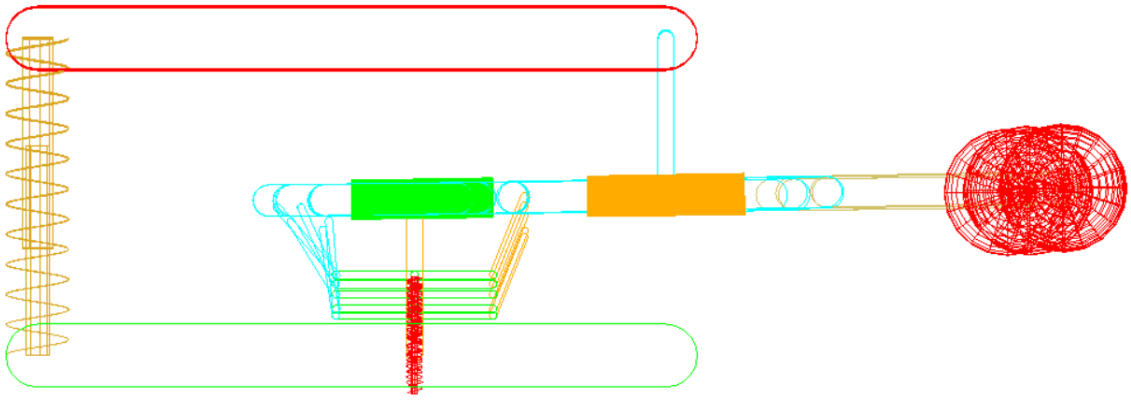


Figure 3.3. 1st mode shape at 7.4 Hz.

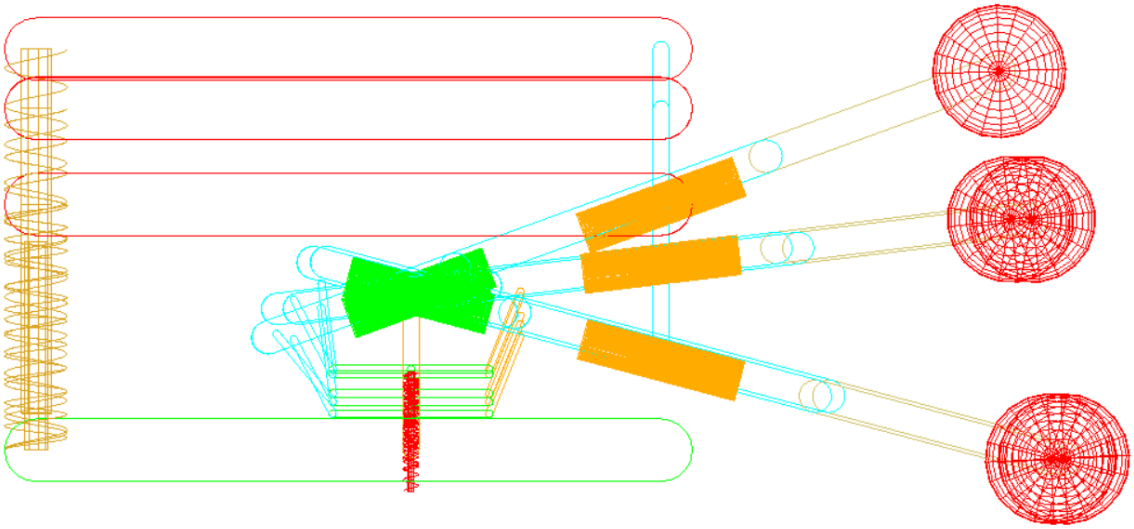


Figure 3.4. 2nd mode shape at 22.5 Hz.

The system can be harmonically excited from the base with a single frequency and the system is expected to tune to this frequency with the help of the self-tuning mechanism. The excitation frequency (ω) can be below or above initial natural frequency of the system. Once tuning is accomplished the natural frequency will be at the excitation frequency and the system will be in resonance condition. The excitations will be expressed as:

$$A\sin(\omega t). \tag{3.1}$$

In Equation (3.1), A is the amplitude and for very small amplitudes, the tuning time can be very large and for large amplitudes the system can become highly nonlinear and the self-tuning action cannot be achieved. The first example is given for A = 0.4 mm. Moreover, in order to view both conditions of excitation frequency being greater and lower than the initial natural frequency (22.5 Hz = 45π rad/s), step functions are used for base excitation as:

$$0.4\big(sin(64\pi t) - STEP(t, 10, 0, 10.25, 1)\ sin(64\pi t) + STEP(t, 10.25, 0, 10.5, 1)sin(40\pi t)\big). \tag{3.2}$$

Figure 3.5 shows that the horizontal displacement of the levered mass converges to a fix value in about 5 seconds when the excitation frequency is 32 Hz. Moreover, Figure 3.6 shows that during the tuning time of the first 5 seconds the vertical vibration amplitude of the main absorber mass increases and reaches a steady state value. Notice that for 0.4 mm input, the output amplitude is 3mm, hence there is significant amplification, hence the

system is close to resonance condition. After the 10.25 seconds the excitation frequency is reduced to 20 Hz. Between 10.25 and 35 seconds, the system self-tunes to the new excitation frequency. After a small overshoot, the steady state amplitude is 2.3 mm, which is again significantly higher than the input amplitude (0.4 mm). Figure 3.7 shows initial position of the levered mass and the vibration amplitude of the main absorber mass. Figure 3.8 shows that after self-tuning to 32 Hz the levered mass displaces to the left. Moreover, Figure 3.9 shows that after self-tuning to 20 Hz the levered mass displaces to the right.

Note that the tuning time and the steady state output displacement values are different for tuning to a high and low excitation frequency compared to the initial natural frequency. The aim in this thesis is to reduce the tuning time and increase resonance amplitude.

The numerical studies are carried out in the absence of gravity. If gravity is included, the V-shaped tuning mechanism would have been subjected to vertical loads. Moreover, the main absorber mass and the levered absorber mass would also deflect due to gravity. In that case, there should be an adjustment system to adjust the equilibrium level of the system so that the two wings of the V-shaped tuning mechanism touch the lever with equal amount of forces in the absence of base-excitation.

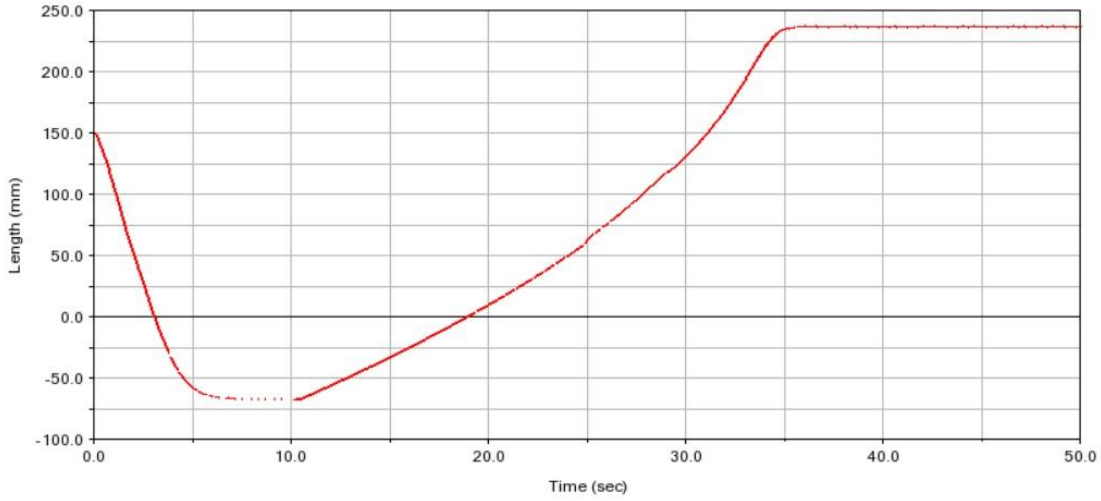


Figure 3.5. Displacement of levered absorber mass.

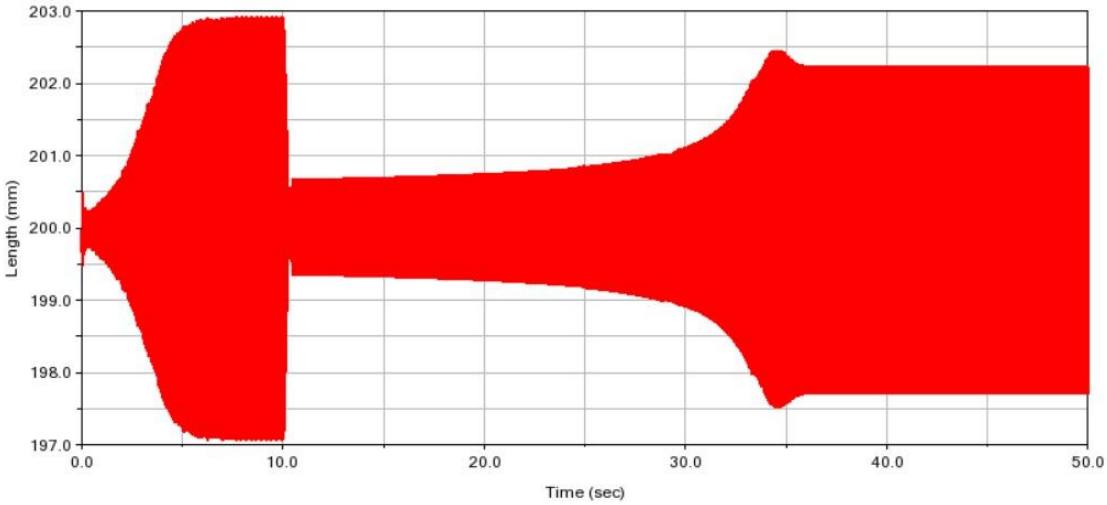


Figure 3.6. Amplitude of the main absorber mass.

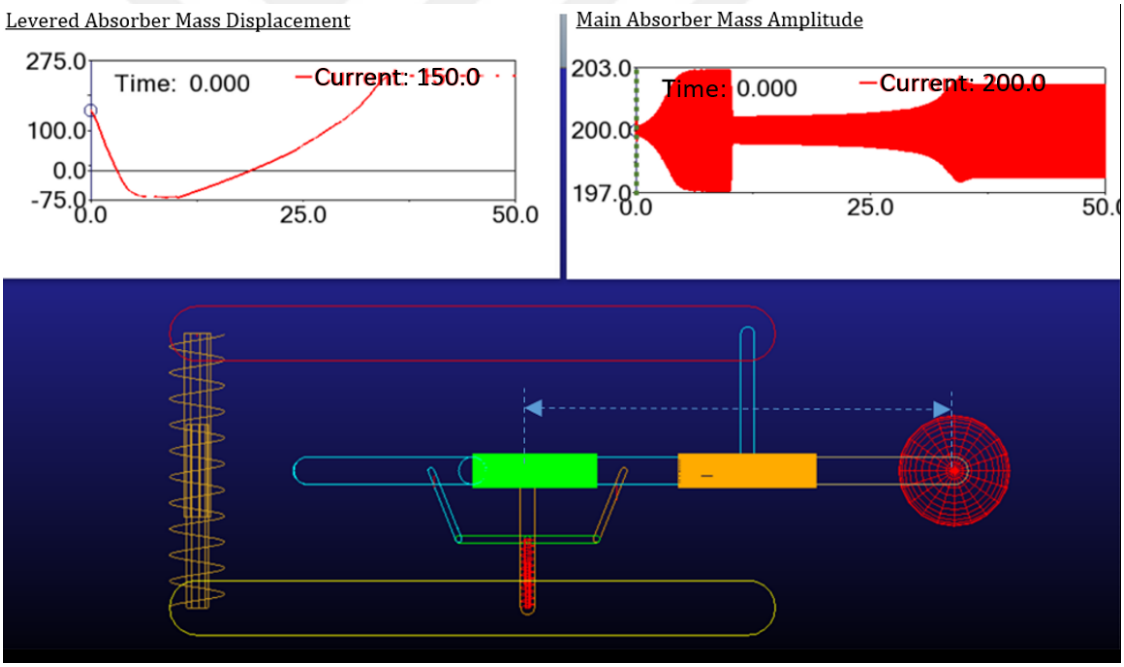


Figure 3.7. Equilibrium position for the initial resonance frequency (22.5 Hz).

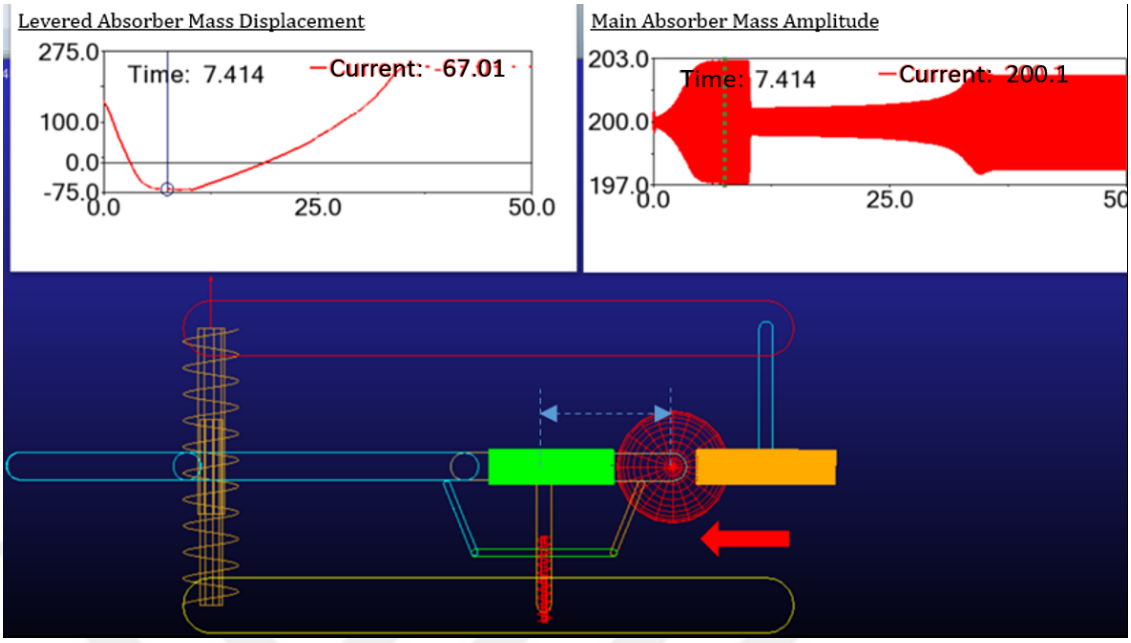


Figure 3.8. Equilibrium position after tuning to 32 Hz.

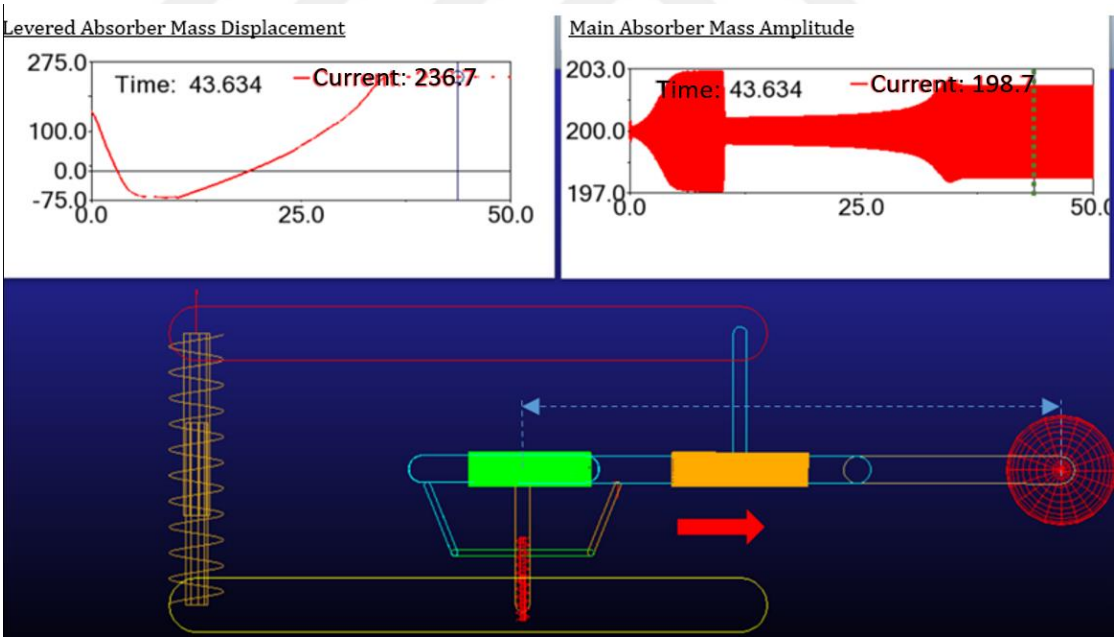


Figure 3.9. Equilibrium position after tuning to 20 Hz.

3.2. Parametric Design Studies

In order to have a more robust and faster tuning system, optimization studies are carried out. Main goal is to change certain parameters in such way that the equilibrium convergence and resonance reach durations are decreased.

Five parameters are selected, i.e., friction coefficients of the contact condition, vertical spring (under V-shaped tuning mechanism) stiffness, vertical damping constant, torsional spring (between V-shaped tuning mechanism wings & base) stiffness, torsional damping constant. Moreover, tuning convergence time is investigated for different input vibration amplitude. Each parameter is individually changed and its effect on the tuning time is compared with the original model.

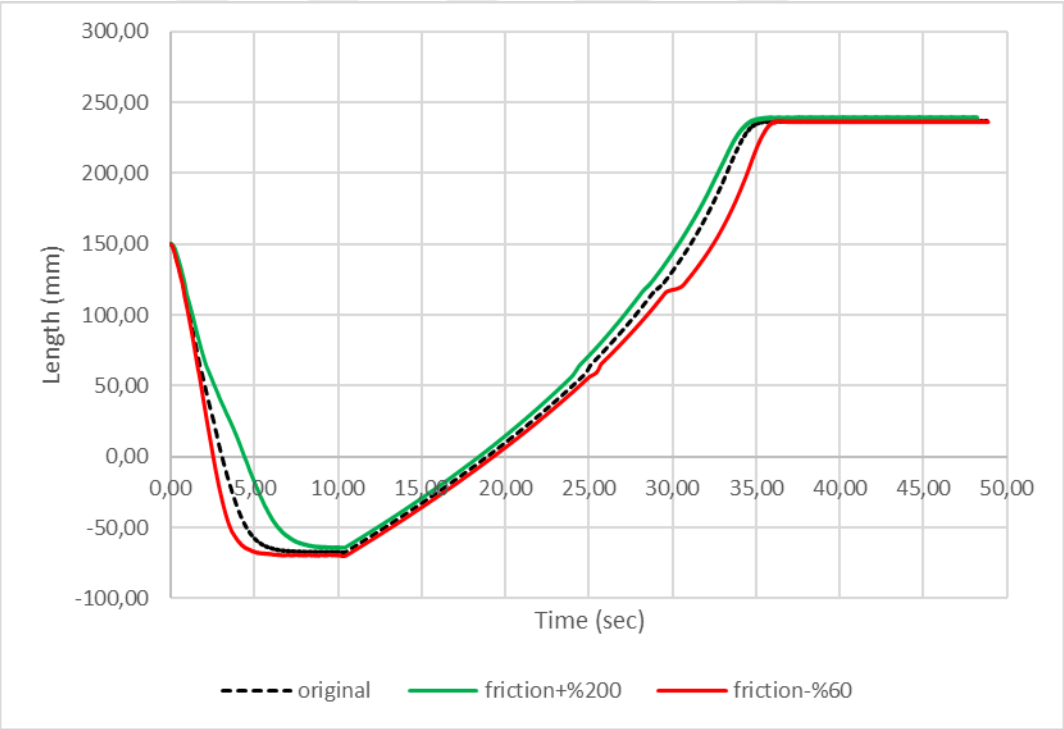


Figure 3.10. Effect of friction coefficient on the displacement of the levered absorber mass during self-tuning to high and low excitation frequencies compared to the natural frequency.

Figure 3.10 shows that when both static and dynamic friction coefficients are decreased, the tuning time to a high excitation frequency decreases, however, tuning time to a low excitation frequency increases. On the other hand, when both static and dynamic friction coefficients are increased, the tuning time to a high excitation frequency increases, however, tuning time to a low excitation frequency decreases. Hence, friction coefficient affects tuning time differently for high and low excitation frequencies.

In order to examine the effect of friction in more detail, intermediate values of friction coefficient are examined. Higher values up to +%50 and lower values down to -%50 are tested. It is seen that there is no specific trend and in some friction coefficient values faster tuning for low frequency and slower tuning for high frequency excitation is achieved; however, for some other values, tuning time is increased for both high and low frequency excitations. It is also seen that when the friction coefficient is very low, the lever cannot converge to an equilibrium position and overshooting increases. Moreover, very high friction coefficients increase the tuning durations. Therefore, the initial value of the friction coefficient is not changed.

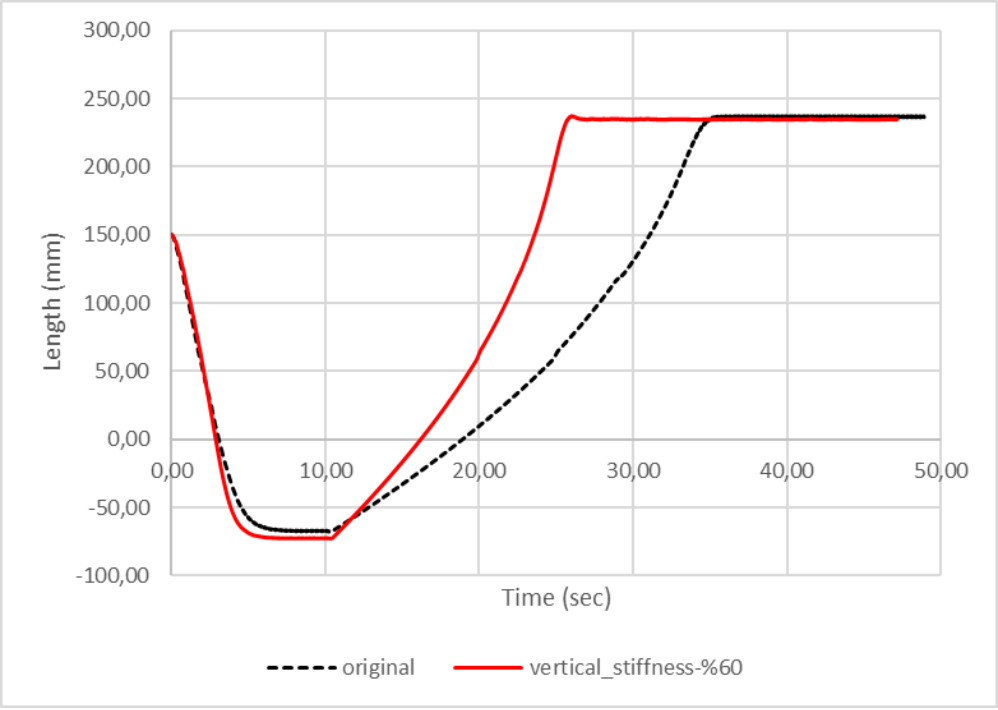


Figure 3.11. Effect of vertical spring stiffness on the displacement of the levered absorber mass during self-tuning to high and low excitation frequencies compared to the natural frequency.

Figure 3.11 shows that when the vertical stiffness decreases tuning time to both high excitation frequency and low excitation frequency decreases. The below figure on the other hand, shows that although the vertical damping constant is changed significantly, the tuning time is not much affected.

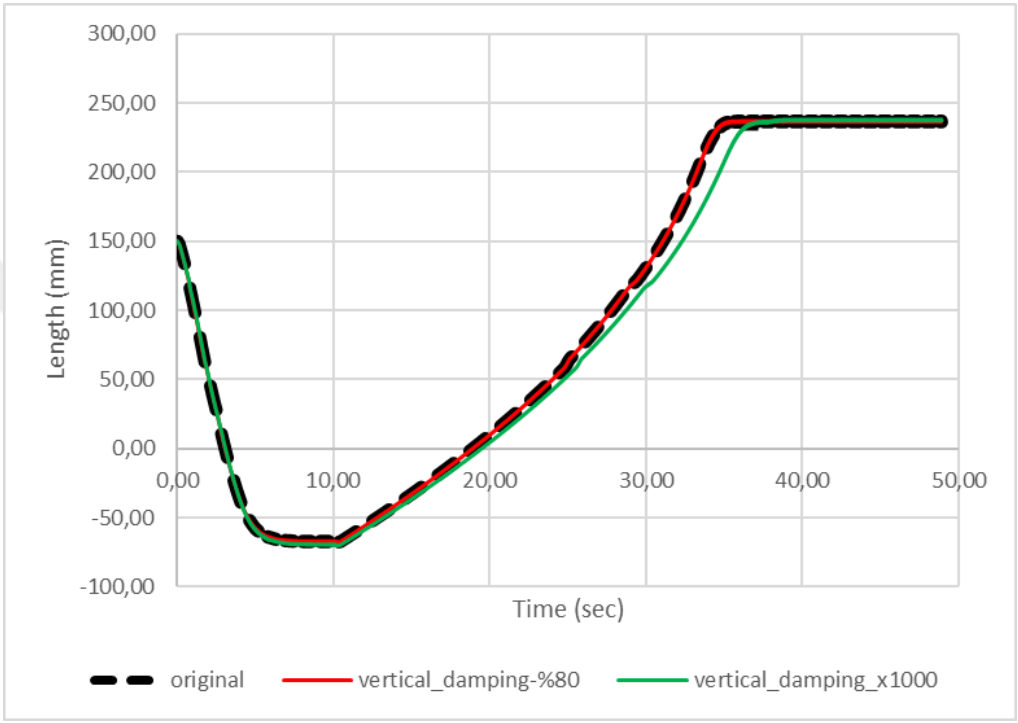


Figure 3.12. Effect of vertical damping constant on the displacement of the levered absorber mass during self-tuning to high and low excitation frequencies compared to the natural frequency.

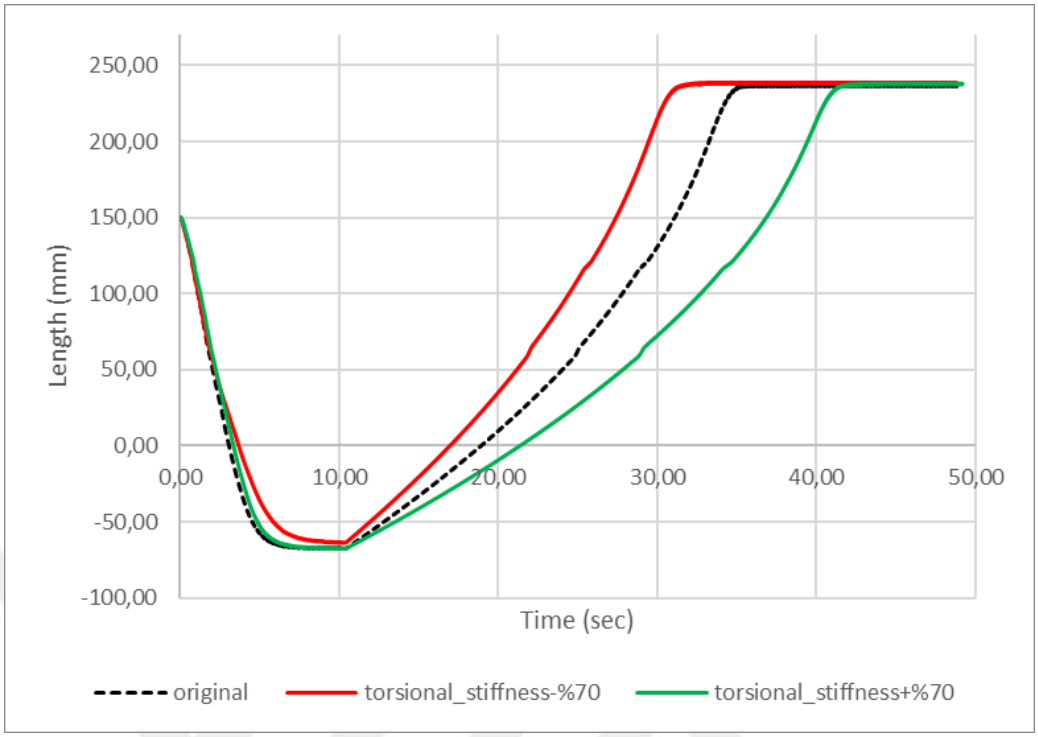


Figure 3.13. Effect of torsional spring stiffness on the displacement of the levered absorber mass during self-tuning to high and low excitation frequencies compared to the natural frequency.

Figure 3.13 shows that when torsional spring stiffness is decreased, the tuning time to a high excitation frequency increases, however, tuning time to a low excitation frequency decreases. On the other hand, when torsional spring stiffness is increased, the tuning time to a high excitation frequency is not affected much, but, tuning time to a low excitation frequency increases. As the tuning time is quite long for a low excitation frequency, using low torsional stiffness is more beneficial.

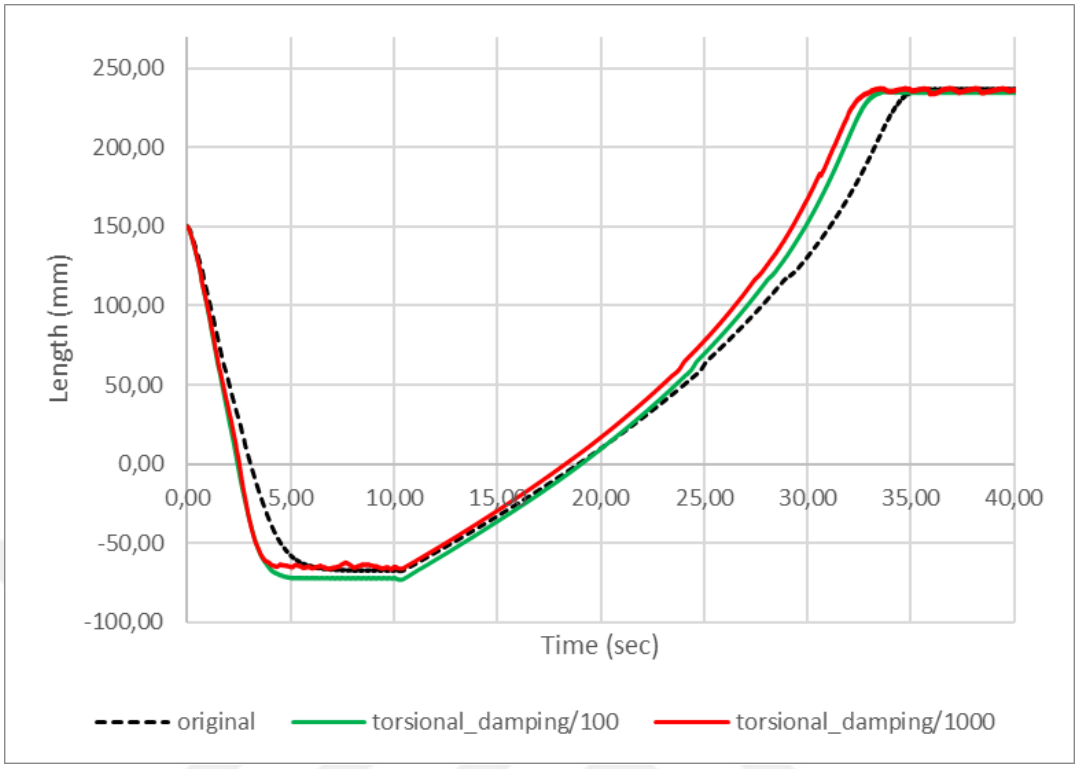


Figure 3.14. Effect of torsional damping constant on the displacement of the levered absorber mass during self-tuning to high and low excitation frequencies compared to the natural frequency.

Figure 3.14 shows that when the torsional damping constant decreases tuning time to both high excitation frequency and low excitation frequency decreases. However, when the torsional damping constant is reduced to very low values, some instability occurs.

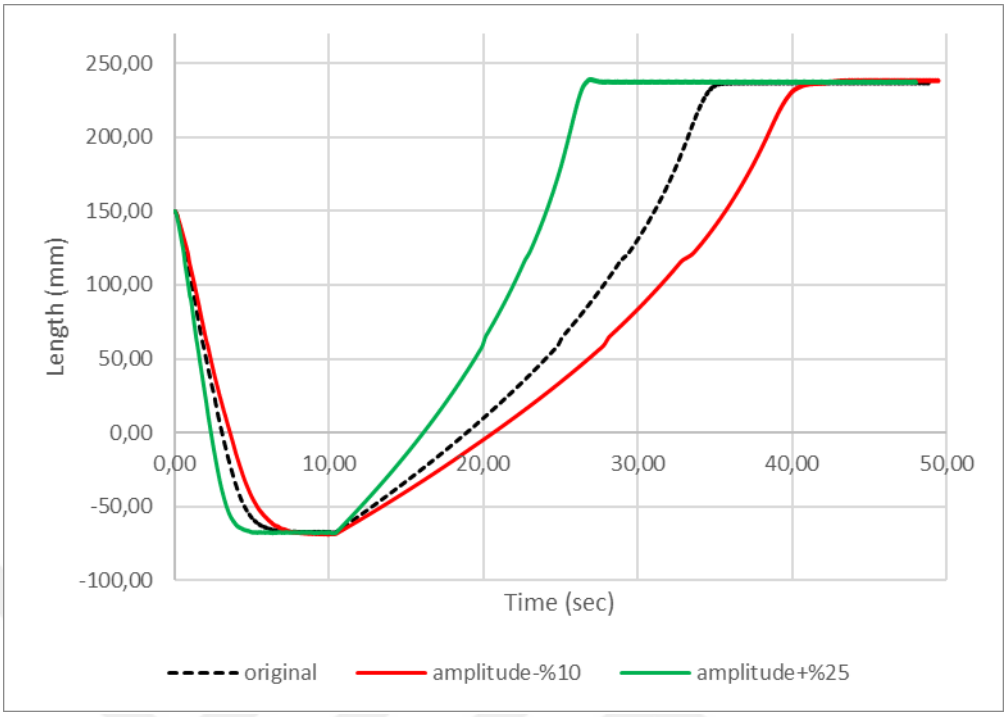


Figure 3.15. Effect of input excitation amplitude on the displacement of the levered absorber mass during self-tuning to high and low excitation frequencies compared to the natural frequency.

Figure 3.15 shows that when the excitation amplitude is increased, tuning time to both high excitation frequency and low excitation frequency decreases. This parameter and the stiffness parameter modifications result in the most significant positive changes in the optimization studies.

In order to minimize the tuning time to both high and low excitation frequencies, the most effective parameters are modified, i.e., vertical spring stiffness, torsional spring stiffness and torsional damping constant. Moreover, input excitation amplitude is also increased to minimize tuning time. Table 3.4 shows the modified parameter values.

Table 3.4. Parameter modifications to minimize self-tuning time.

	Revision	Old Value	New Value
Vertical Spring Stiffness	-%60	0.3 [N/mm]	0.12 [N/mm]
Torsional Spring Stiffness	-%70	100 [N-mm/deg]	30 [N-mm/deg]
Torsional Damping Constant	/100	1 [N-mm-sec/deg]	0.01 [N-mm-sec/deg]
Amplitude	+%25	0.4	0.5

After applying all the aforementioned changes, the modified system self-tunes to both high and low excitation frequencies much faster than the original system (see Figure 3.16). When the initial natural frequency of the original system is 22.5 Hz, the original system self-tunes to 32 Hz in 5 seconds whereas the modified system self-tunes in 2.5 seconds. After these systems are self-tuned to 32 Hz, the input excitation frequency is changed to 20 Hz. The original system self-tunes to 20 Hz in 25 seconds whereas the modified system self-tunes in 7 seconds.

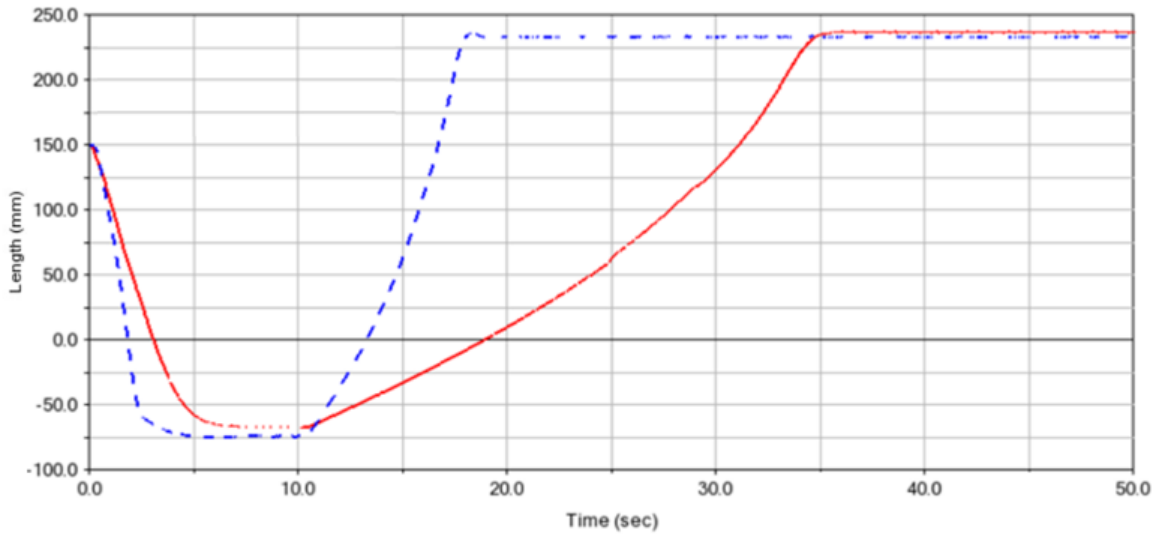


Figure 3.16. Displacement of the levered absorber mass during self-tuning to high and low excitation frequencies compared to the natural frequency for the original system (red solid line) and modified system (blue dashed line).

In addition to the displacements of the levered absorber mass, amplitude of the main absorber mass is also checked in the modified system and is given in Figure 3.17.

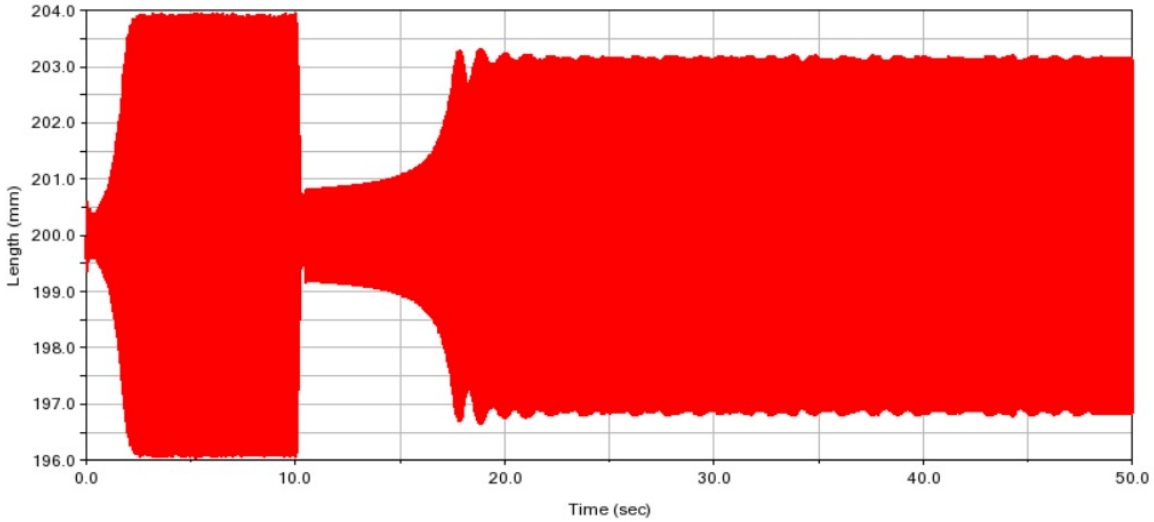


Figure 3.17. Amplitude of the main absorber mass in the modified system.

The resonance amplitude of the main absorber mass is larger compared to the original model as shown in Figure 3.18. In other words, shortening the self-tuning process time led to an increase in the resonance amplitude, which is beneficial.

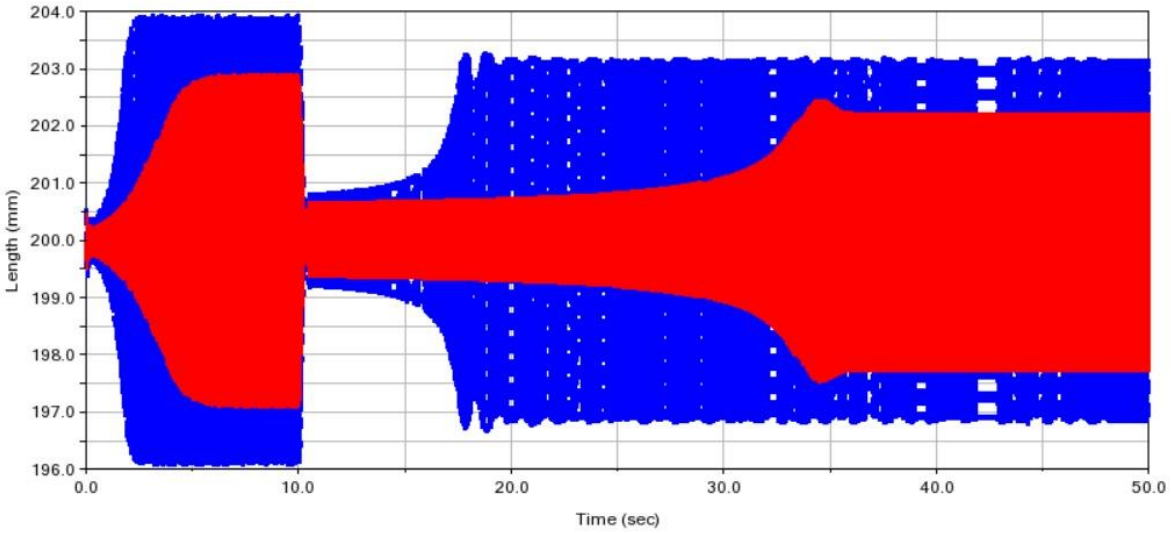


Figure 3.18. Amplitude of the main absorber mass during self-tuning to high and low excitation frequencies compared to the natural frequency for the original system (red solid line) and modified system (blue dashed line).

After obtaining a robust and fast-tuning system, in order to push the limits further and decreasing the self-tuning durations even more, main damping constant specified in Table 3.1 is modified and tested. In the initial optimized model this value was 0.028 N-sec/mm. Firstly, it is decreased to 0.026 N-sec/mm which is the lowest value in which the system kept functioning in a stable manner and later on increased to double its value which is 0.056 N-sec/mm. Decreasing this parameter increased the overshooting and the resonance amplitudes, however the tuning durations are not affected. On the other hand, increasing this parameter significantly decreased the overshooting and resonance amplitudes, however, the tuning duration is extended. The displacement of the levered absorber mass, which indicates the tuning durations are shown in Figure 3.19 and the change of resonance amplitude for different main damping constant values is shown in Figure 3.20.

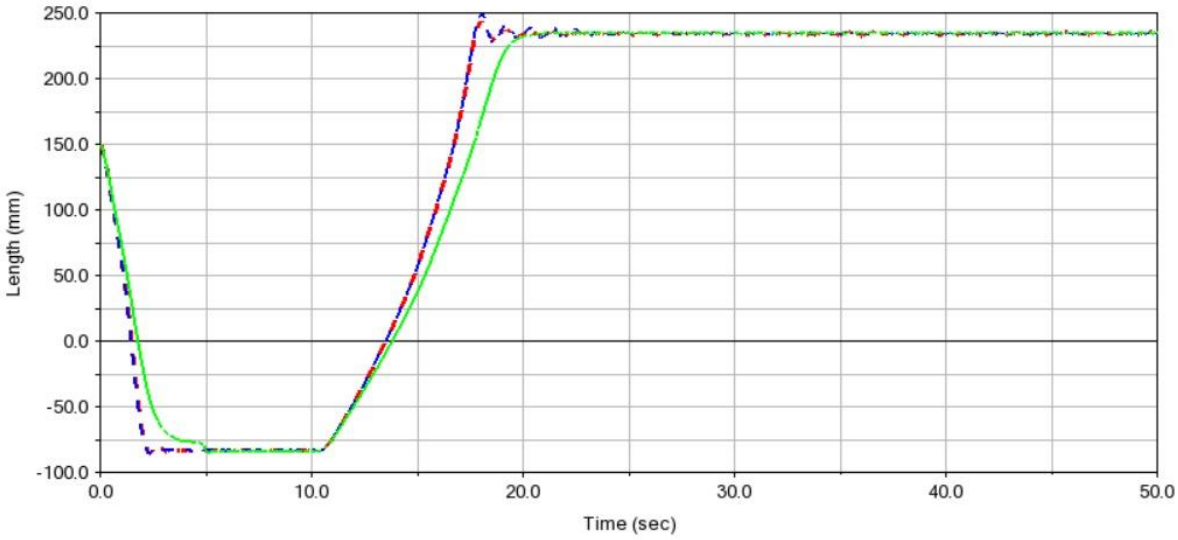


Figure 3.19. Displacement of the levered absorber mass during self-tuning to high and low excitation frequencies compared to the natural frequency for the optimized system (red dotted line), lower main damping constant value (blue dashed line), and larger main damping constant value (green solid line).

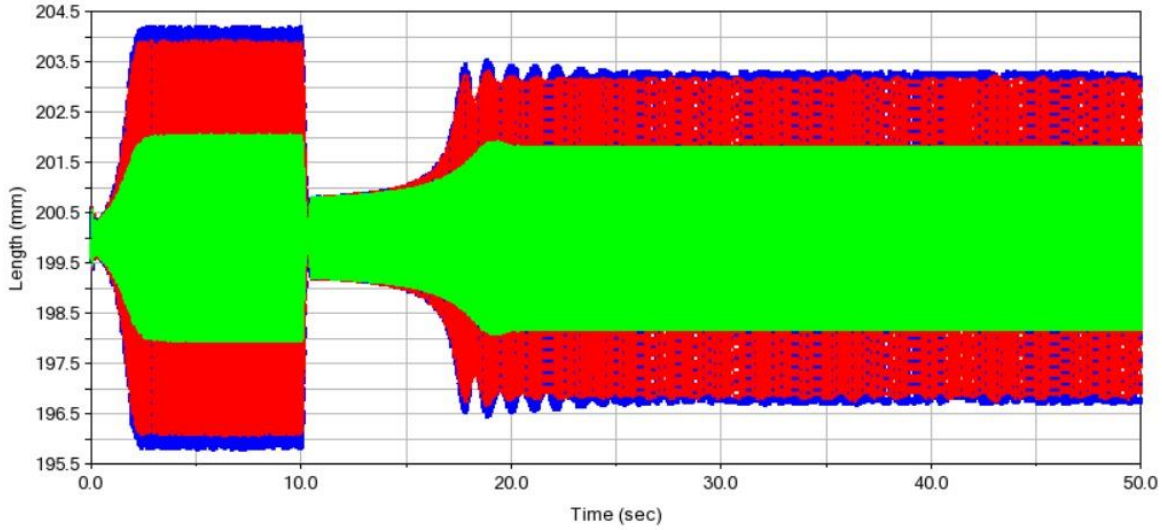


Figure 3.20. Amplitude of the main absorber mass during self-tuning to high and low excitation frequencies compared to the natural frequency for the optimized system (red dotted line), lower main damping constant value (blue dashed line), and larger main damping constant value (green solid line).

3.3. Tracking Performance of the Modified System Under Changing Frequency Condition

In order to test how the system performs under increasing excitation frequency, the input excitation frequency is varied according to the below equation. Notice that the frequency increases from 20 Hz to 25 Hz in 10 seconds. Moreover, the initial natural frequency of the system is 22.5 Hz. The excitation is defined as:

$$0.5\ sin(40\ (1 + 0.025t)\pi t). \tag{3.3}$$

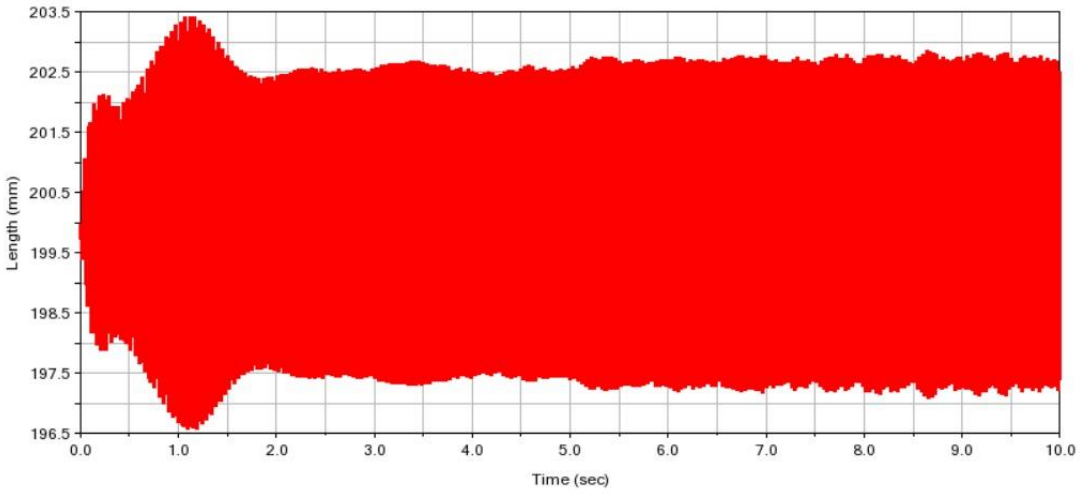


Figure 3.21. Amplitude of the main absorber mass under increasing excitation frequency.

Figure 3.21 shows that when the input excitation frequency is varied, the modified system quickly self-tunes and tracks the input excitation frequency. Notice that the input excitation amplitude is 0.5 mm whereas the output excitation amplitude is 2.5 mm for varying input excitation frequency between 20-25 Hz. Thus, the system remains in resonance condition although the input excitation frequency is varied. Moreover, Figure 3.22 shows that after 1 second, the system self-tunes to the varying excitation condition and tracks it.

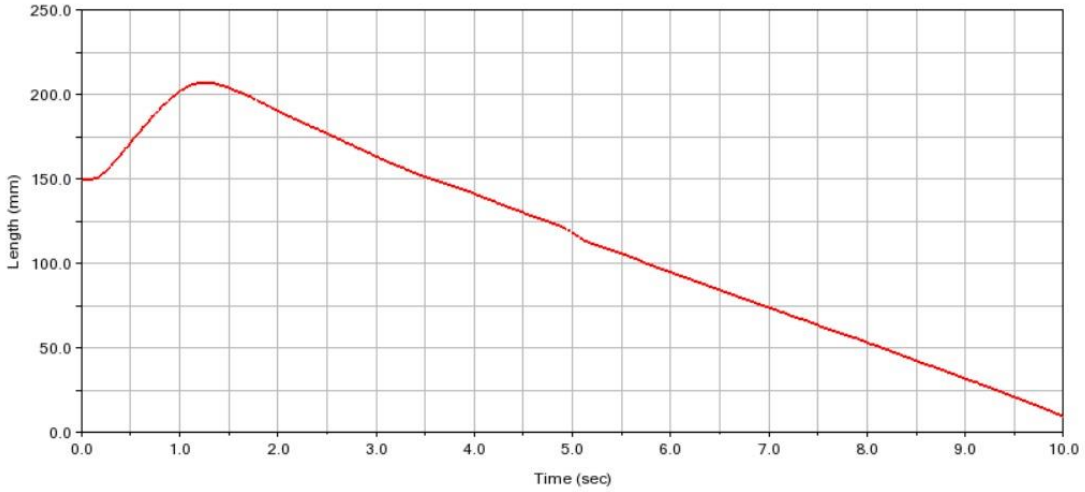


Figure 3.22. Displacement of the levered absorber mass during self-tuning to increasing excitation frequency.

In order to test how the system performs under decreasing excitation frequency, the input excitation frequency is varied according to below equation. Notice that the frequency decreases from 30 Hz to 25 Hz in 10 seconds. Moreover, the initial natural frequency of the system is 22.5 Hz. The excitation is defined as:

$$0.5\ sin(60(1 - 0.01666\ t)\pi t). \tag{3.4}$$

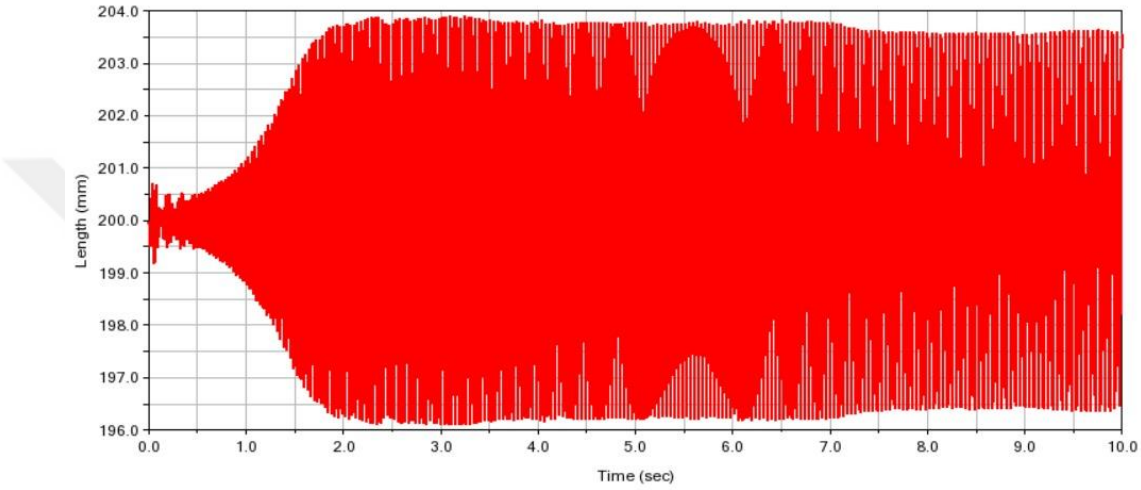


Figure 3.23. Amplitude of the main absorber mass under decreasing excitation frequency.

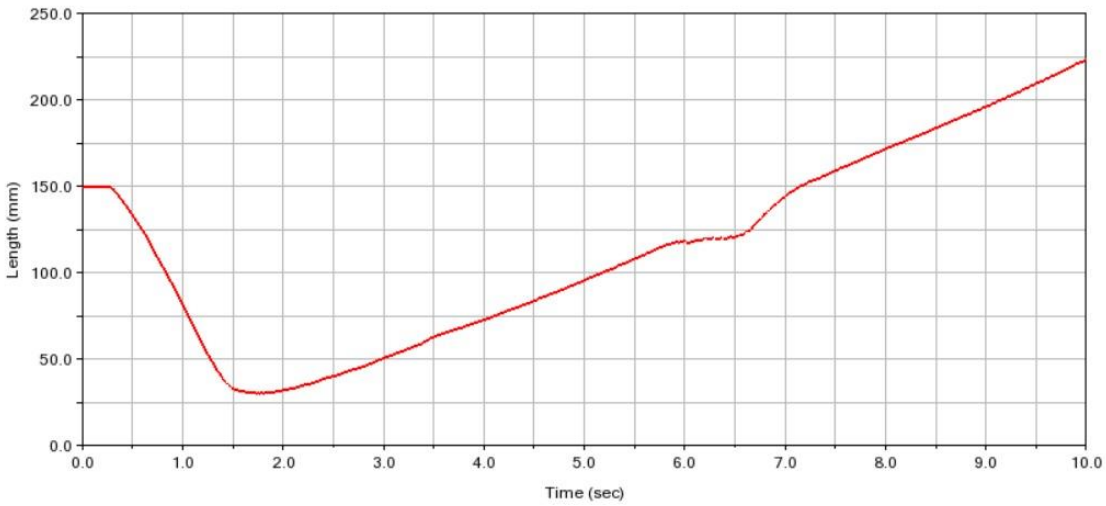


Figure 3.24. Displacement of the levered absorber mass during self-tuning to decreasing excitation frequency.

Consequently, for both increasing and decreasing frequency inputs, system still operates successfully. Hence, it can be said that system is able to adapt to changing excitation frequency conditions.

3.4. Implementation of the Self-Tuning Vibration Absorber

In Figure 2.2, the frequency response of a mass equipped with a passive absorber system was depicted. It was shown that when the absorber mass is 1/10th of the main mass and the absorber natural frequency is tuned to the main system natural frequency, there was very small bandwidth for vibration absorption. In fact, when the excitation frequency shifts up or down by 5%, the system cannot offer isolation and the main mass experiences large amount of vibration.

In this section, the self-tuning absorber system is used on a main mass (indicated with yellow in Figure 3.25) which weighs 10 times the absorber mass identified Table 3.1. Hence, the main mass is 12.3 kg and it is supported by a main spring with stiffness 246 N/mm with no damping. This system is base-excited and in the absence of the self-tuning absorber system, the natural frequency of the 12.3 kg main mass on the main spring with 246 N/mm stiffness corresponds to 22.5 Hz. When the self-tuning absorber system is implemented, it is expected that the motion of the 12.3 kg main mass will not be amplified in the vicinity of 22.5 Hz even if the excitation frequency is varied by 5%.

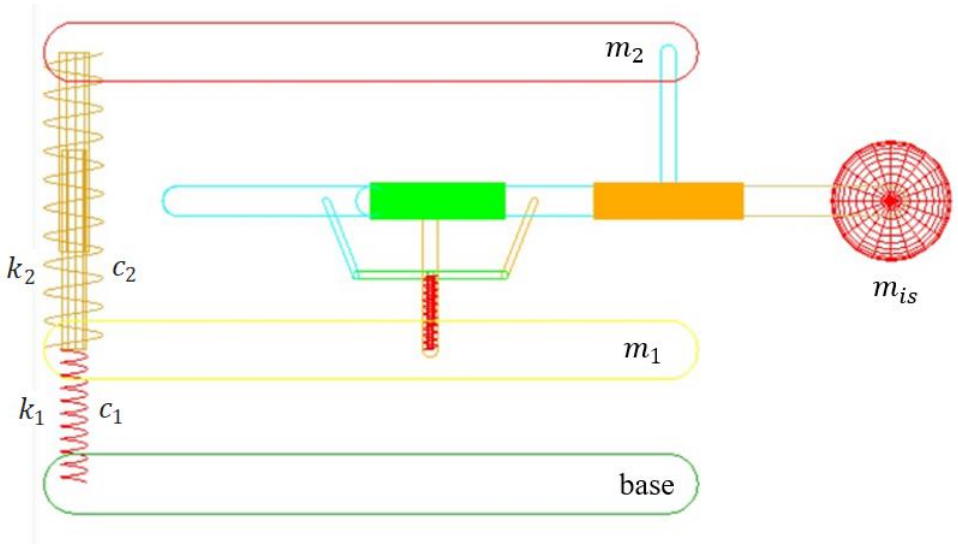


Figure 3.25. The self-tuning absorber system implemented on a main mass suspended by a main spring.

The new parameters can be used to obtain the transmissibility of a similar passive DVA system as in Figure 2.1. Since there is no levered absorber mass in Figure 2.1, the absorber stiffness is chosen as 1/10th of main spring stiffness (246 N/mm). In that case, antiresonance frequency is tuned to 22.5 Hz. However, the passive DVA will have the self-tuning response so its antiresonance and resonance frequencies are fixed. In Equation 2.9, transmissibility of an undamped passive vibration absorber was given. As there is damping in the self-tuning absorber, it should be compared with a damped passive vibration absorber whose transmissibility is given as:

$$\left|\frac{X_1}{Y}\right| = \left|\frac{(k_2-\omega^2 m_2+i\omega c_2)k_1}{(k_1+k_2-\omega^2 m_1+i\omega c_2)(k_2-\omega^2 m_2+i\omega c_2)-(k_2+i\omega c_2)^2}\right|. \quad (3.5)$$

Moreover, absorber damping (c_2) is chosen as 15.6 Ns/m so that the stiffness and damping values are scaled proportionally. There is no main damping in the system so c_1 does not appear in Equation 3.5. Due to non-zero absorber damping, transmissibility cannot reach zero at the antiresonance frequency. The isolation frequency range in which transmissibility is less than 1 is between 22.10 - 23.03 Hz. The input vibration will be significantly amplified when the frequency is varied by ±5% of the antiresonance frequency. Specifically, when the excitation frequency is at 20 Hz, the output amplitude of the main mass will be 6.21 times the base-excitation input amplitude. Moreover, when the excitation frequency is at 25 Hz, the output amplitude of the main mass will be 3.28 times the base-excitation input amplitude. Hence, in both cases significant amplification occurs. It will be shown that the self-tuning absorber will have small amount of vibration of the main mass for these frequencies.

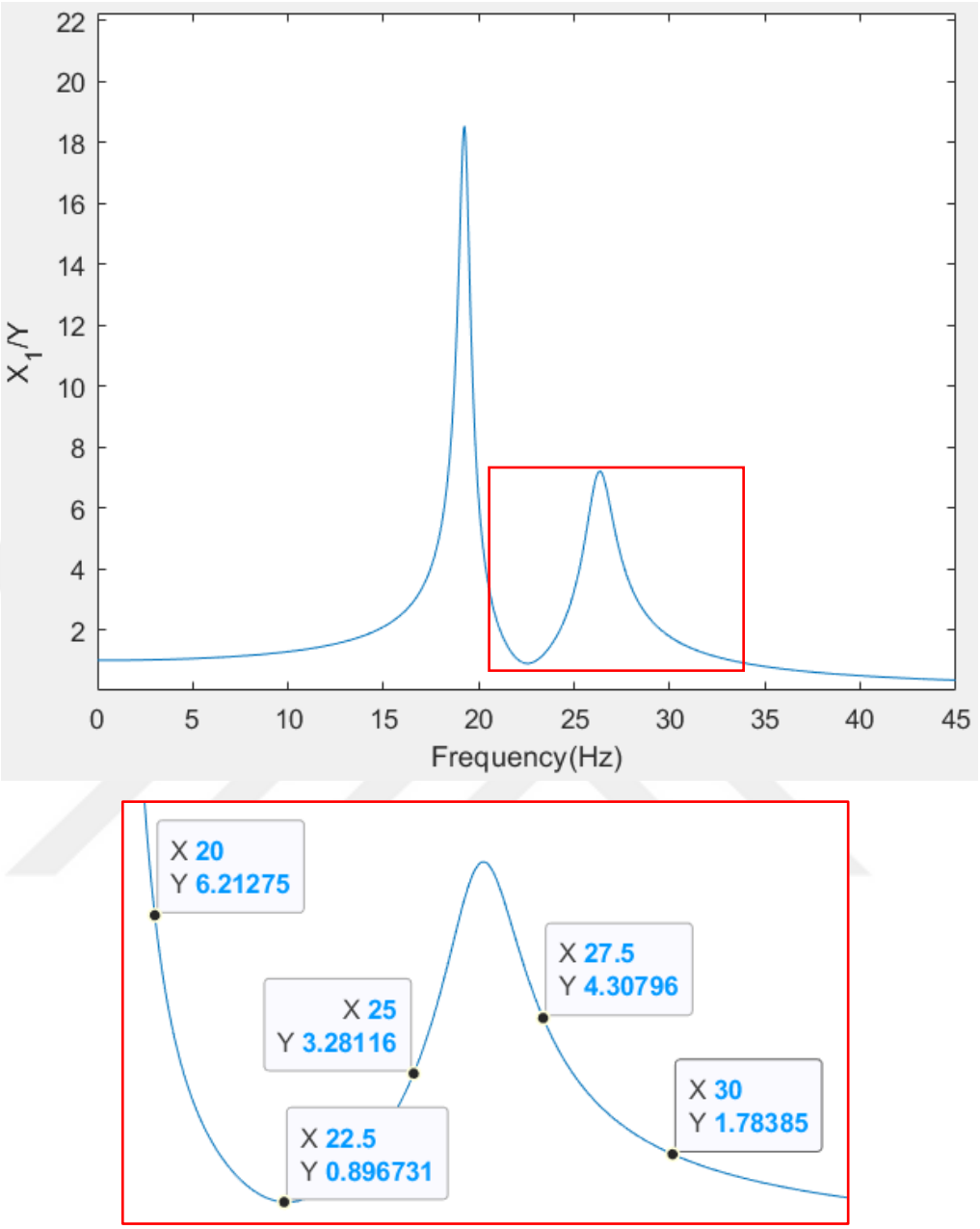


Figure 3.26. Transmissibility plot for a passive dynamic vibration absorber with $k_1 = 246$ N/m, $k_2 = 24.6$ N/m, $m_1 = 12.3$ kg, $m_2 = 1.23$ kg, $c_1 = 0$ Ns/m, $c_2 = 15.6$ Ns/m.

The self-tuning absorber system is tested in 5 different frequency inputs according to the below equation. In order to examine response of the system in detail, main mass amplitude graph is plotted in addition to the main absorber mass amplitude & levered absorber mass displacement graphs. The excitation is defined as:

$$0.1 \sin(\omega t). \tag{3.6}$$

Firstly, system is subjected to 20 Hz excitation frequency in which self-tuning equilibrium is achieved towards the right of the initial position as shown in Figure 3.27. Then, the system is subjected to its natural frequency (22.5 Hz) and the lever almost maintains its initial position as shown in Figure 3.28. Consequently, frequency values larger the natural frequency value are tested which are 25, 27.5 and 30 Hz as shown in Figures 3.29, 3.30, 3.31. The self-tuning system reached different equilibrium positions in which the lever moved towards left as excitation frequency is increased. When the lever moves towards left, the lever ratio and the effective mass of the absorber system decreases and its natural frequency increases to match the excitation frequency. However, tuning to higher frequencies are harder. Overshooting and tuning durations are increased as the excitation frequency is increased.

Figure 3.27(a) shows that the main mass amplitude reaches steady state amplitude of 0.14 mm when the excitation frequency is 20 Hz. As the base-excitation amplitude is 0.1 mm, there is small amount of amplification in the system. However, according to Figure 3.26, at 20 Hz the equivalent passive DVA would have 0.62 mm amplitude for the main mass (6.21 times amplification). Hence, the self-tuning absorber system effectively reduces the output amplitude.

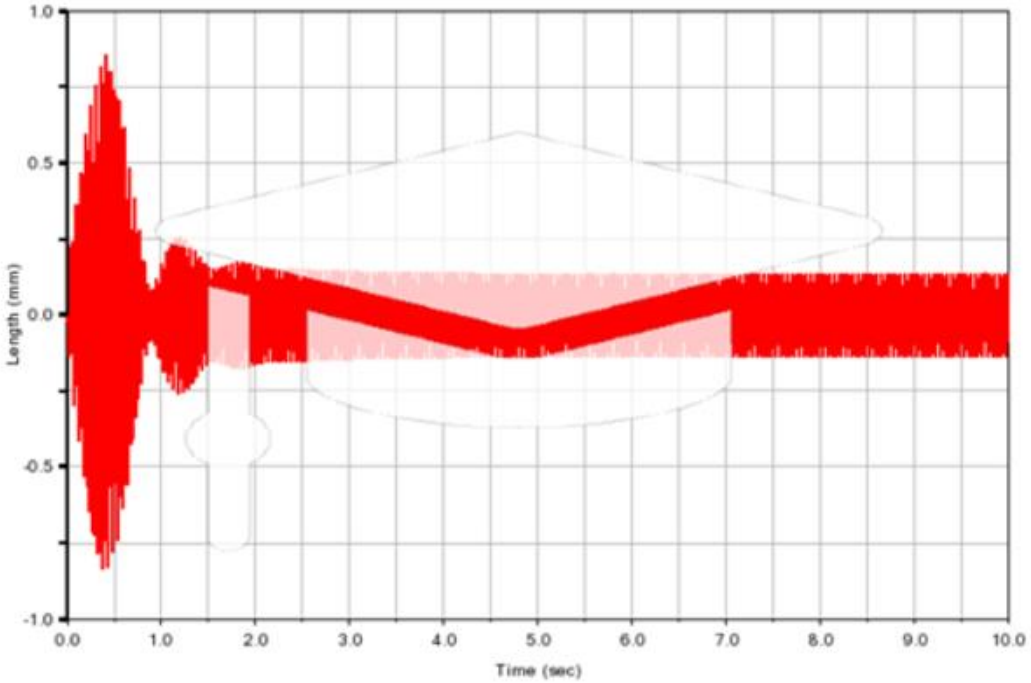
Figure 3.28(a) shows that the main mass amplitude reaches steady state amplitude of 0.17 mm when the excitation frequency is 22.5 Hz. As the base-excitation amplitude is 0.1 mm, there is small amount of amplification in the system. According to Figure 3.26, at 22.5 Hz the equivalent passive DVA would have 0.09 mm amplitude for the main mass. As there is some damping in both of these systems, output amplitude cannot reach zero at the antiresonance frequency.

Figure 3.29(a) shows that the main mass amplitude reaches steady state amplitude of 0.1 mm when the excitation frequency is 25 Hz. As the base-excitation amplitude is also 0.1 mm, there is no amplification in the system. However, according to Figure 3.26, at 25 Hz the equivalent passive DVA would have 0.33 mm amplitude for the main mass (3.28 times amplification). Hence, the self-tuning absorber system effectively reduces the output amplitude.

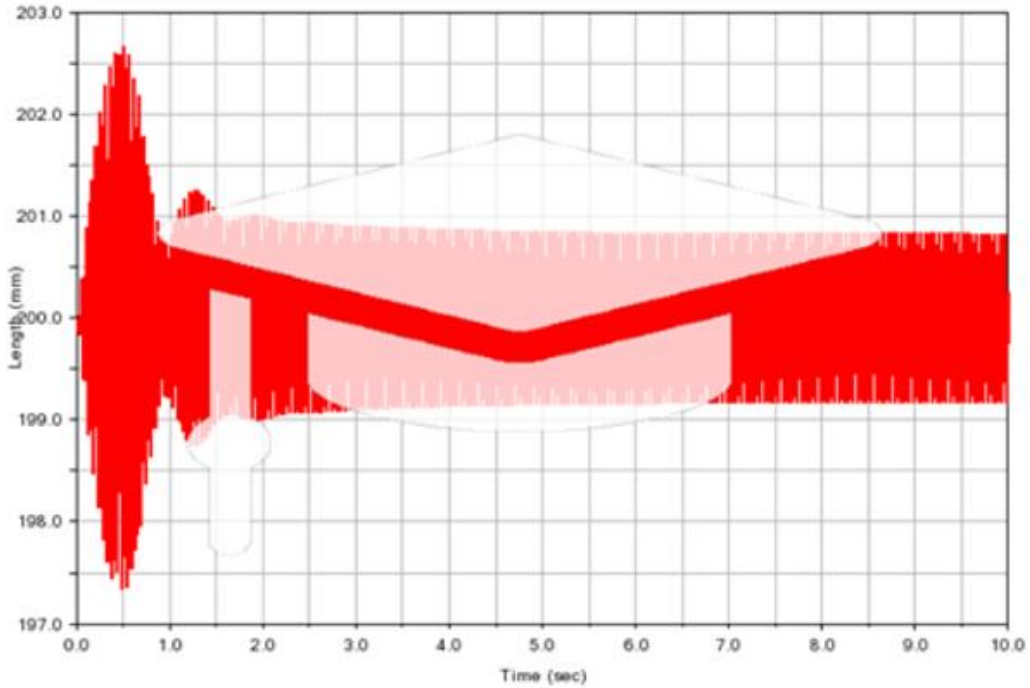
Figure 3.30(a) shows that the main mass amplitude reaches steady state amplitude of 0.1 mm when the excitation frequency is 27.5 Hz. As the base-excitation amplitude is also 0.1 mm, there is no amplification in the system. However, according to Figure 3.26, at 27.5 Hz the equivalent passive DVA would have 0.43 mm amplitude for the main mass (4.3 times amplification). Hence, the self-tuning absorber system effectively reduces the output amplitude.

Figure 3.31(a) shows that the main mass amplitude reaches steady state amplitude of 0.065 mm when the excitation frequency is 30 Hz. As the base-excitation amplitude is 0.1 mm, there is no amplification in the system. However, according to Figure 3.26, at 30 Hz the equivalent passive DVA would have 0.18 mm amplitude for the main mass (1.78 times amplification). Hence, the self-tuning absorber system effectively reduces the output amplitude.

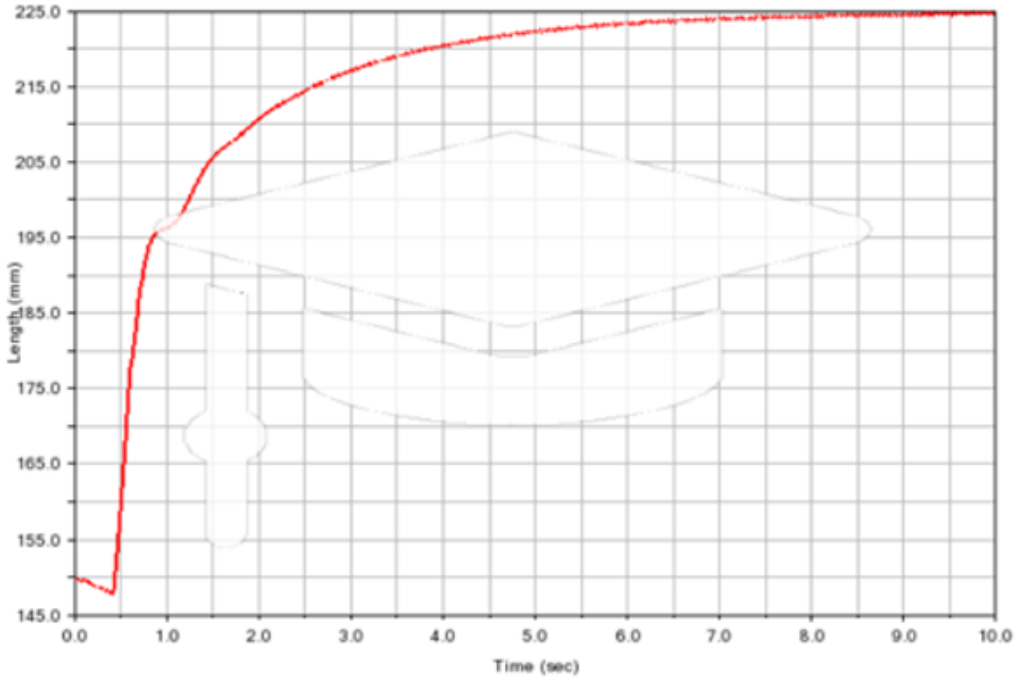
(a)


1.0
0.5
0.0
-0.5
-1.0
Length (mm)
0.0
1.0
2.0
3.0
4.0
5.0
6.0
7.0
8.0
9.0
10.0
Time (sec)

(b)


203.0
202.0
201.0
200.0
199.0
198.0
197.0
Length (mm)
0.0
1.0
2.0
3.0
4.0
5.0
6.0
7.0
8.0
9.0
10.0
Time (sec)

(c)



(d)

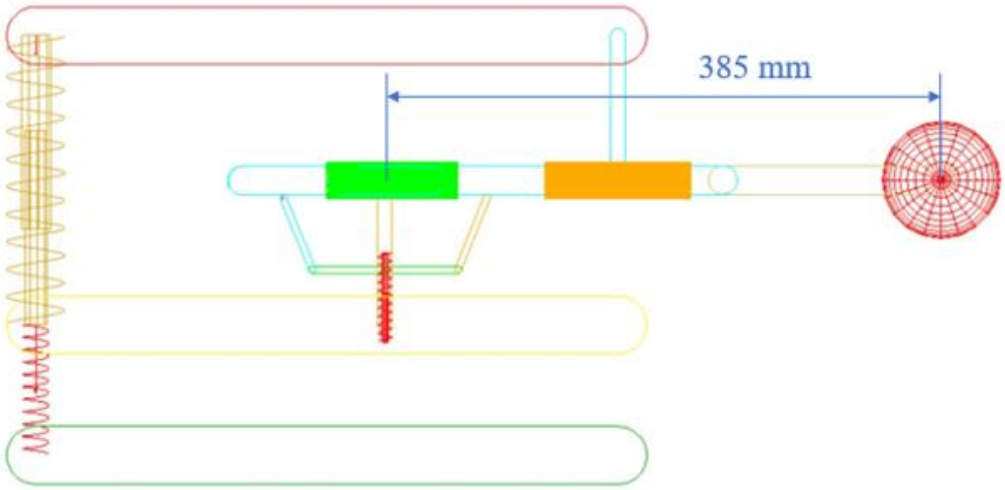
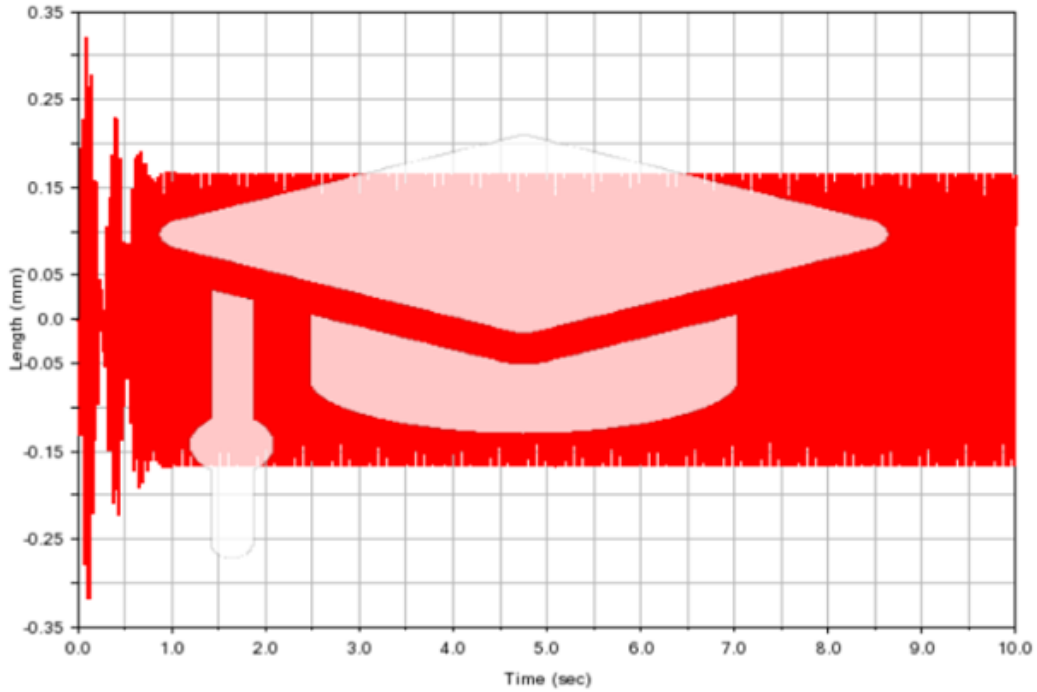
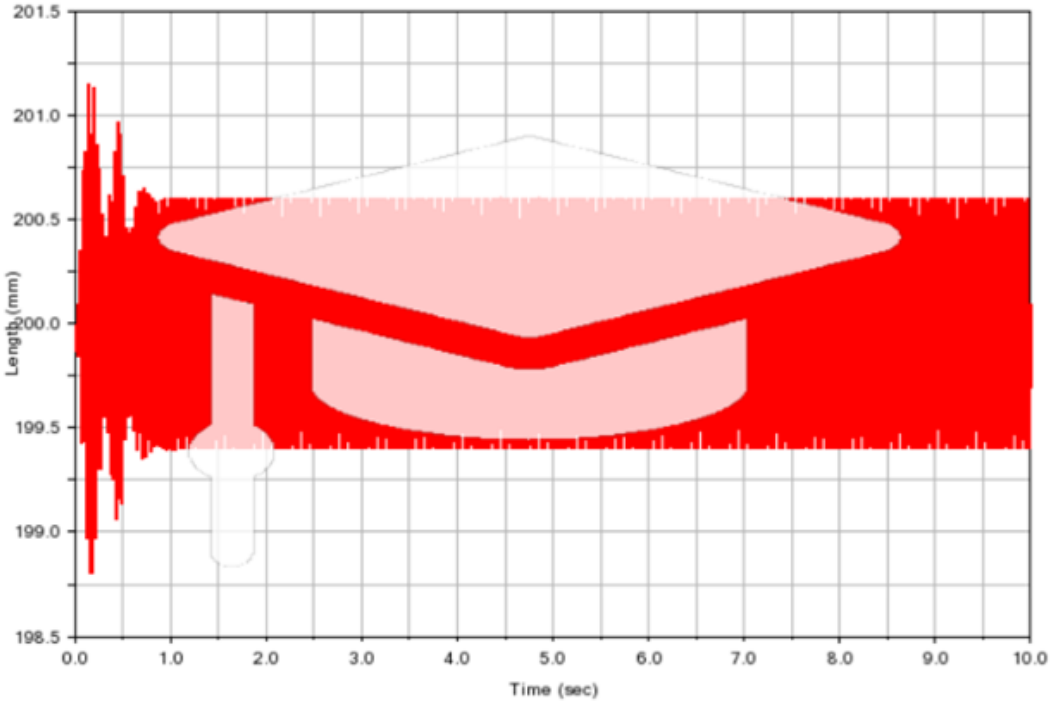


Figure 3.27. Response of the self-tuning absorber system implemented on a main mass suspended by a main spring when subject to 20 Hz base-excitation. (a) Main mass amplitude, (b) Main absorber mass amplitude, (c) Lever absorber mass displacement, (d) Position of the levered mass after self-tuning to 20 Hz.

(a)


0.35
0.25
0.15
0.05
0.0
-0.05
-0.15
-0.25
-0.35
Length (mm)
0.0
1.0
2.0
3.0
4.0
5.0
6.0
7.0
8.0
9.0
10.0
Time (sec)

(b)


201.5
201.0
200.5
200.0
199.5
199.0
198.5
Length (mm)
0.0
1.0
2.0
3.0
4.0
5.0
6.0
7.0
8.0
9.0
10.0
Time (sec)

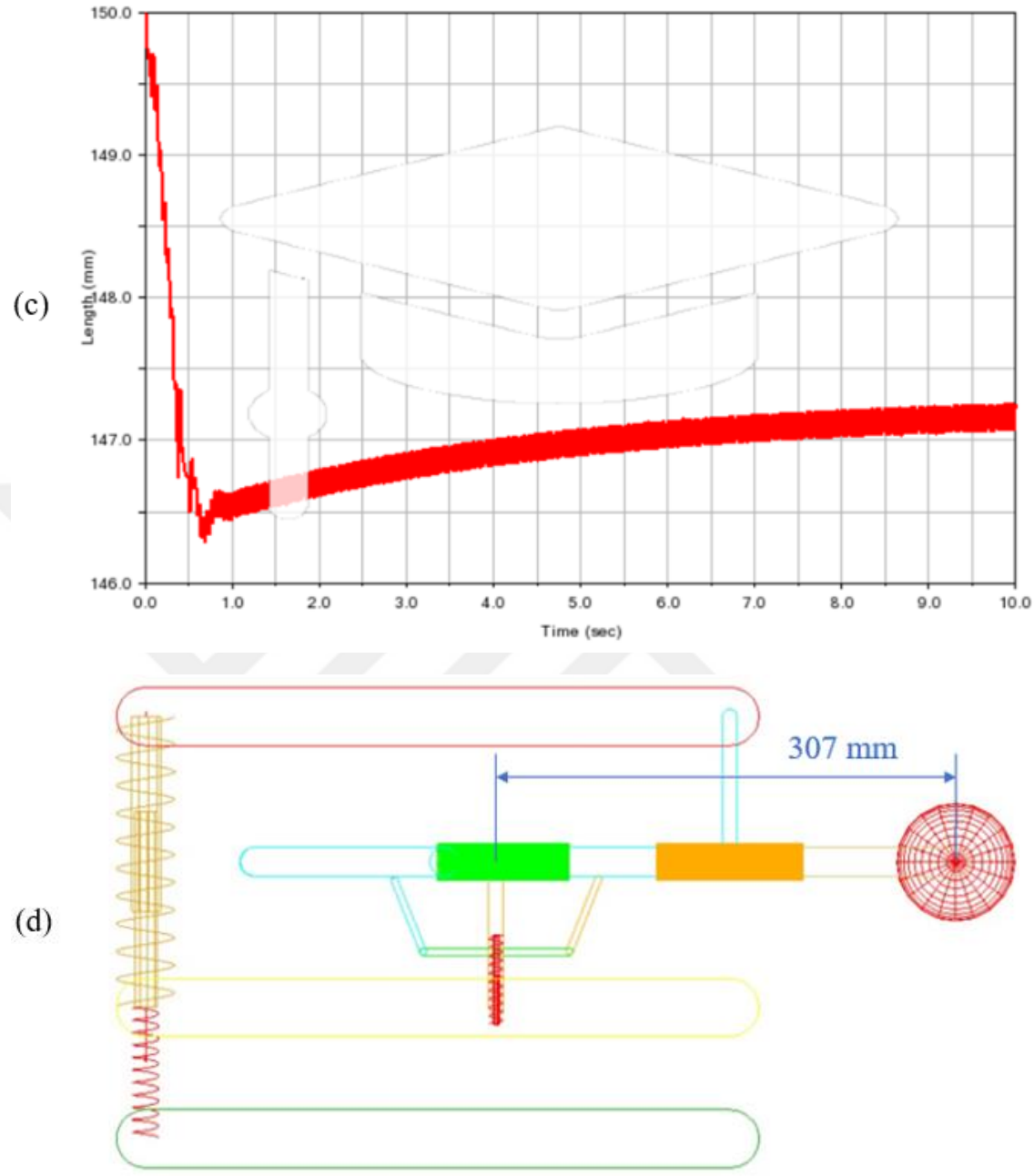
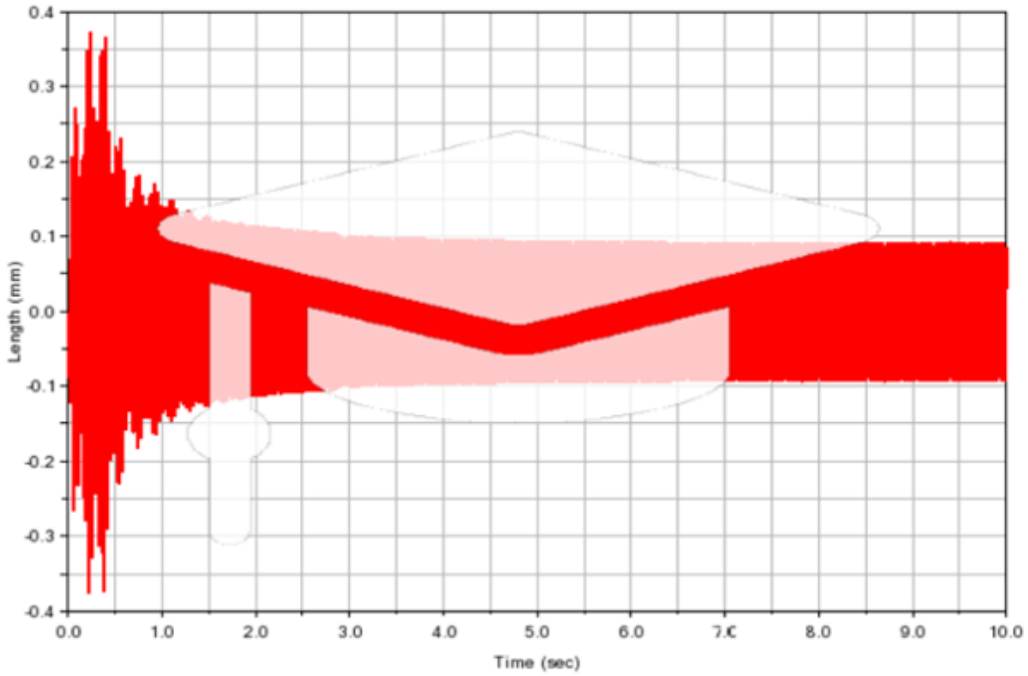
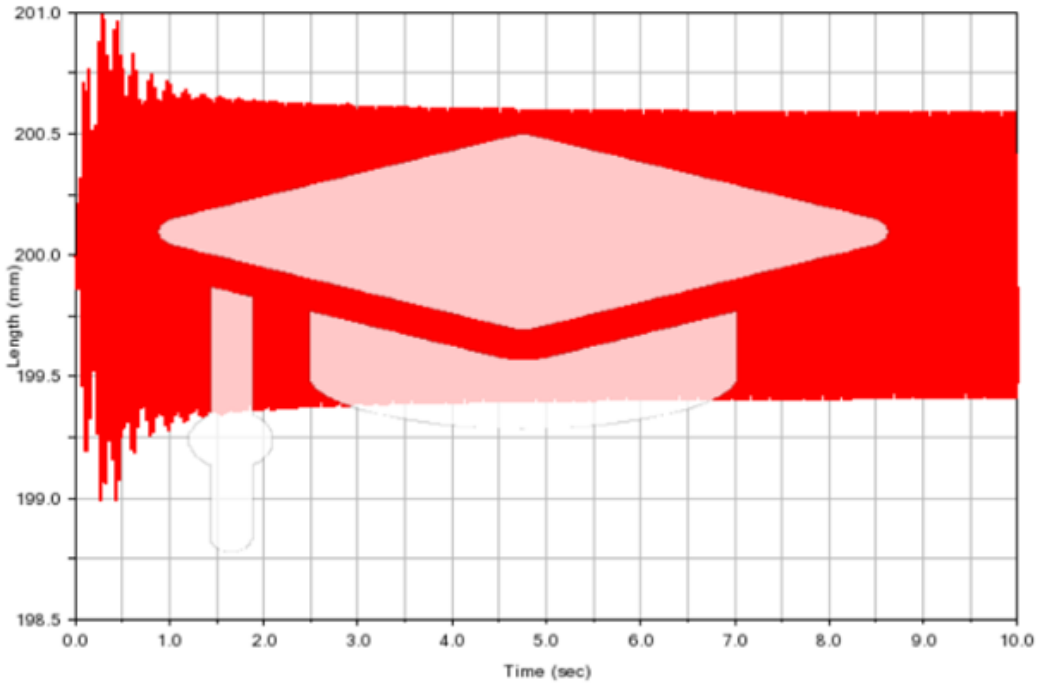


Figure 3.28. Response of the self-tuning absorber system implemented on a main mass suspended by a main spring when subject to 22.5 Hz base-excitation. (a) Main mass amplitude, (b) Main absorber mass amplitude, (c) Lever absorber mass displacement, (d) Position of the levered mass after self-tuning to 22.5 Hz.

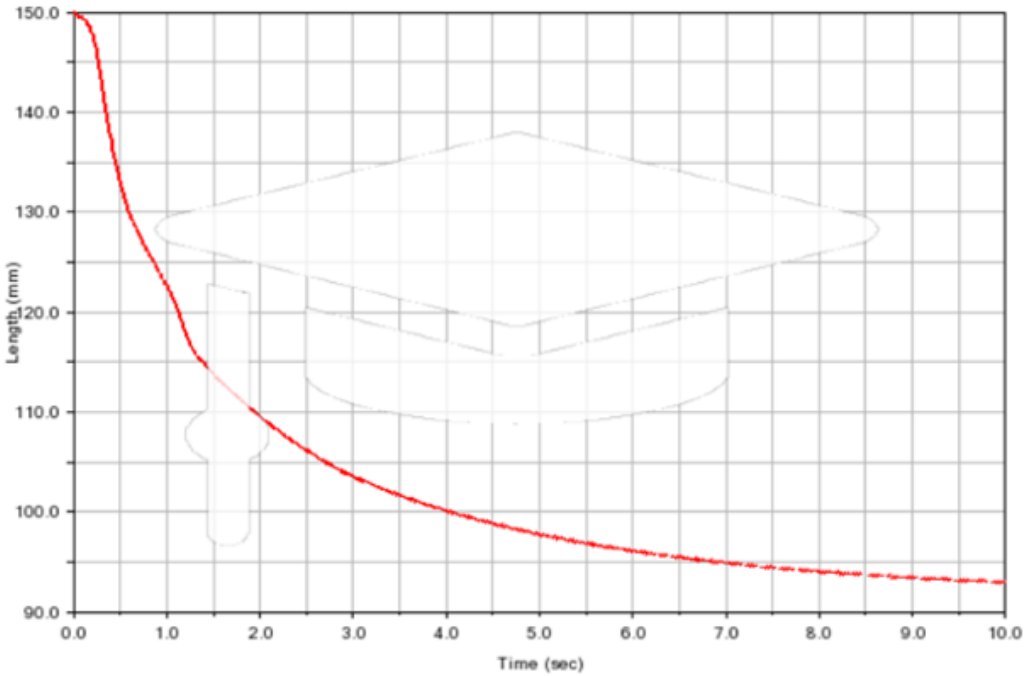
(a)


0.4
0.3
0.2
0.1
0.0
-0.1
-0.2
-0.3
-0.4
Length (mm)
0.0
1.0
2.0
3.0
4.0
5.0
6.0
7.0
8.0
9.0
10.0
Time (sec)

(b)


201.0
200.5
200.0
199.5
199.0
198.5
Length (mm)
0.0
1.0
2.0
3.0
4.0
5.0
6.0
7.0
8.0
9.0
10.0
Time (sec)

(c)



(d)

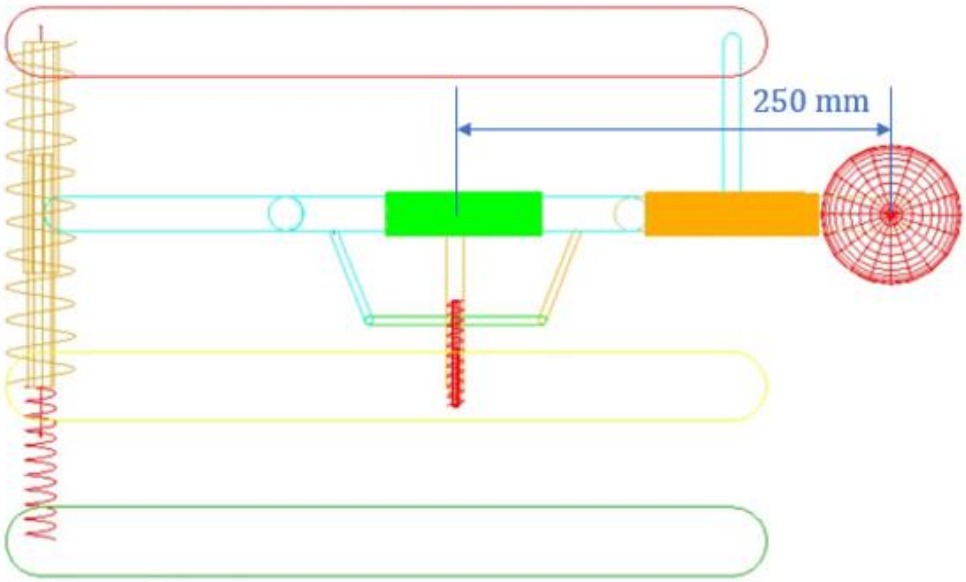
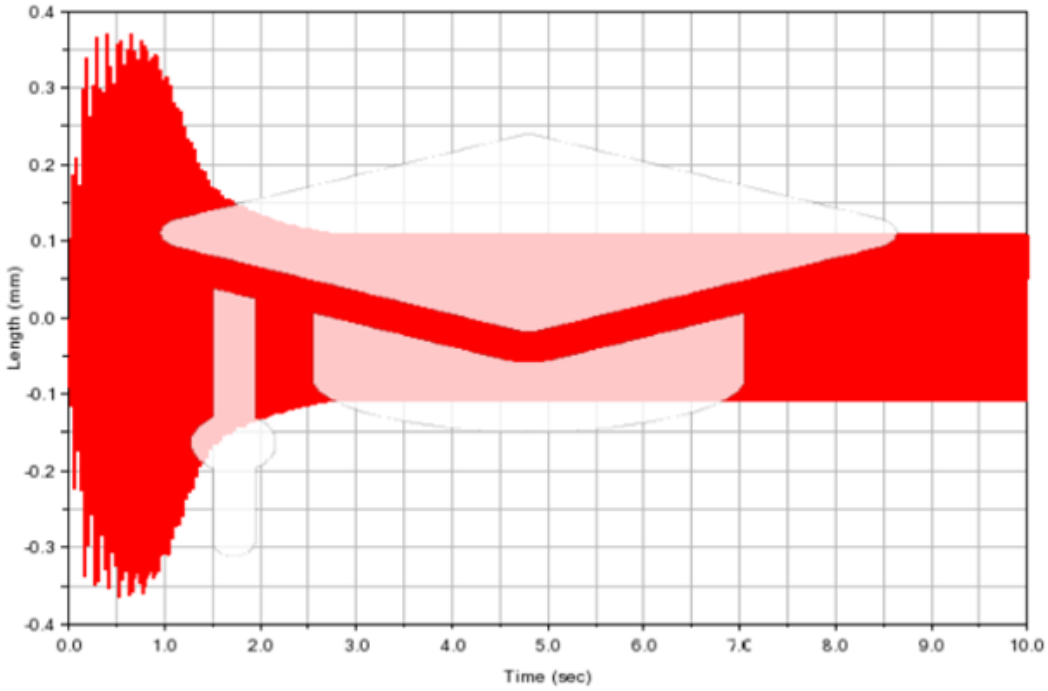
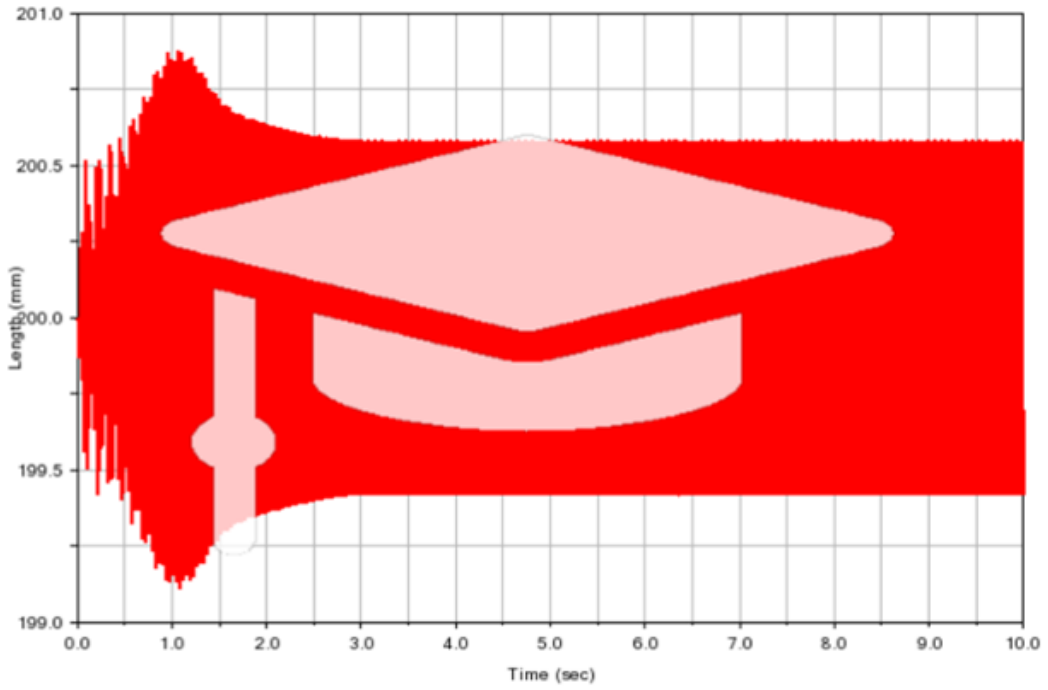


Figure 3.29. Response of the self-tuning absorber system implemented on a main mass suspended by a main spring when subject to 25 Hz base-excitation. (a) Main mass amplitude, (b) Main absorber mass amplitude, (c) Lever absorber mass displacement, (d) Position of the levered mass after self-tuning to 25 Hz.

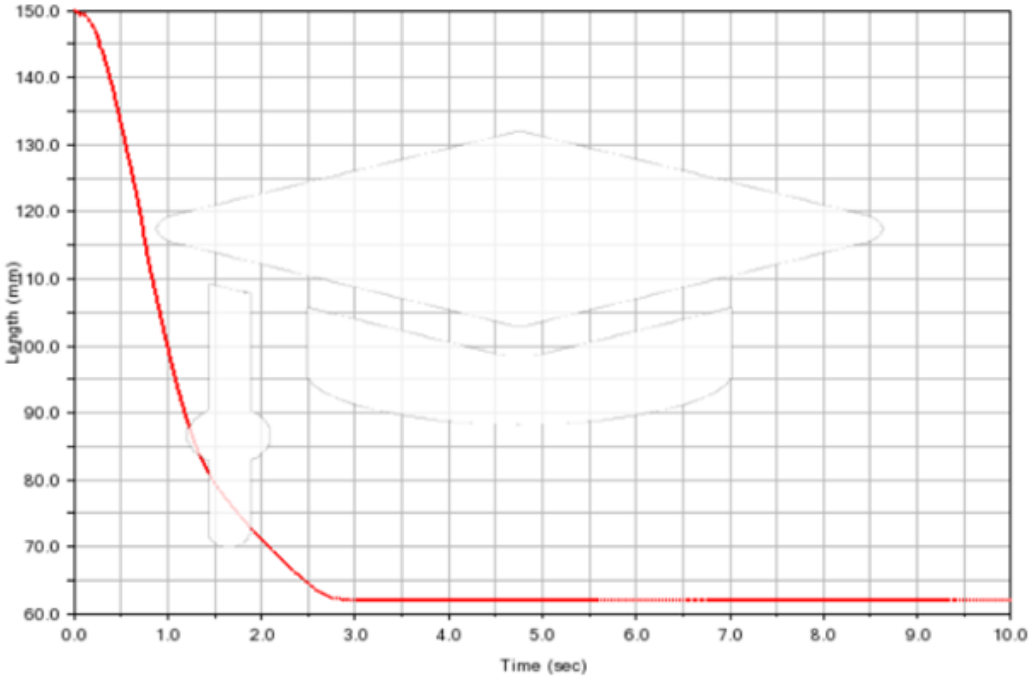
(a)


0.4
0.3
0.2
0.1
0.0
-0.1
-0.2
-0.3
-0.4
Length (mm)
0.0
1.0
2.0
3.0
4.0
5.0
6.0
7.0
8.0
9.0
10.0
Time (sec)

(b)


201.0
200.5
200.0
199.5
199.0
Length (mm)
0.0
1.0
2.0
3.0
4.0
5.0
6.0
7.0
8.0
9.0
10.0
Time (sec)

(c)



(d)

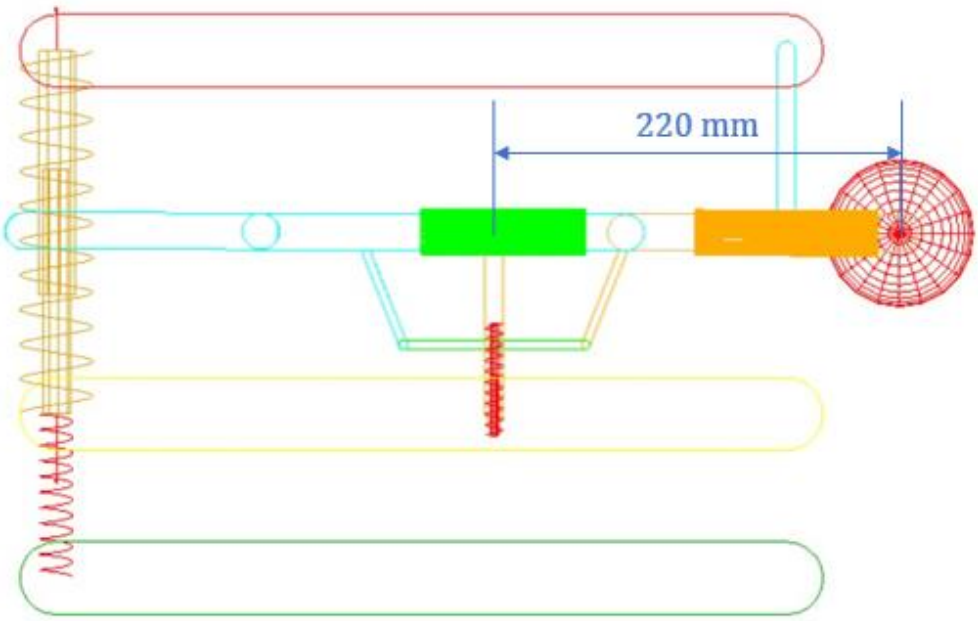
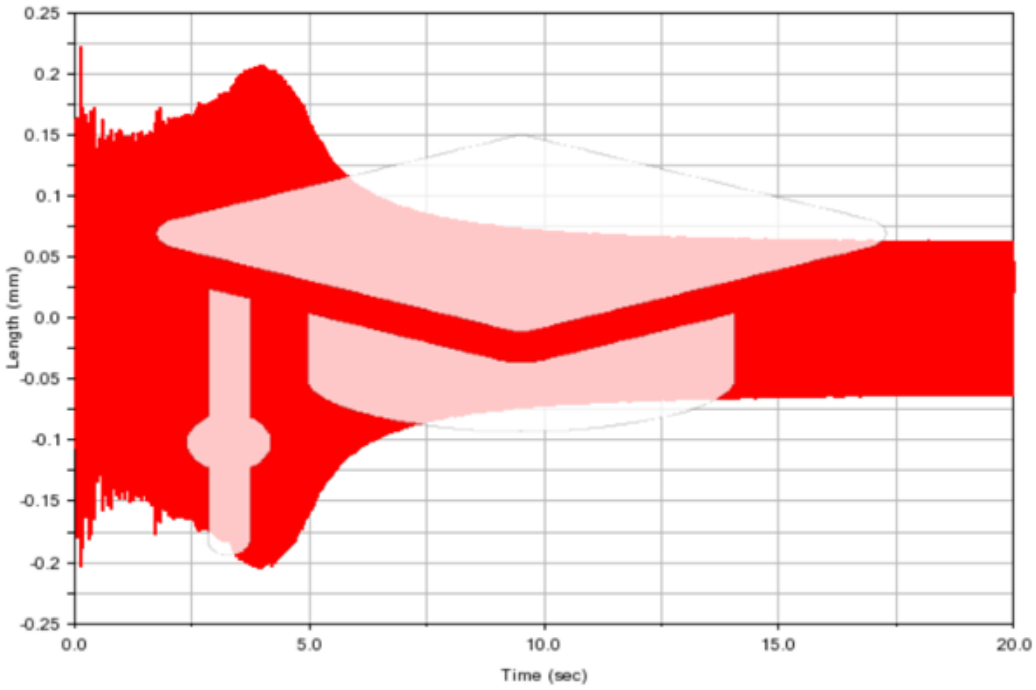
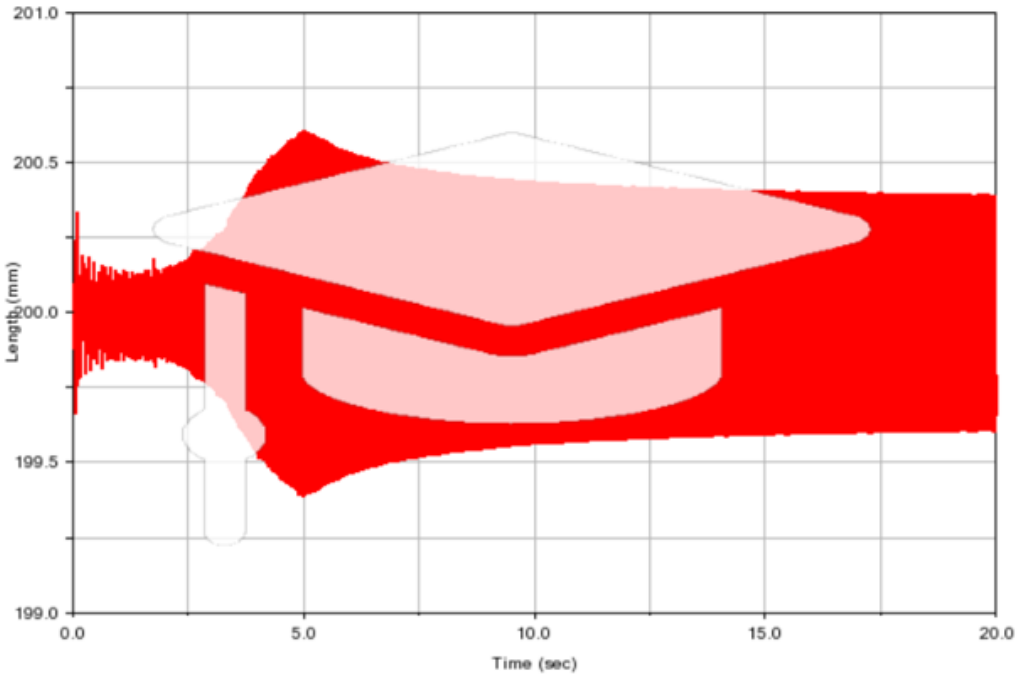


Figure 3.30. Response of the self-tuning absorber system implemented on a main mass suspended by a main spring when subject to 27.5 Hz base-excitation. (a) Main mass amplitude, (b) Main absorber mass amplitude, (c) Lever absorber mass displacement, (d) Position of the levered mass after self-tuning to 27.5 Hz.

(a)


0.25
0.2
0.15
0.1
0.05
0.0
-0.05
-0.1
-0.15
-0.2
-0.25
Length (mm)
0.0
5.0
10.0
15.0
20.0
Time (sec)

(b)


201.0
200.5
200.0
199.5
199.0
Length (mm)
0.0
5.0
10.0
15.0
20.0
Time (sec)

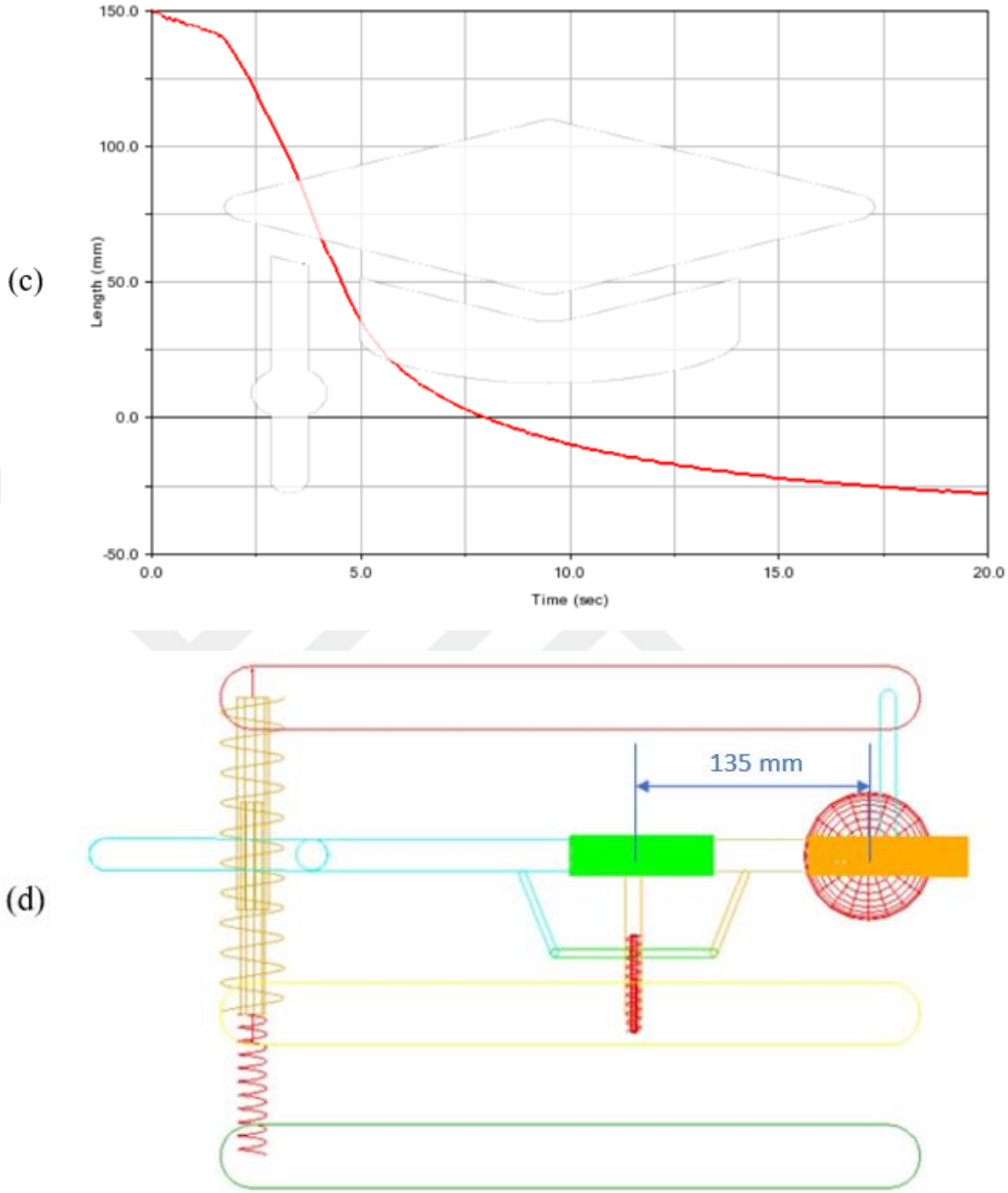


Figure 3.31. Response of the self-tuning absorber system implemented on a main mass suspended by a main spring when subject to 30 Hz base-excitation. (a) Main mass amplitude, (b) Main absorber mass amplitude, (c) Lever absorber mass displacement, (d) Position of the levered mass after self-tuning to 30 Hz.

In Figures 3.27-3.31 it is shown that the output amplitude of the main mass remains between 0.065 - 0.17 mm for input amplitude of 0.1 mm. In order to improve the vibration isolation performance of the self-tuning absorber system, the output amplitude of the main mass should be reduced further. To that end, main absorber damping constant

is reduced from 28 Ns/m to 7 Ns/m. As the damping constant is reduced to $1/4^{th}$ of the previous value, output amplitude around the antiresonance frequency is expected to reduce to $1/4^{th}$, as well. Numerical studies show that reducing damping constant further causes instabilities and the self-tuning absorber system cannot converge to an equilibrium position given a fixed excitation frequency.

Figures 3.32-3.36 show the response of the system with reduced damping and they can be compared with Figures 3.27-3.31. Figures 3.32-3.36(a) show that main mass amplitude is significantly reduced especially at higher frequency inputs. Hence, the vibration isolation performance of the system is significantly improved.

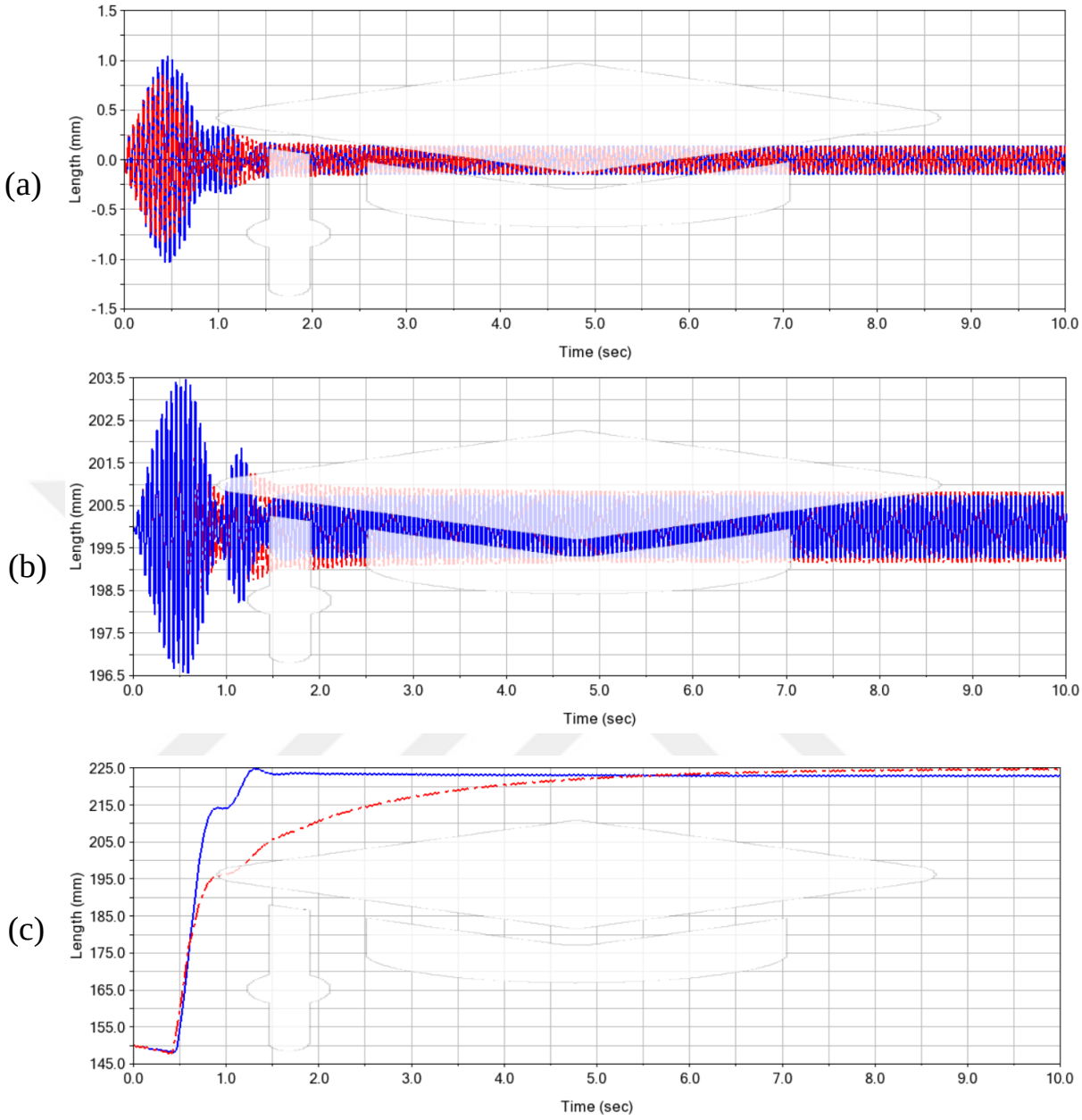


Figure 3.32. Response of the self-tuning absorber system implemented on a main mass suspended by a main spring when subject to 20 Hz base-excitation. (a) Main mass amplitude, (b) Main absorber mass amplitude, (c) Lever absorber mass displacement. Here, the red dashed line represents the system with original damping (28 Ns/m) and the blue solid line represents the system with reduced damping (7 Ns/m).

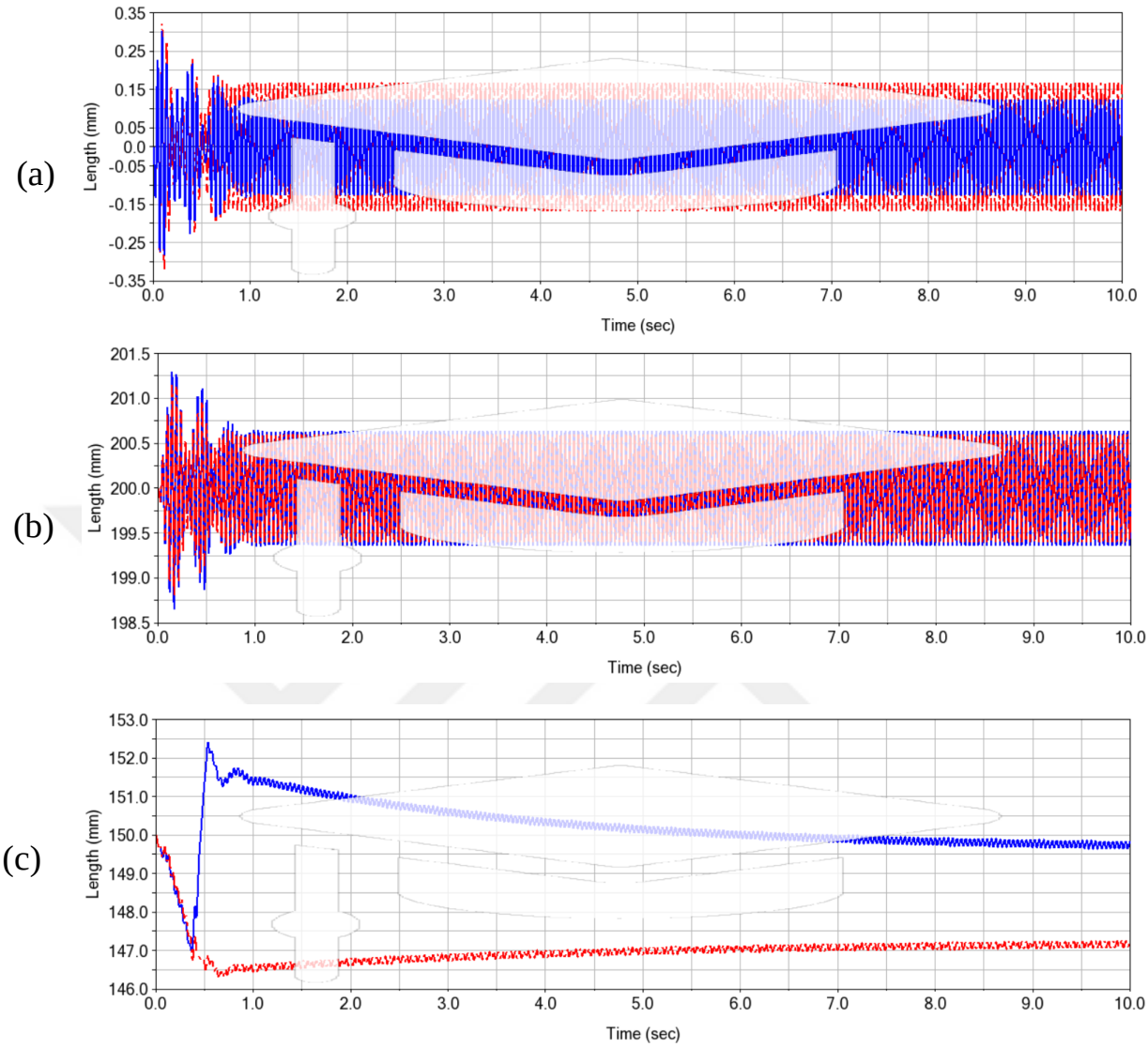


Figure 3.33. Response of the self-tuning absorber system implemented on a main mass suspended by a main spring when subject to 22.5 Hz base-excitation. (a) Main mass amplitude, (b) Main absorber mass amplitude, (c) Lever absorber mass displacement. Here, the red dashed line represents the system with original damping (28 Ns/m) and the blue solid line represents the system with reduced damping (7 Ns/m).

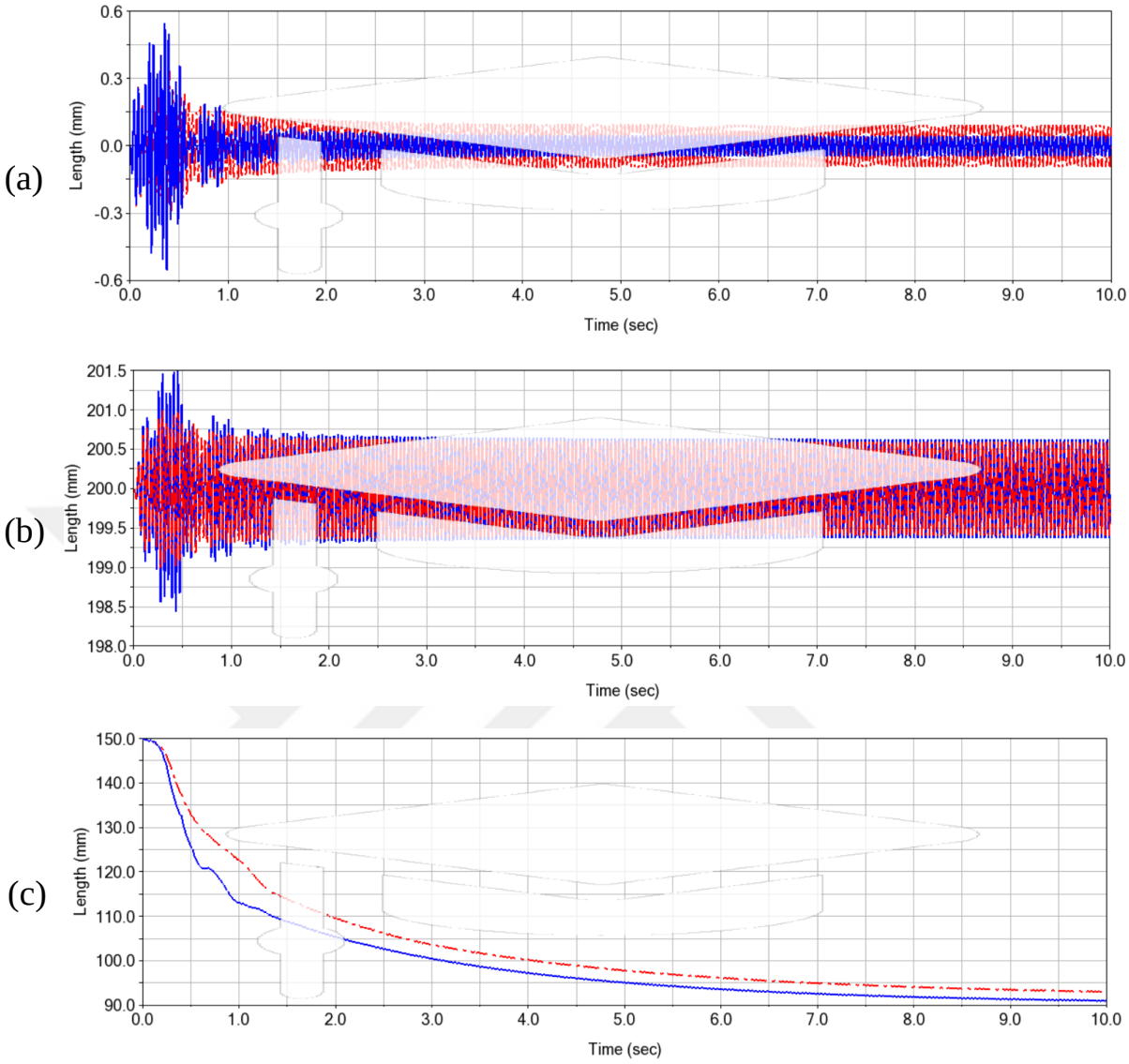


Figure 3.34. Response of the self-tuning absorber system implemented on a main mass suspended by a main spring when subject to 25 Hz base-excitation. (a) Main mass amplitude, (b) Main absorber mass amplitude, (c) Lever absorber mass displacement. Here, the red dashed line represents the system with original damping (28 Ns/m) and the blue solid line represents the system with reduced damping (7 Ns/m).

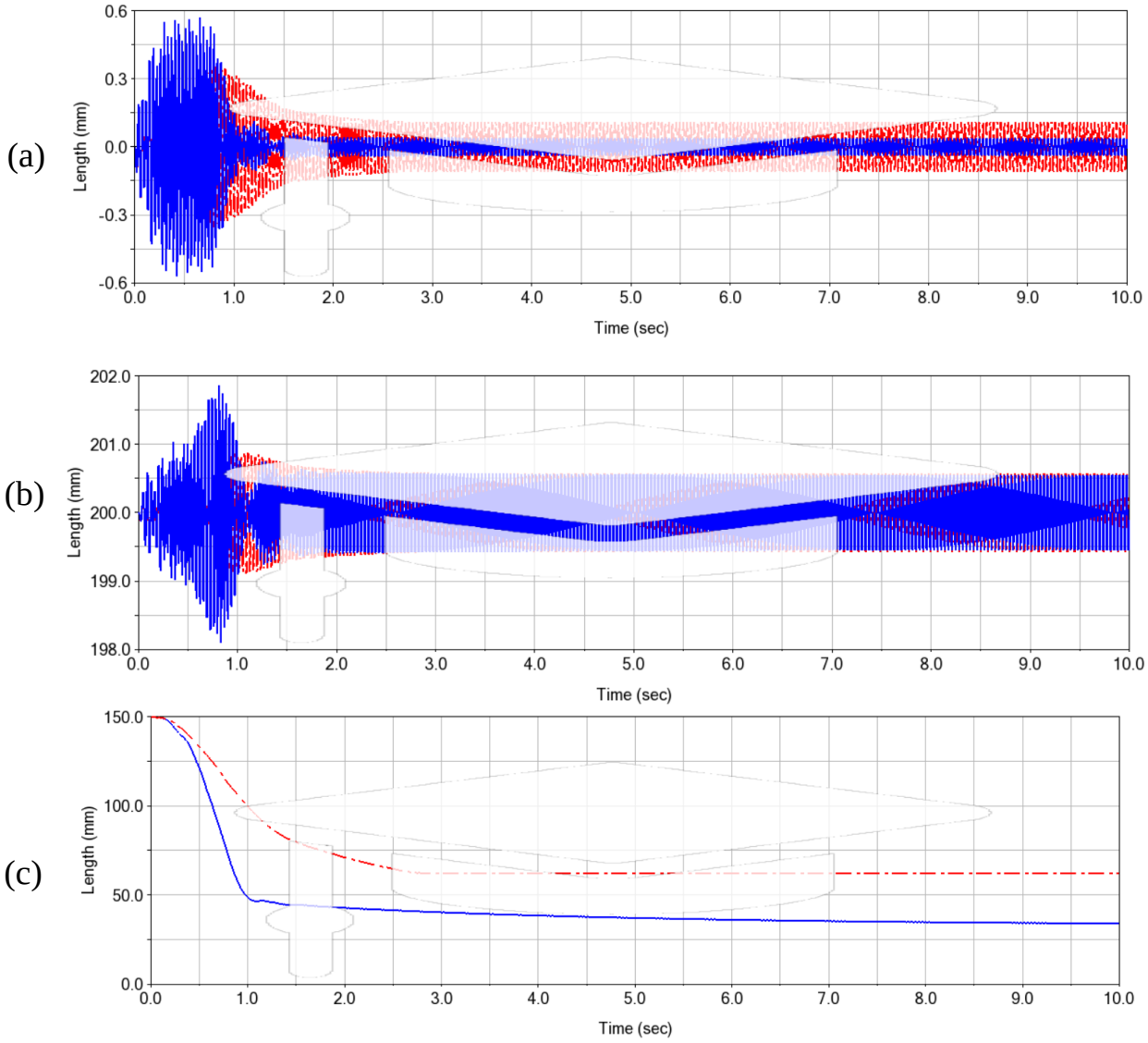


Figure 3.35. Response of the self-tuning absorber system implemented on a main mass suspended by a main spring when subject to 27.5 Hz base-excitation. (a) Main mass amplitude, (b) Main absorber mass amplitude, (c) Lever absorber mass displacement. Here, the red dashed line represents the system with original damping (28 Ns/m) and the blue solid line represents the system with reduced damping (7 Ns/m).

(a)

(b)

(c)

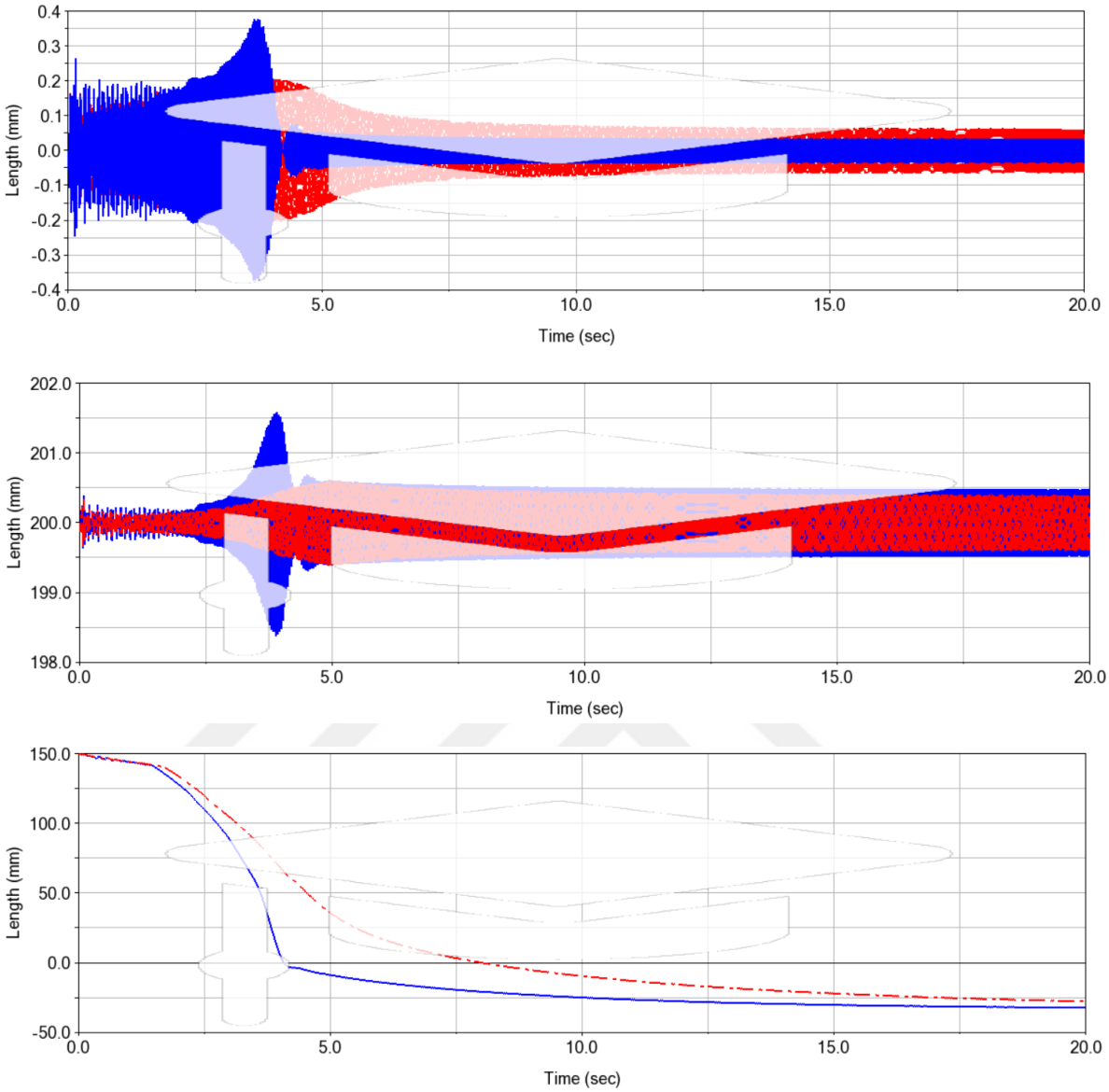


Figure 3.36. Response of the self-tuning absorber system implemented on a main mass suspended by a main spring when subject to 30 Hz base-excitation. (a) Main mass amplitude, (b) Main absorber mass amplitude, (c) Lever absorber mass displacement. Here, the red dashed line represents the system with original damping (28 Ns/m) and the blue solid line represents the system with reduced damping (7 Ns/m).

In order to compare the response of the self-tuning absorber system having reduced absorber damping (7 Ns/m) with a passive DVA, a model is created (see Figure 3.37). In the passive DVA model, every element of the self-tuning mechanism is removed and the main spring stiffness is determined as 24.6 N/mm which is 1/10th of the additional spring stiffness (246 N/mm). Moreover, the absorber damping coefficient is chosen as 3.9 Ns/m, which is 1/4th of the damping used in the earlier passive DVA system (15.6 Ns/m).

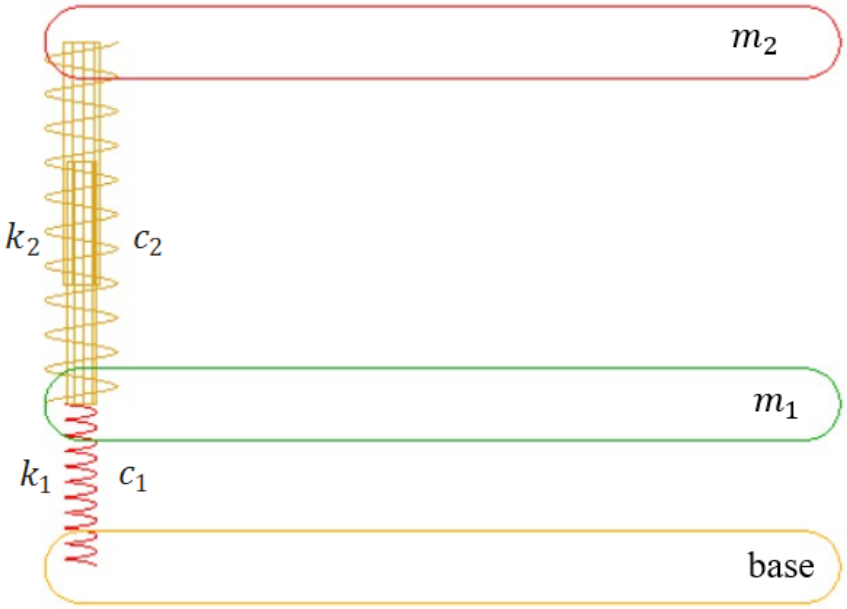


Figure 3.37. The passive dynamic vibration absorber system.

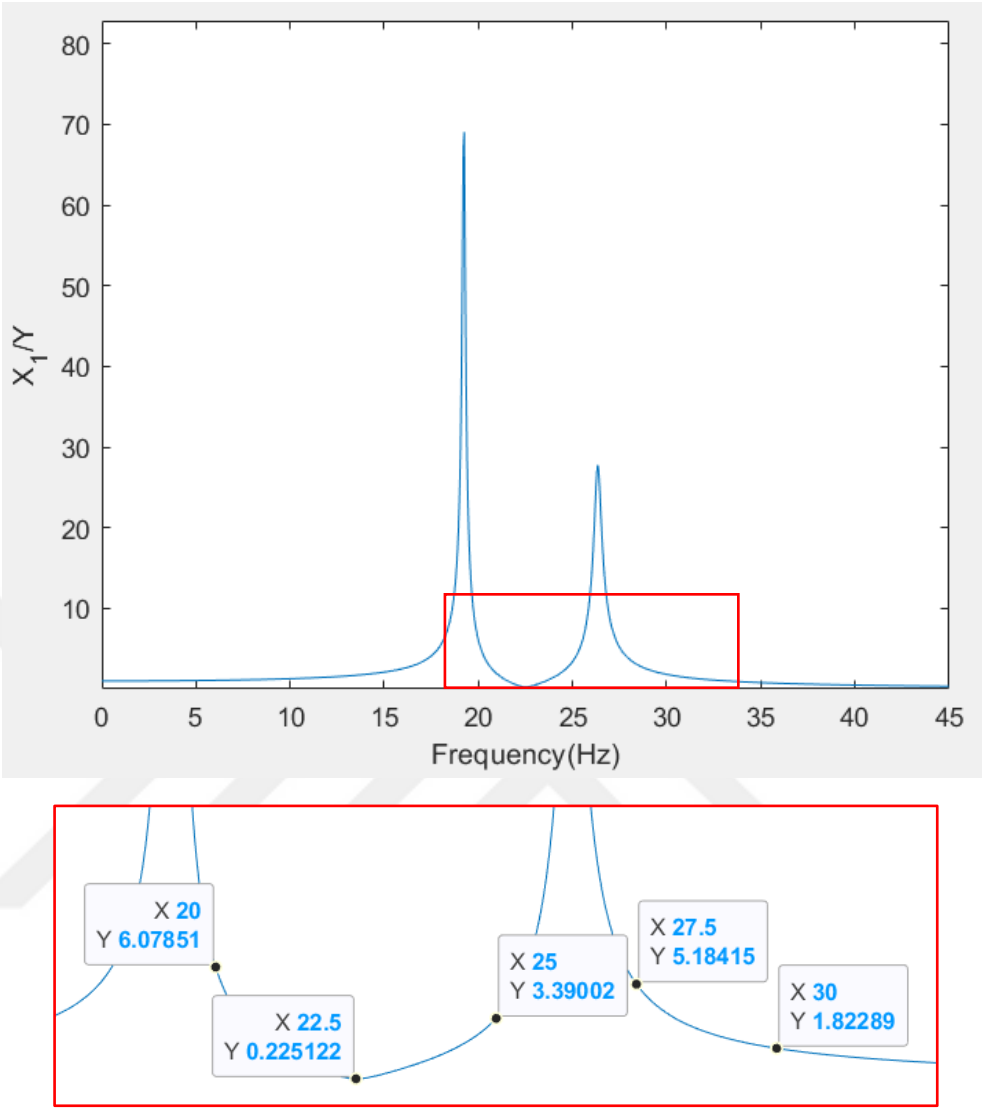


Figure 3.38. Transmissibility plot for a passive dynamic vibration absorber with $k_1 = 246$ N/m, $k_2 = 24.6$ N/m, $m_1 = 12.3$ kg, $m_2 = 1.23$ kg, $c_1 = 0$ Ns/m, $c_2 = 3.9$ Ns/m.

Figure 3.39(a) shows that the main mass amplitude reaches steady state amplitude of 0.5 mm when the excitation frequency is 20 Hz. As the base-excitation amplitude is 0.1 mm, the amplification ratio of the system is 5. According to Figure 3.38, at 20 Hz the passive DVA should have 0.61 mm amplitude for the main mass (6.1 times amplification). Hence, the results are close and there is 18% difference.

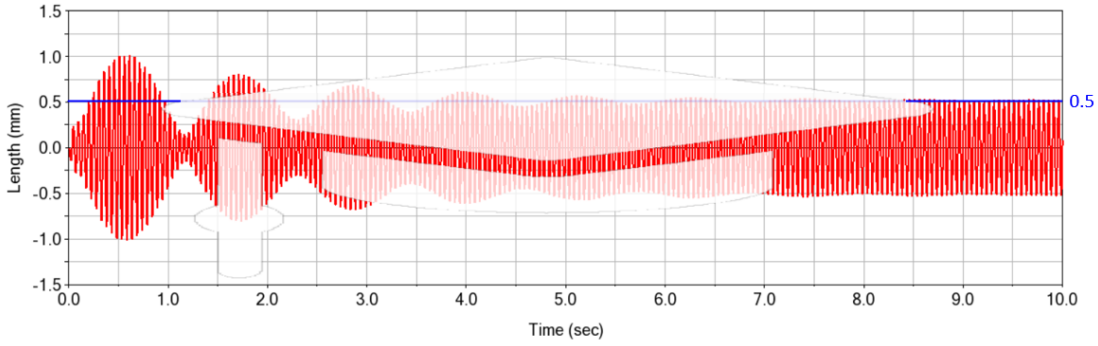
Figure 3.39 (b) shows that the main mass amplitude reaches steady state amplitude of 0.025 mm when the excitation frequency is 22.5 Hz. According to Figure 3.38, at 22.5 Hz the passive DVA should have 0.0225 mm amplitude for the main mass. Hence, the results are close and there is 11% difference.

Figure 3.39(c) shows that the main mass amplitude reaches steady state amplitude of 0.38 mm when the excitation frequency is 25 Hz. As the base-excitation amplitude is 0.1 mm, the amplification ratio of the system is 3.8. According to Figure 3.38, at 25 Hz the passive DVA should have 0.34 mm amplitude for the main mass (3.4 times amplification). Hence, the results are close and there is 11% difference.

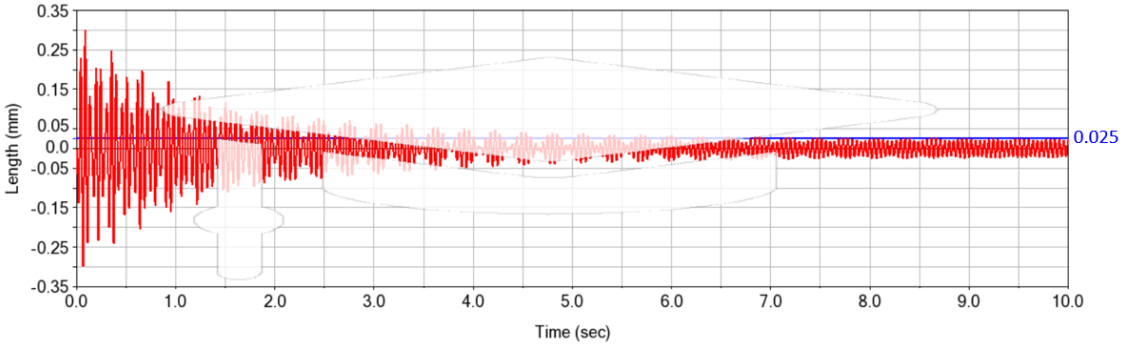
Figure 3.39(d) shows that the main mass amplitude reaches steady state amplitude of 0.45 mm when the excitation frequency is 27.5 Hz. As the base-excitation amplitude is 0.1 mm, the amplification ratio of the system is 4.5. According to Figure 3.38, at 27.5 Hz the passive DVA should have 0.52 mm amplitude for the main mass (5.2 times amplification). Hence, the results are close and there is 13% difference.

Figure 3.39(e) shows that the main mass amplitude reaches steady state amplitude of 0.17 mm when the excitation frequency is 30 Hz. As the base-excitation amplitude is 0.1 mm, the amplification ratio of the system is 1.7. According to Figure 3.38, at 30 Hz the passive DVA should have 0.18 mm amplitude for the main mass (1.8 times amplification). Hence, the results are close and there is 6% difference.

(a)



(b)



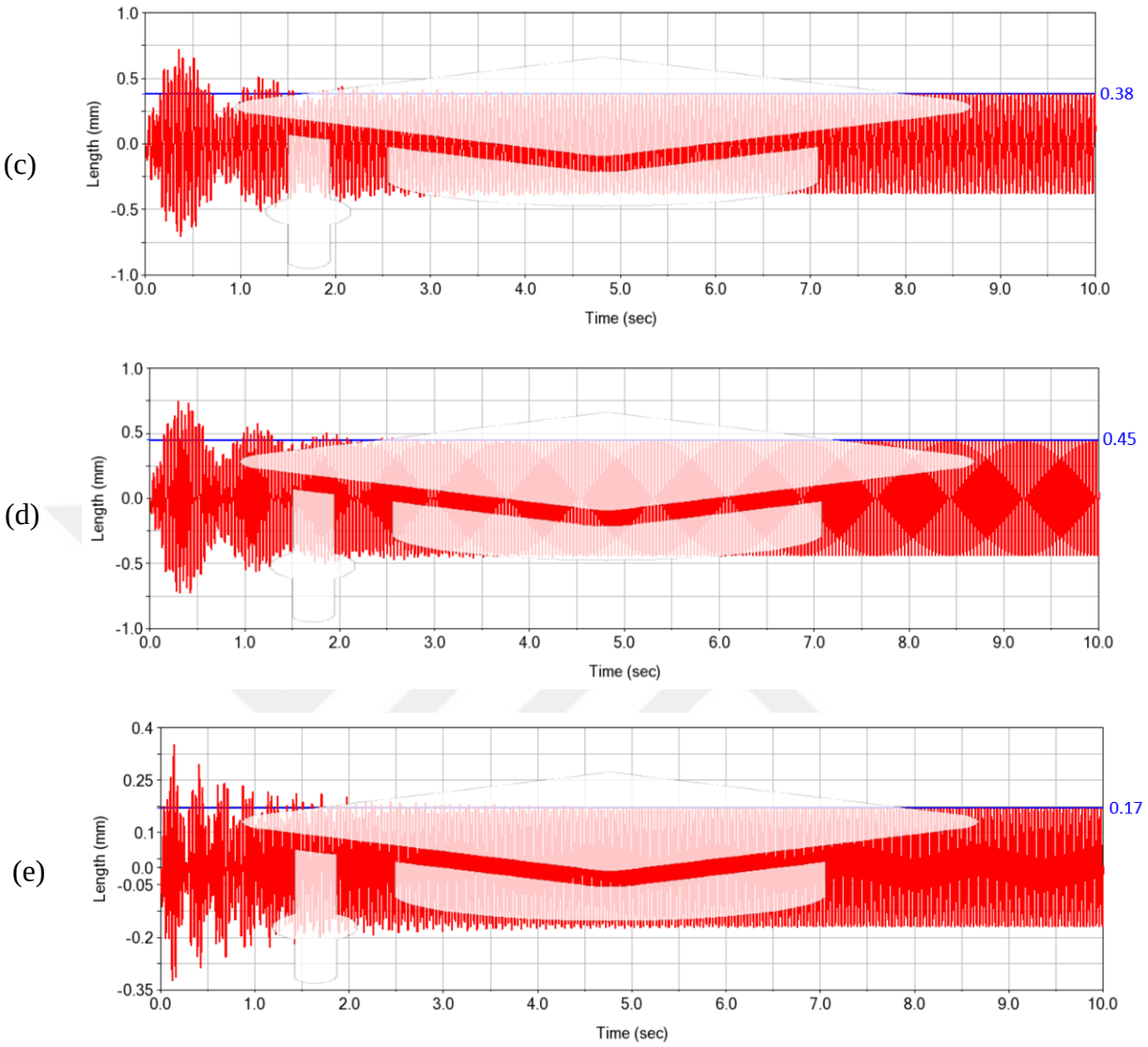


Figure 3.39. Main mass amplitude of the dynamic vibration absorber system when subject to 0.1 mm base-excitation at different frequencies (a) 20 Hz, (b) 22.5 Hz, (c) 25 Hz, (d) 27.5 Hz, (e) 30 Hz.

Table 3.5 summarizes the steady state amplitude of the main mass for various excitation frequencies for both the self-tuning DVA system and the passive DVA system with different absorber damping constants. Notice that passive DVA's can only provide isolation at 22.5 Hz whereas they amplify the motion significantly at other frequencies. Moreover, the best isolation performance is achieved by the self-tuning DVA with c_2=7 Ns/m.

Table 3.5. Steady state amplitude of the main mass for various excitation frequencies for 0.1mm input amplitude.

Excitation Frequency (Hz)	**Self-tuning DVA (c_2=28 Ns/m)**	**Self-tuning DVA (c_2=7 Ns/m)**	**Passive DVA (c_2=15.6 Ns/m)**	**Passive DVA (c_2=3.9 Ns/m)**
20	0.14	0.14	0.62	0.61
22.5	0.17	0.125	0.089	0.022
25	0.1	0.045	0.33	0.34
27.5	0.1	0.038	0.43	0.52
30	0.065	0.035	0.18	0.18

3.4.1. Tracking Performance of the Self-Tuning Absorber System Under Changing Frequency Condition

Similar to Section 3.3, in order to test how the system performs under changing excitation frequency, the input excitation frequency is varied according to the below equation. Notice that the frequency increases from 20 Hz to 25 Hz in 10 seconds. Moreover, the initial natural frequency of the system is 22.5 Hz. The excitation is defined as:

$$0.1\sin(40\,(1+0.0125t)\pi t). \tag{3.7}$$

Figures 3.40 and 3.41 show that when the input excitation frequency is varied, the implemented system quickly self-tunes and tracks the input excitation frequency. Thus, the amplitudes do not exceed a certain limit although the input excitation frequency is varied. Moreover, Figure 3.42 shows that after 1 second, the system self-tunes to the varying excitation condition and tracks it.

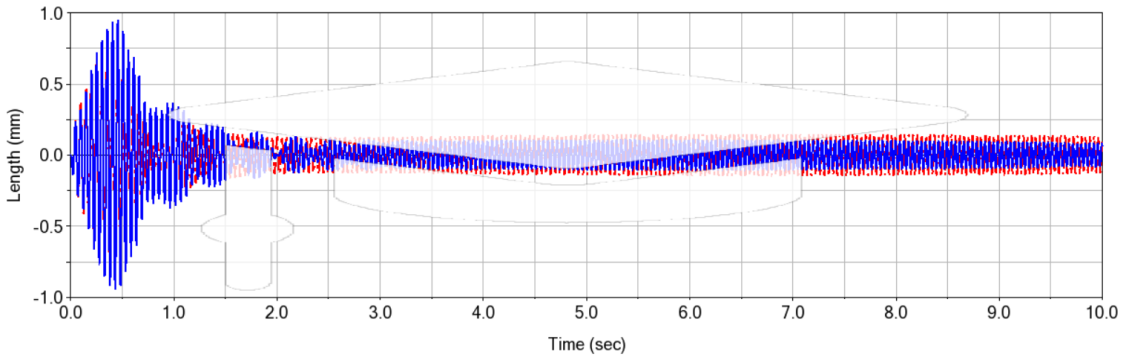


Figure 3.40. Amplitude of the main mass under changing excitation frequency. Here, the red dashed line represents the system with original damping (28 Ns/m) and the blue solid line represents the system with reduced damping (7 Ns/m).

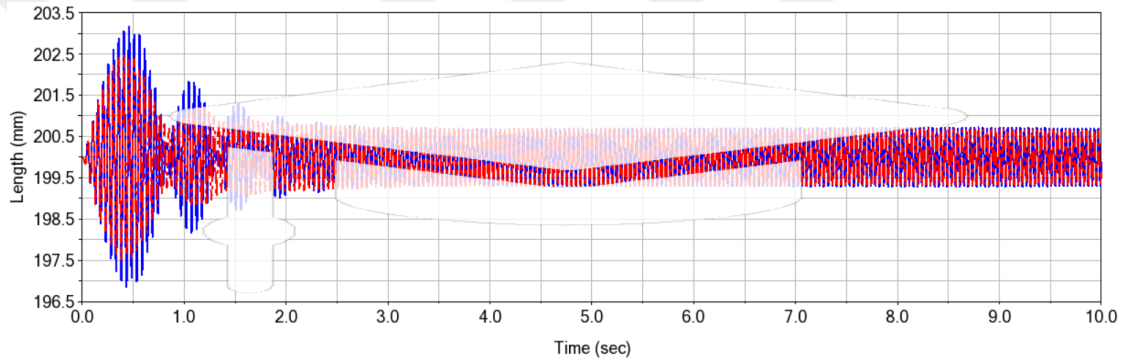


Figure 3.41. Amplitude of the main absorber mass under changing excitation frequency. Here, the red dashed line represents the system with original damping (28 Ns/m) and the blue solid line represents the system with reduced damping (7 Ns/m).

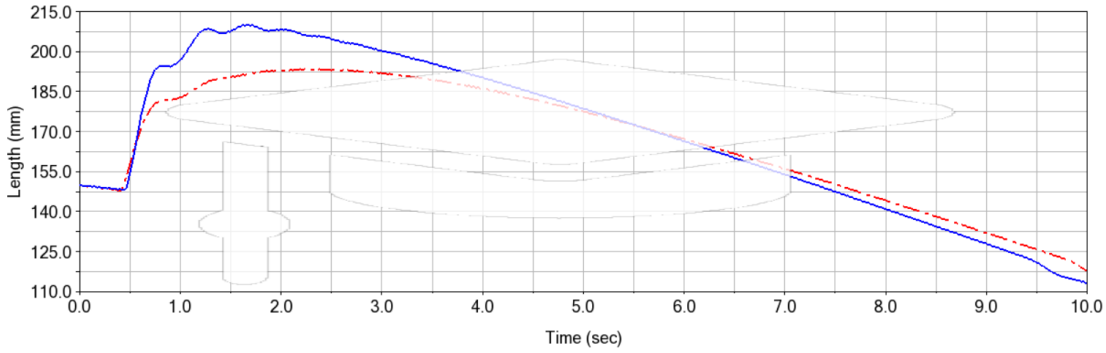


Figure 3.42. Displacement of the levered absorber mass during self-tuning to changing excitation frequency. Here, the red dashed line represents the system with original damping (28 Ns/m) and the blue solid line represents the system with reduced damping (7 Ns/m).

Consequently, for both conditions, the system still operates successfully. Hence, it can be said that system is able to adapt to changing excitation frequency conditions.

3.5. Modification of the System to Increase Working Frequency Range

In order to increase the working frequency range of the system, the lever ratio should be varied over a wider range. To that end, the hinges are brought closer. In the original system the hinge spacing was 160 mm, currently it is reduced to 60 mm.

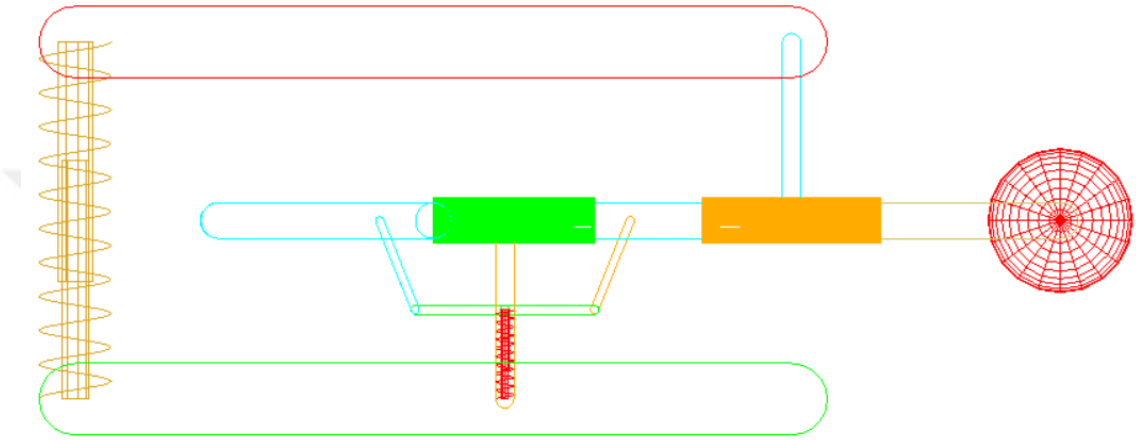


Figure 3.43. Original system with 160 mm hinge spacing.

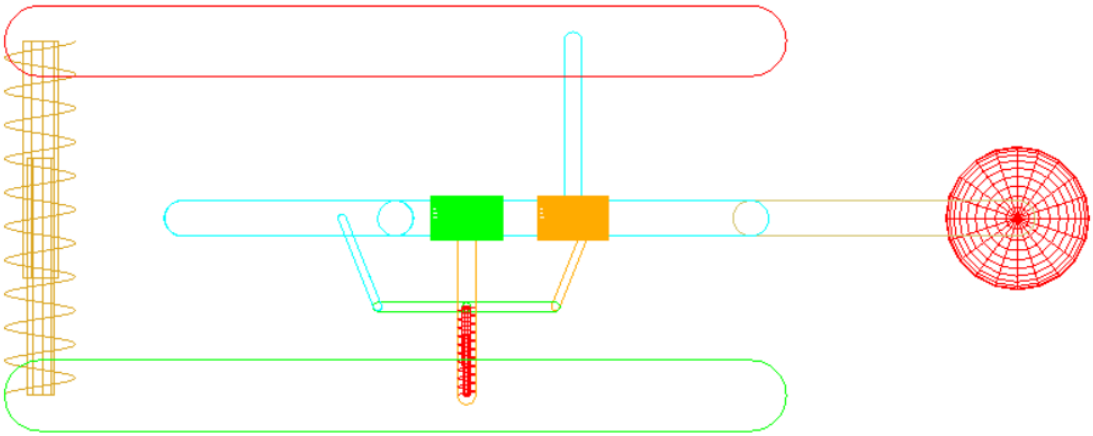


Figure 3.44. New system with 60 mm hinge spacing.

In the original model the natural frequency was 22.5 Hz and its working frequency range was 20-32 Hz. Ratio of the upper limit of the working frequency range to the lower limit is 1.6. When the hinge spacing is modified as in Figure 3.44, the natural frequency

reduces to 10.6 Hz and the working frequency range is 10-25 Hz. Ratio of the upper limit of the working frequency range to the lower limit is 2.5. Hence, the bandwidth of operation is significantly increased.

In order to view both conditions of excitation frequency being greater and lower than the initial natural frequency (10.6 Hz), step functions are used for base excitation as in:

$$0.6\ (\sin(50\pi t) - STEP(t, 5, 0, 5.25, 1)\sin(50\pi t) + STEP(t, 5.25, 0, 5.5, 1)\sin(20\pi t)). \quad (3.8)$$

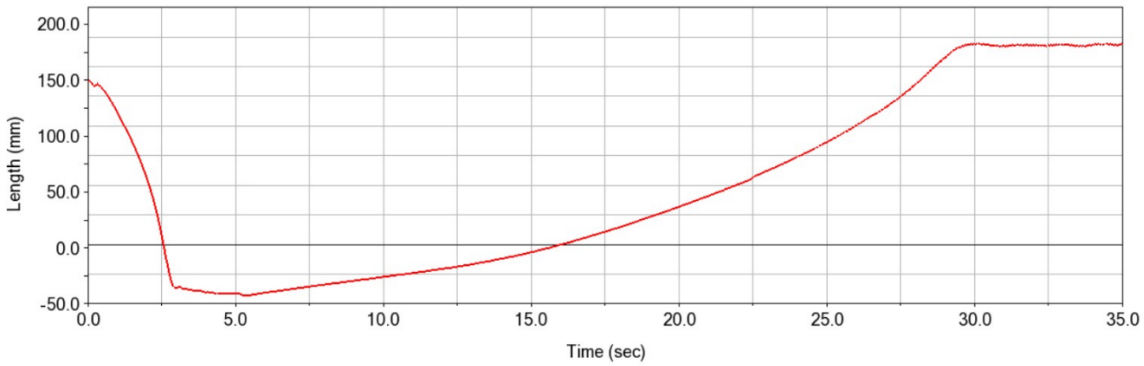


Figure 3.45. Displacement of levered absorber mass for the system with modified hinge spacing.

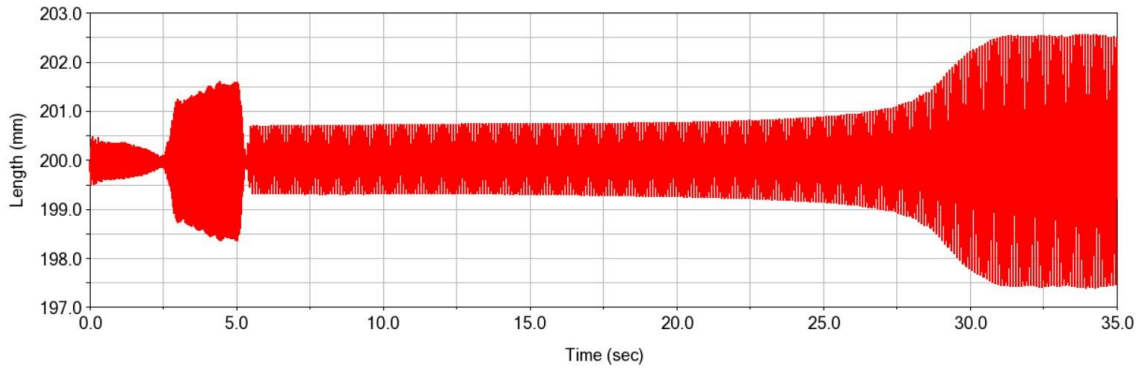


Figure 3.46. Amplitude of the main absorber mass for the system with modified hinge spacing.

Notice that although the initial natural frequency of the system is at 10.6 Hz, the system self-tunes to 25 Hz in about 3 seconds.

When the initial natural frequency of the original system is 10.6 Hz, the system self-tunes to 25 Hz in 3 seconds. After the system is self-tuned to 25 Hz, the input excitation frequency is changed to 10 Hz. The system self-tunes to 10 Hz in 27 seconds.

4. CONCLUSION

4.1. Summary

In this thesis, an adaptive self-tuning base-excited resonator, which can be used a vibration absorber system, is designed. A self-tuning algorithm is developed and implemented to the numerical model of the system.

The performance of a passive vibration absorber system may not meet the performance requirements due to changing operating conditions. However, the designed self-tuning mechanical system can respond to these changes by altering its parameters without the help of an external power source.

The self-tuning algorithm is developed for a base-excited dynamic vibration resonator system which auto-tunes within the operational frequency range. The parameters of the system are modified systematically to minimize self-tuning response time, which also improved the output resonance amplitude.

System was tested in changing excitation frequency conditions to see if it can successfully track and tune accordingly. Hence, it was subjected to increasing and decreasing excitation frequency. The system successfully adapted to varying excitation conditions.

In order to increase operational frequency range, system design was modified in which hinge spacing was reduced. The operational frequency range increased but the self-tuning duration was increased.

4.2. Future Work

This study is aimed to fill the gap in the knowledge of adaptive, self-tuned and self-powered vibration absorbers which can act as resonators. The study concentrates on the creation and validation of a self-tuning algorithm. The system is assumed to be linear and the detrimental effects of nonlinearities on the performance are not diagnosed or improved,

the effect of gravity was neglected. Gravitational deflection, vibro-impact effects, and non-linearities due to large amplitude excitations can be investigated in future studies.

In addition, the current system works for a limited frequency range constrained by the system design and geometrical constraints. The design of the system can be modified so that the working frequency range can be increased while minimizing self-tuning response time.

REFERENCES

1. Williams, K., G. Chiu and R. Bernhard, "Adaptive-Passive Absorbers Using Shape Memory Alloys", *Journal of Sound and Vibration*, Vol. 249, No. 5, pp. 835-848, 2002.

2. Ahmadi, S., K. Jacob, F. Wendler and M. Kohl, "Shape Memory Alloy Film Damping for Smart Miniature Systems", *International Journal of Smart and Nano Materials*, Vol. 9, No. 3, pp. 199–215, 2018.

3. Rustighi, E., M. J. Brennan and B. R. Mace, "A Shape Memory Alloy Adaptive Tuned Vibration Absorber: Design and Implementation", *Smart Materials and Structures*, Vol. 14, No. 1, pp. 19-28, 2004.

4. Savi M., A. De Paula and D. Lagoudas, "Numerical Investigation of an Adaptive Vibration Absorber Usign Shape Memory Alloys", *Journal of Intelligent Material Systems and Structures*, Vol. 22, No. 1, pp. 67-80, 2011.

5. Hodgson, D. E., "Damping Applications of Shape-Memory Alloys", *Materials Science Forum*, Vol. 394-395, pp. 69-74, 2002.

6. Acar, M. A. and C. Yilmaz, "Design of an Adaptive-Passive Dynamic Vibration Absorber Composed of a String-mass System Equipped with Negative Stiffness Tension Adjusting Mechanism", *Journal of Sound and Vibration*, Vol. 332, No. 2, pp. 231-245, 2013.

7. Lee, C., V. Goverdovskiy and A. Temkinov, "Design of Springs with Negative Stiffness to Improve Vehicle Driver Vibration Isolation", *Journal of Sound and Vibration*, Vol. 302, No. 4-5, pp. 865-874, 2007.

8. Wang, Y. and R. Lakes, "Extreme Stiffness Systems Due to Negative Stiffness Elements", *American Journal of Physics*, Vol. 72, No. 1, pp. 40-50, 2004.

9. Carella, A., M. Brennan and T. Waters, “Static Analysis of a Passive Vibration Isolator with Quasi-Zero-Stiffness Characteristics”, *Journal of Sound and Vibration*, Vol. 301, No. 3-5, pp. 678-874, 2007.

10. Shen, Y., H. Peng, X. Li and S. Yang, “Analytically Optimal Parameters of Dynamic Vibration Absorber with Negative Stiffness”, *Mechanical Systems and Signals Processing*, Vol. 85, pp. 193-203, 2017.

11. Hoang, N., N. Zhang and H. Du, “An Adaptive Tunable Vibration Absorber Using a New Magnetorheological Elastomer for Vehicular Powertrain Transient Vibration Reduction”, *Smart Structures and Materials*, Vol. 20, No. 1, p. 015019, 2010.

12. Hoang, N., N. Zhang and H. Du, “A Dynamic Absorber with a Soft Magnetorheological Elastomer for Powertrain Vibration Suppresion”, *Smart Materials and Structures*, Vol. 18, No. 7, p. 074009, 2009.

13. Hirunyapruk, C., M. J. Brennan, B. R. Mace and W. H. Li, “A Tunable Magneto-rheological Fluid-Filled Beam-Like Vibration Absorber”, *Smart Materials and Structures*, Vol. 19, No. 5, p. 055020, 2010.

14. Nagaya, K., A. Kurusu, S. Ikai and Y. Shitani, “Vibration Control of a Structure by Using a Tunable Absorber and an Optimal Vibration Absorber Under Auto-Tuning Control”, *Journal of Sound and Vibration*, Vol. 228, No. 4, pp. 773-792, 1999.

15. Lerner, A. A. and K. A. Cunefare, “Performance of MRE-Based Vibration Absorbers”, *Journal of Intelligent Material Systems and Structures*, Vol. 19, No. 5, pp. 551-563, 2008.

16. Rasooli, A., R. Sedaghati, and M. Hemmatian, “A Novel Magnetorheological Elastomer-Based Adaptive Tuned Vibration Absorber: Design, Analysis and Experimental Characterization”, *Smart Materials and Structures*, Vol. 29, No. 11, p. 115042, 2020.

17. Cronje, M. J., P. Heyns, N. Theron and P. Loveday, “Developement of a Variable Stiffness and Damping Tunable Vibration Isolator”, *Journal of Vibration and Control*, Vol. 11, No. 3, pp. 381-396, 2005.

18. Bonello, P., M. J. Brennan and S.J. Elliott, “Vibration Control Using an Adaptive Tuned Vibration Absorber with a Variable Curvature Stiffness Element”, *Smart Materials and Structures*, Vol. 14, No. 5, pp. 1055–1065, 2005.

19. Cronje, M. J., P. Stephans, N. J. Theron and P. W. Loveday, “Development of a Variable Stiffness Spring for Adaptive Vibration Isolators”, *Proceedings of SPIE - The International Society for Optical Engineering*, Vol. 5386, 2004.

20. Xu, Z., X. Gong and X. Chen, “Development of a Mechanical Semi-Active Vibration Absorber”, *Advances in Vibration Engineering*, Vol. 10, No. 3, pp. 229–38, 2011.

21. Yilmaz, C. and N. Kikuchi, “Analysis and Design of Passive Band-Stop Filter-Type Vibration Isolators for Low-Frequency Applications”, *Journal of Sound and Vibration*, Vol. 291, No. 3-5, pp. 1004-1028, 2006.

22. Masjedi, P. K. and P. M. Weaver, “Variable Stiffness Composite Beams Subject to Non-Uniformly Distributed Loads: An Analytical Solution”, *Composite Structures*, Vol. 256, p. 112975, 2020.

23. Bonello, P., M. Brennan, S. Elliot, J. Vincent and G. Jeronimidis, “Designs for an Adaptive Tuned Vibration Absorber with Variable Shape Stiffness Element”, *Proceedings of the Royal Society A: Mathematical, Physical and Engineering Science*, Vol. 461, No. 2064, pp. 3955-3976, 2005.

24. Franchek, M. A., M. W. Ryan and R. J. Bernhard, “Adaptive Passive Vibration Control”, *Journal of Sound and Vibration*, Vol. 189, No. 5, pp. 565-585, 1996.

25. Behrooz, F., “Self-Tuning Vibration Absorber”, US Patent 8044629 B2, 25 October 2010, https://patents.google.com/patent/US8044629B2/.

26. Changrong, Z., T. Fengchen and H. Caichun, “Self-Tuning Dynamic Vibration Absorber”, CN Patent 205078688 U, 3 September 2016, https://patents.google.com/patent/CN205078688U/.

27. Almashhor, A. and S. Asiri, “Development of a New Tuned Vibration Absorber Based on One Degree-of-Freedom of Translational Motion”, *Cogent Engineering*, Vol. 8, No. 1, p. 1976929, 2021.

28. Borowski, V. J., H. H. Denman, D. L. Cronin, S. W. Shaw, J. P. Hanisko, L. T. Brooks, D. A. Mikulec, W. B. Crum and M. P. Anderson, “Reducing Vibration of Reciprocating Engines with Crankshaft Pendulum Vibration Absorbers”, *SAE Transactions*, Vol. 100, No. 2, pp. 376–382, 1991.

29. Bruce, G., B. Christopher, R. William, H. Imran, P. Michael and M. Stan, “Pendulum Vibration Absorber on a Crankshaft”, US Patent 8813604 B2, 26 August 2014, https://patents.google.com/patent/US8813604B2/.

30. Shen, Y., Z. Xing, S. Yang and J. Sun, “Parameters Optimization for a Novel Dynamic Vibration Absorber”, *Mechanical Systems and Signals Processing*, Vol. 113, p. 106282, 2019.

31. Ozyar, O. and C. Yilmaz, “A Self-Tuning Adaptive-Passive Lever-Type Vibration Isolation System”, *Journal of Sound and Vibration*, Vol. 505, p. 116159, 2021.

APPENDIX A: ELSEVIER LICENSE NUMBER

5375511216243

ELSEVIER LICENSE
TERMS AND CONDITIONS

Aug 24, 2022

This Agreement between Mr. Bedri Seyhan ("You") and Elsevier ("Elsevier") consists of your license details and the terms and conditions provided by Elsevier and Copyright Clearance Center.

License Number	5375511216243
License date	Aug 24, 2022
Licensed Content Publisher	Elsevier
Licensed Content Publication	Journal of Sound and Vibration
Licensed Content Title	ADAPTIVE-PASSIVE ABSORBERS USING SHAPE-MEMORY ALLOYS
Licensed Content Author	K. WILLIAMS,G. CHIU,R. BERNHARD
Licensed Content Date	Jan 31, 2002
Licensed Content Volume	249
Licensed Content Issue	5
Licensed Content Pages	14
Start Page	835
End Page	848
Type of Use	reuse in a thesis/dissertation
Portion	figures/tables/illustrations
Number of figures/tables/illustrations	1
Format	both print and electronic
Are you the author of this Elsevier article?	No
Will you be translating?	No
Title	DESIGN OF A SELF-ADJUSTING AND SELF-POWERED DYNAMIC VIBRATION ABSORBER
Institution name	BOGAZICI UNIVERSITY
Expected presentation date	Aug 2022

Figure A.1. Elsevier license of Ref. [1] for Figure 1.1.

APPENDIX B: ELSEVIER LICENSE NUMBER

5375510063227

ELSEVIER LICENSE
TERMS AND CONDITIONS

Aug 24, 2022

This Agreement between Mr. Bedri Seyhan ("You") and Elsevier ("Elsevier") consists of your license details and the terms and conditions provided by Elsevier and Copyright Clearance Center.

License Number	5375510063227
License date	Aug 24, 2022
Licensed Content Publisher	Elsevier
Licensed Content Publication	Journal of Sound and Vibration
Licensed Content Title	Design of an adaptive–passive dynamic vibration absorber composed of a string–mass system equipped with negative stiffness tension adjusting mechanism
Licensed Content Author	M.A. Acar,C. Yilmaz
Licensed Content Date	Jan 21, 2013
Licensed Content Volume	332
Licensed Content Issue	2
Licensed Content Pages	15
Start Page	231
End Page	245
Type of Use	reuse in a thesis/dissertation
Portion	figures/tables/illustrations
Number of figures/tables/illustrations	1
Format	both print and electronic
Are you the author of this Elsevier article?	No
Will you be translating?	No
Title	DESIGN OF A SELF-ADJUSTING AND SELF-POWERED DYNAMIC VIBRATION ABSORBER
Institution name	BOGAZICI UNIVERSITY
Expected presentation date	Aug 2022

Figure B.1. Elsevier license of Ref. [6] for Figure 1.2.

APPENDIX C: ELSEVIER LICENSE NUMBER

5375500220278

ELSEVIER LICENSE
TERMS AND CONDITIONS

Aug 24, 2022

This Agreement between Mr. Bedri Seyhan ("You") and Elsevier ("Elsevier") consists of your license details and the terms and conditions provided by Elsevier and Copyright Clearance Center.

License Number	5375500220278
License date	Aug 24, 2022
Licensed Content Publisher	Elsevier
Licensed Content Publication	Journal of Sound and Vibration
Licensed Content Title	A self-tuning adaptive-passive lever-type vibration isolation system
Licensed Content Author	Onur Özyar,Çetin Yılmaz
Licensed Content Date	Aug 4, 2021
Licensed Content Volume	505
Licensed Content Issue	n/a
Licensed Content Pages	1
Start Page	116159
End Page	
Type of Use	reuse in a thesis/dissertation
Portion	figures/tables/illustrations
Number of figures/tables/illustrations	3
Format	both print and electronic
Are you the author of this Elsevier article?	No
Will you be translating?	No
Title	DESIGN OF A SELF-ADJUSTING AND SELF-POWERED DYNAMIC VIBRATION ABSORBER
Institution name	BOGAZICI UNIVERSITY
Expected presentation date	Aug 2022

Figure C.1. Elsevier license of Ref. [31] for Figures 2.3-2.9.